

Characterization of Discontinuous Carbon Fibre Mat Produced by Hydrodynamic Processes

By

Zhe Liu

MSc.

Thesis submitted to the University of Nottingham for the degree of Doctor of Philosophy

May 2017

Abstract

It is estimated that in 2017 global demand for carbon fibre may be as much as 111 thousand tonnes and with an annual growth rate (AGR) of 10% to 13% this number will increase to 191 thousand tonnes by 2022. Commercial operations to recover carbon fibre from waste composites are now developing and as more recovered fibre becomes available new applications for recovered fibre are required. Mats with random in-plane fibre orientation can readily be produced using existing commercial processes, however, due to a random fibre orientation distribution, over 100bar is required to achieve 40% fibre volume fraction during moulding. Under this pressure, fibre breakage significantly reduces the mean fibre length and the properties of the composite manufactured. Nonwoven mats made from short carbon fibres which are aligned in a preferential direction can achieve higher fibre volume fractions with lower fibre breakage even at high moulding pressure. A hydrodynamic alignment process has been developed in the University of Nottingham which consists of three stages; dispersing, depositing and dewatering. In this thesis, the influencing factors in the depositing and dewatering processes will be explored.

In the depositing process, the dispersed fibre suspension flows through a converging nozzle which can generate the aligned fibre orientation. A careful nozzle design is required to improve the fibre alignment quality. At the same time, a high level of jet stability will help to maintain this aligned orientation. Thus, both experimental work and CFD simulation were used to increase understanding of both the fibre suspension jet stability behaviour and the effects of nozzle shape on fibre orientation. When the fibre suspension jet is

depositing, many processing factors (e.g. fibre length, fibre volume concentration, dewatering vacuum level) will affect the fibre orientation on the mat. A series of experimental work was undertaken following a 2-level full factorial experiment design. Furthermore, a composite of 46% fibre volume fraction has been produced moulded at a pressure of just 7 bar in an autoclave, exhibiting good mechanical properties (with 98GPa tensile moudulus) which compete with higher grade materials. This demonstrates the potential for high value applications for recovered carbon fibre by preferential fibre alignment.

The fundamental theory of this hydrodynamic alignment process is similar to the paper making process: the fibre suspension flows through the headbox to form a moist paper sheet and then the water residual is removed in the forming section (vacuum suction), press section and drying section. However, the drying section takes 85% energy consumption of the whole dewatering process and a 1% reduction in sheet moisture after the vacuum dewatering results in a 4% reduction in dryer load. Thus, to reduce the energy costs, the optimization of vacuum dewatering is important in paper making process and this hydrodynamic alignment process. The dewatering behaviour of the aligned fibre mat is investigated in this thesis. As one of the main factors which can determine the dewatering rate, permeability was measured and predicted. Based on the predicted permeability, the required suction pressure in dewatering process for an aligned fibre mat with target areal density is evaluated. To maintain the suction pressure with a low energy cost, a pump selection analytical model is developed with the performance curves of liquid ring pump, high pressure radial blower and 2-stage channel blower.

Furthermore, to increase the dewatering efficiency and protect the aligned fibre orientation, the evenly distributed vacuum pressure through the fibre mat is required. Therefore, in this thesis, the optimised opening geometry for the deposition drum is identified. The lay-up configuration of nylon meshes with different wire sizes was studied to raise the best pressure distribution media.

Acknowledgements

The author wishes to acknowledge the patient, advice and support of her supervisors, Dr K. H. Wong, Dr T. A. Turner and Prof. S.J. Pickering.

Many thanks to the technicians who have assisted with various practical parts of this work; Paul Johns and Ben Jennison.

The author would also gratefully acknowledge the support of the Boeing Company under the Boeing / University of Nottingham strategic collaboration in carbon fibre recycling.

Finally, I would appreciate my parents and friends for their love, support and encouragement.

Contents

Abstract....1
1. Introduction....9
1.1 Summary of Carbon Fibre Recycling Methods....9
1.1.1 Mechanical recycling process....10
1.1.2 Chemical recycling process....11
1.1.3 Thermal recycling process....12
1.1.4 Reuse challenge of recycled carbon fibre....13
1.2 Project objectives....14
References....17
2. Literature review....19
2.1 Hydrodynamic Alignment Process....19
2.1.1 ERDE process....20
2.1.2 Hydrodynamic alignment process for recycled carbon fibre....22
2.2 Effect of fibre suspension jet stability on alignment quality of discontinuous carbon fibre mat....24
2.2.1 Liquid jet break up regime....24
2.2.2 Influences of nozzle design on the jet stability behaviour....26
2.3 Fibre orientation in a jet of fibre – liquid suspension....28
2.3.1 Jeffery's orbit and orientation tensors....28
2.3.2 Nozzle geometry effects....35
2.4 Performance of discontinuous fibre composites....39
2.4.1 Fibre length effects....39
2.4.2 Volume fraction effects....39
2.4.3 Analytical models for determining mechanical properties of discontinuous fibre composites....40
2.5 Permeability measurement and prediction....43
2.5.1 Darcy's law....43
2.5.2 Analytical permeability prediction method....44

2.6 Summary of literature review 48

References 49

3. Characterisation of liquid jets and nozzle design 54

3.1 Introduction 54

3.2 Materials and methods 56

3.2.1 Jet stability test 56

3.2.2 The effects of nozzle geometries on fibre alignment 59

3.3 Results and discussion 60

3.3.1 Liquid jet break-up regimes validation 60

3.3.2 Break-up regime exploration of short fibre suspension jet 62

3.3.3 The effects of nozzle geometries on flow kinematics and fibre alignment 67

3.4 Conclusion 72

References 73

4. Characterisation of aligned mats and composites 74

4.1 Introduction 74

4.2 Materials and methods 75

4.2.1 Materials 75

4.2.2 Dry fibre mat compaction testing 76

4.2.3 Glycerine washing methods 77

4.2.4 Manufacture of aligned fibre composite in an autoclave and tensile testing 79

4.2.5 Fibre orientation determination 81

4.3 Results and discussion 82

4.3.1 Dry fibre mats compaction results 82

4.3.2 Self-compaction behaviour of aligned fibre mats 86

4.3.3 Glycerine washing methods results 87

4.3.4 Fibre orientation evaluation 90

4.3.5 Mechanical properties 91

4.4 Conclusion 97
References 98
5. Characterisation of through thickness permeability 99
5.1 Introduction 99
5.2 Methodology and materials 102
5.2.1 Design of permeability testing rig 102
5.2.2 Testing material 103
5.2.3 Permeability testing experimental design 104
5.2.4 Permeability prediction 105
5.2.5 Fan performance analytical model 106
5.3 Results and discussion 110
5.3.1 Effects of fibre orientation on fibre mat permeability 110
5.3.2 Aligned fibre mat permeability prediction 111
5.3.3 Fan selection and energy cost analytical model 114
5.4 Conclusion 117
References 118
6. Characterisation of dewatering behaviour 119
6.1 Introduction 119
6.2 Material and method 120
6.2.1 Vacuum plate dewatering test 120
6.2.2 Nylon mesh selection 122
6.3 Results and analysis 123
6.3.1 Slot vacuum plate dewatering behaviour 123
6.3.2 Perforated plate dewatering behaviour 125
6.3.3 Nylon mesh permeability and mats 127
6.4 Conclusion 130
7. Conclusions 132

7.1 Behaviour of fibre suspension jet and improvements in nozzle design 132
7.2 Characterisation of aligned mats and composites.....133
7.3 Through thickness permeability of aligned fibre mat.....133
7.4 Characterisation of dewatering behaviour.....134
7.5 Future research recommendations.....135
Appendix – publications.....137

1. Introduction

Thermoset composite materials have been widely used in industry, construction, automotive and aerospace areas due to their attractive and competitive mechanical properties. Figure 1.1 presents the development of global carbon fibre demand in tonnes [1]. From 2010 to 2015, it shows a 12.3% compound annual growth rate (CAGR). To estimate the further development in the global demand for carbon fibre, an annual growth rate (AGR) of 10% to 13% was applied. It is estimated that by 2022 global demand for carbon fibre may be as much as 191 thousand tonnes.

1.1 **Summary of Carbon Fibre Recycling Methods**

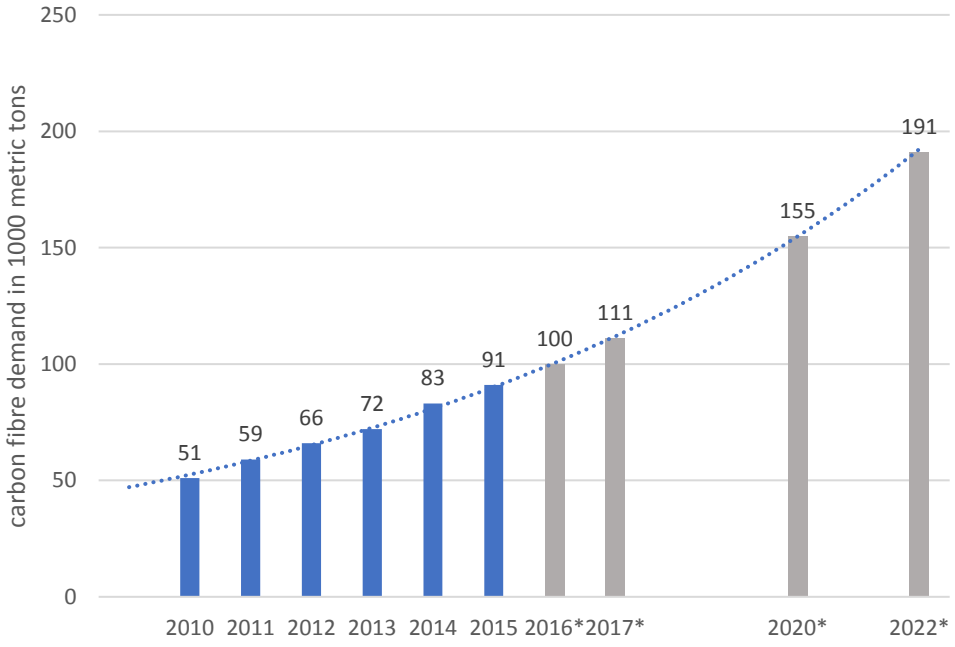


Figure 1.1 Global demand for Carbon Fibres in thousand tonnes from 2009 to 2022 (* estimates) [1]

The application distribution of carbon composites is described in Figure 1.2. Aerospace and automotive industries consume 52% of the total global carbon composites demand of 116,500 tonnes in 2015 [1]. However, since the increasing speed of the development of sustainable materials and resource,

the lack of recyclability has become one of the most important factors which will affect the material developing future.

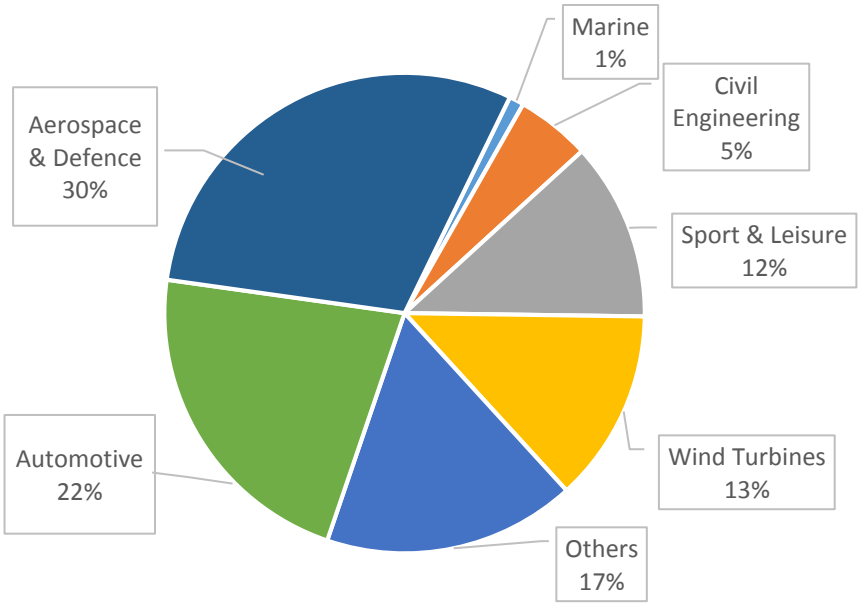


Figure 1.2 Carbon composites demand in 1,000t according to application (2015)

With the increasing needs of sustainable materials and stronger environmental legislations, several recycling technologies have been developed for composite materials in the past decades. The majority of research directed to the recycling of carbon fibre composites is concerned with thermoset composites as thermoset polymers cannot be melted down and remoulded. There are three main types of composite recycling: mechanical, thermal, and chemical methods.

1.1.1 Mechanical recycling process

The mechanical recycling process starts with the size reduction of large composite scrap by low-speed cutting or crushing (to 50–100 mm). Then it is further reduced to 10 mm to 50μm by using a hammer mill or other high-speed millings for fine grinding. Afterwards, the fine particles of the waste composites are classified with cyclones and sieves to fibre-rich (coarser) and

matrix-rich (finer) fractions [2]. This process requires the scrap material to be relatively clean and uncontaminated and from known origin [3]. Most of the mechanical treatment by crushing and milling is relatively straightforward, but it can be energy intensified and is only able to produce short milled fibres with poor mechanical properties which are used as a filler material.

1.1.2 Chemical recycling process

In the chemical recycling process, as its name suggests, chemical compounds, catalysts or solvents are applied. These chemicals will react with the resin of composites and remove it. A catalytic pyrolysis process has been developed by Adherent Technologies, Inc. which applied an aid of a catalyst to free individual carbon fibres from the matrix resin under 200°C. The fibres which are recovered from this process, with a 1% -17% reduction in tensile strength comparing with virgin fibre properties [3][7]. This process could take a relatively long time (can be hours with acids) in dissolving the resin with a conventional chemical such as acids. Although much time can be saved by using solvolysis, a lot of hazardous chemicals used in this process which makes researchers have more concerns about this process [4].

Most research into chemical recycling methods is aimed at supercritical fluids It was found that the use of an alkaline catalyst (e.g. KOH, potassium hydroxide) gives a resin elimination efficiency of over 90% in supercritical water, and the recovered carbon fibre has only 2–10% degradation in the mechanical strength [5]. In the case of supercritical alcohol, a resin elimination efficiency of 98% was reported at 350ºC, and the recovered carbon fibres retain 85–99% of the strength of the virgin fibres [6]. However, these recent tests were conducted on a small scale in the labs. Much more

research work is needed to scale-up the reactor system. Furthermore, the efficiency of the chemical dissolution process (solvolysis) depends on the type of the organic resin, and pre-separation of the types of composites is critical. Thus, the process could be applicable to the production scrap composites which have a clear description of characteristics but can be difficult to treat the post-consumer composite scrap which could be a mixture of various composites.

1.1.3 Thermal recycling process

The thermal recycling processes include the fluidised-bed combustion recycling process and the pyrolysis recycling process. In a pyrolysis recycling process, materials are recycled in an atmosphere without oxygen and often with nitrogen. Thus, the resin will be broken down in to lower molecular weight components and form char on the surface of the fibre. As a result, an extra oxidation step is needed to remove the residual char.

For another thermal recycling process – fluidised bed recycling, a bed of silica sand is used. The sand is fluidised by a stream of hot air at a temperature of 550ºC at a certain superficial velocity [3]. High temperature condition inside the bed burns off polymer resin and also oxidises char, which immediately liberate the fibres. The fibres are carried away from the hot bed by the outgoing stream of gases to a cyclone for fibre collection. The gases are finally sent to an after burner for complete decomposition before releasing to the atmosphere. The heat exchanger can be installed after the cyclone for potential energy recovery. However, compared with the virgin continuous fibres, the fibres recycled through the fluidised-bed process are individual short glass or carbon filaments in a low density fluffy form [2].

1.1.4 Reuse challenge of recycled carbon fibre

In most cases, the scrap being processed in thermal recycling process would be in a variety of physical forms, as shown in Figure 1.3, and so a short fibre product could be produced by either chopping the waste before processing or by chopping the carbon fibre recyclate after recycling. The recycled fibre products are in a fluffy form as there is no longer any size holding the fibres bundles together. Figure 1.4 shows the recycled carbon fibre from fluidized bed process, in which the carbon fibre is in the form of individual filaments with a distribution of fibre length.



Figure 1.3 End of life laminate scrap after primary size reduction (Left) and secondary size reduction (right)



Figure 1.4 Recycled fibre in raw form showing fluffy, discontinuous, 3D random and highly entangled structure with areas of higher fibre packing due to retained bundle integrity

For recycled fibre, having an economically viable conversion processes is pivotal for them to be established away from markets associated with a

perception of lower quality, such as being used as a filler in injection moulding, and to reach out to wider markets offering higher grade applications. Using milled recycled fibre in injection moulding is the earliest conversion process to enable the recycled fibre to be used in high volume basis. This application will have a long-term presence, but wider routes are required as the market will become saturated. Attention is focusing on seeking out established technology in which recycled fibre can be used directly, and the papermaking industry may be able to offer not only a process for direct use of recycled fibre but also an economically viable process for turning the fluffy fibre into a nonwoven form. Work is still ongoing to optimise the process and to establish markets for the nonwovens. Meanwhile, the recycling industry is continuing to develop new processes for higher value usage, and fibre alignment is considered one of the important conversion options as it not only offers higher fibre volume fractions to be achieved with lower moulding pressure, but it will also reduce high pressure fibre-to-fibre contact points and preserve fibre length for much needed structural application development.

1.2 **Project objectives**

A hydrodynamic alignment process has been developed in the University of Nottingham. And the aim of this thesis is to explore the factors which can affect the fibre alignment quality and optimize the process basing on the outcomes.

In the depositing process, a carefully designed nozzle shape is required to improve the aligned fibre orientation through the flow kinematics and maintain this aligned orientation with good jet stability. Furthermore, the

processing factors, such as fibre length, fibre volume concentration, dewatering vacuum level can affect fibre orientation on the fibre mat. Thus, fibre architecture is affected by the nozzle design and processing factors and this architecture determines the composites material properties and performance. However, the material properties of the fibre mat, such as fibre volume fraction and permeability will affect the dewatering rate and fibre orientation. The theme of this thesis is explained in Figure 1.5, and the objectives of the thesis can be listed as:

- Understand the fundamental behaviour of hydrodynamic process
- Indicate the main principal factors affecting the alignment quality in deposition process
- Determine the mechanical properties of aligned fibre products (mats and laminates) from the current process
- Measure and predict through thickness permeability of fibre mat
- Consider the energy consumption estimation of dewatering process

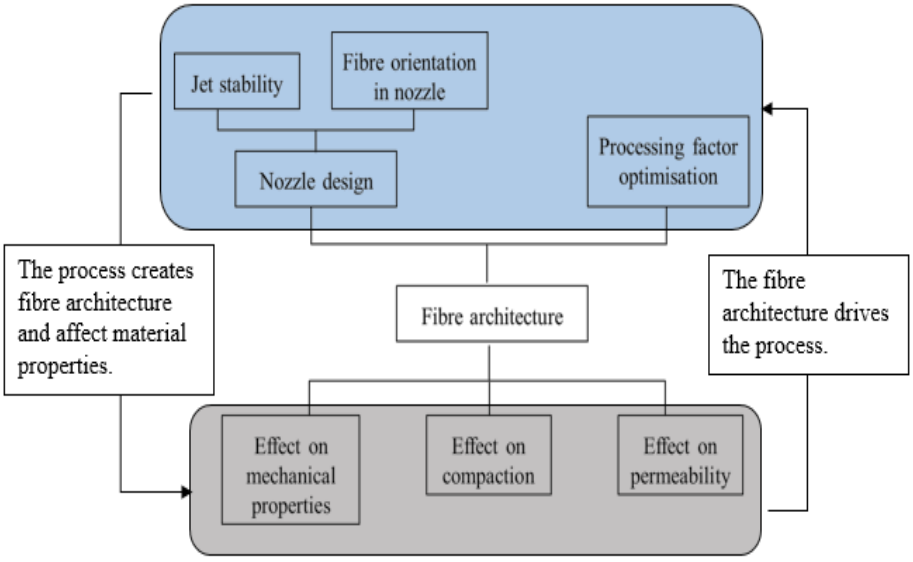


Figure 1.5 The theme of this work

Chapter 2 contains a literature review of the research work about the main objective area of this thesis. Chapter 3 studies the influences of fibre suspension jet stability and nozzle internal geometry on deposited fibre orientation. The stability of fibre suspension jet is not as expected in the previous research work in the hydrodynamic alignment process. In the present work, it is shown to display both a varicose and sinuous shape depending on the input parameters. These types of instability have been described in spray technology research work according to the liquid jet break-up regime. With an unstable jet, the aligned fibre orientation will be affected. Thus, understanding the factors influencing the fibre suspension jet break-up regime can help to maintain the jet stability and improve the aligned fibre orientation. Nozzle shape design is important in both spray technology and the paper making industry. In this thesis, CFD simulation is used to predict the velocity gradient profile inside different nozzles to explore the appropriate nozzle geometry which can help to achieve good fibre alignment inside the nozzle and provide an improvement in jet stability.

In Chapter 4 the capability of the rig was investigated with a 2-level full factorial experimental design to provide a better insight into the effect of operating conditions on alignment quality. The four factors under consideration were fibre length, fibre volume concentration in suspension, dewatering vacuum level, the relative speed between the rotating drum and the slurry deposition rate. Dry mat compaction testing [8] was used to evaluate the fibre volume fraction in aligned mats under different loading pressures, and these data were used as an output response to assess the effect of changes from the four input factors. The results of the test allowed the

determining of the best operating conditions for aligning recycled carbon fibre. Finally, tensile testing was used to evaluate the mechanical properties of aligned discontinued carbon fibre moulded laminates.

The through thickness permeability of aligned fibre mat is investigated with both an experimental and an analytical approach in Chapter 5. These permeability results can be applied in evaluating the required suction pressure in dewatering process for an aligned fibre mat with a target areal density. To maintain the suction pressure with a low energy cost, a pump selection and energy consumption analytical model is developed with the performance curves of liquid ring pump, high pressure radial blower and 2-stage channel blower. In Chapter 6, the best opening geometry for the deposition drum is identified to maintain the high pressure difference evenly distributed across the fibre. Vacuum plates are designed with four different open area geometry (3-slots, 5-slots, 21-slots and perforated plate) and dewatering testing is used to investigate their dewatering behaviour. Nylon mesh has been used as pressure distribution media and attached around the dewatering drum. Permeability testing is undertaken to explore the flow resistant capacity of nylon meshes with different lay-up configurations. Light aligned fibre mats are manufactured with these mesh configurations, in order to observe the effects on fibre alignment quality.

References

[1]. T. Kraus, M. Kuhnel, E. Witten, Global carbon fibre market report 2016, http://www.carboncomposites.eu/media/2449/market_report_2016_ccev-avk.pdf

[2]. Yongxiang Yang, Rob Boom, Brijan Irion, Derk-Jan van Heerden, Pieter Kuiper, Hans de Wit, Recycling of composite materials, Chemical Engineering and Processing 51(2012),53-68.

[3]. S.J. Pickering, Recycling technologies for thermoset composite materials-current status, Composites: Part A 37 (2006), 1206-1215

[4]. Chemical recycling of carbon fibre/epoxy composites in a mixed solution of peroxide hydrogen and N, N-dimethylformamide. Xu, P, Li, J and Ding, J. Ningbo: Elsevier, 2013, Composites Science and Technology, Vol. 82, pp. 54-59. 0266-3538.

[5]. R. Pi nero-Hernanz, C. Dodds, J. Hyde, J. García-Serna, M. Poliakoff, E. Lester, M.J. Cocero, S. Kingman, S. Pickering, K.H. Wong, Chemical recycling of carbon fibre reinforced composites in near critical and supercritical water, Composites: Part A (Applied Science and Manufacturing) 39 (2008) 454–461.

[6]. R. Pi nero-Hernanz, J. García-Serna, C. Dodds, J. Hydec, M. Poliakoff, M.J. Cocero, S. Kingman, S. Pickering, E. Lester, Chemical recycling of carbon fibre composites using alcohols under subcritical and supercritical conditions, Journal of Supercritical Fluids 46 (2008) 83–92.

[7]. Allred, R E, et al., et al. Tertiary recycling of cured composite aircraft parts. Dearborn : Society of Manufacturing Engineers, 1997.

[8]. Wong KH, The potential for fibre alignment on the manufacture of polymer composites from recycled carbon fibre. In: Proceedings of SAE international journal of Aero space, 2009. p. 225–31.

2. Literature review

A continuous carbon fibre tow inherently contains a close-packed structure and can readily be aligned according to loading requirement by conventional textile processing technologies. However, for short, fluffy recycled fibres, it is difficult to re-establish this close-packed structure with preferable reinforcement direction. Several approaches have been developed using different means to align discontinuous fibre. The diamagnetic anisotropic property of carbon fibre has been exploited under a magnetic field for alignment development, but this is limited to fibre length less than 500μm [1][2]. Electric fields have also been used for orientation control but generally for carbon nanotubes [3] or polymer fibres [4]. The traditional textile processes such as carding, combing and gilling have been applied in improving orientation for cotton yarn, which is generally long, tough and flexible. However, recycled carbon fibre is unsized, entangled and brittle; these intense mechanical aligning methods could damage the fibre itself. Thus, researchers started to investigate using hydrodynamic force to align the fibres. The Explosives Research and Development Establishment (ERDE), UK devised and developed three hydrodynamic alignment techniques based on extrusion [5], filtration [6] and centrifugal [7] processes in the 1970s. Based on the inspiration from the centrifugal process, a hydrodynamic process for aligning recycled carbon fibres has been developed at the University of Nottingham. The detailed features of these hydrodynamic fibre alignment processes will be described in the following subsections.

2.1 Hydrodynamic Alignment Process

2.1.1 ERDE process

The extrusion process was designed for aligning asbestos and silicon carbide whiskers in an ammonium alginate solution [5]. In the extrusion process (Figure 2.1_(a)), fibre suspension is extruded through a 2mm diameter orifice under low pressure and into an acid precipitating bath and immediately becomes gelled to maintain the aligned orientation. Then the gelled extrude is reeled up on a winding drum and is dried and cleaned afterwards. Then the residual alginic acid is burned off. The level of alignment was not presented, but high volume packing of up to 50% was reported. However, this process was deemed to be impractical and uneconomical as the ammonium alginate itself was not recyclable, and it required a lengthy combustion stage for complete removal of the alginic acid [6].

The filtration approach is the most widely published ERDE fibre alignment process, and it is composed of three stages: dispersion stage, alignment stage, and separation stage. In this process, fibres are dispersed and the suspension is pushed through a slit on a convergent head which repeatedly passes above a fine mesh to form an aligned fibre architecture. Vacuum suction also assists to promote draining of the dispersion medium. The fibre mat is then washed with a gentle water spray and a binder is applied. The degree of alignment attained from this process was good and more than 90% of the fibre population was within ±15° of the desired direction [8]. However, when the mat thickness increases, its through-thickness permeability would decreases, resulting in a longer dwell period to allow completion of glycerine drainage before the next deposition is applied and leading to an economically unacceptable production rate [9]. In addition, due to the reciprocating motion

of the convergent slit, a lower degree of alignment was seen at the end regions of the reciprocating path.

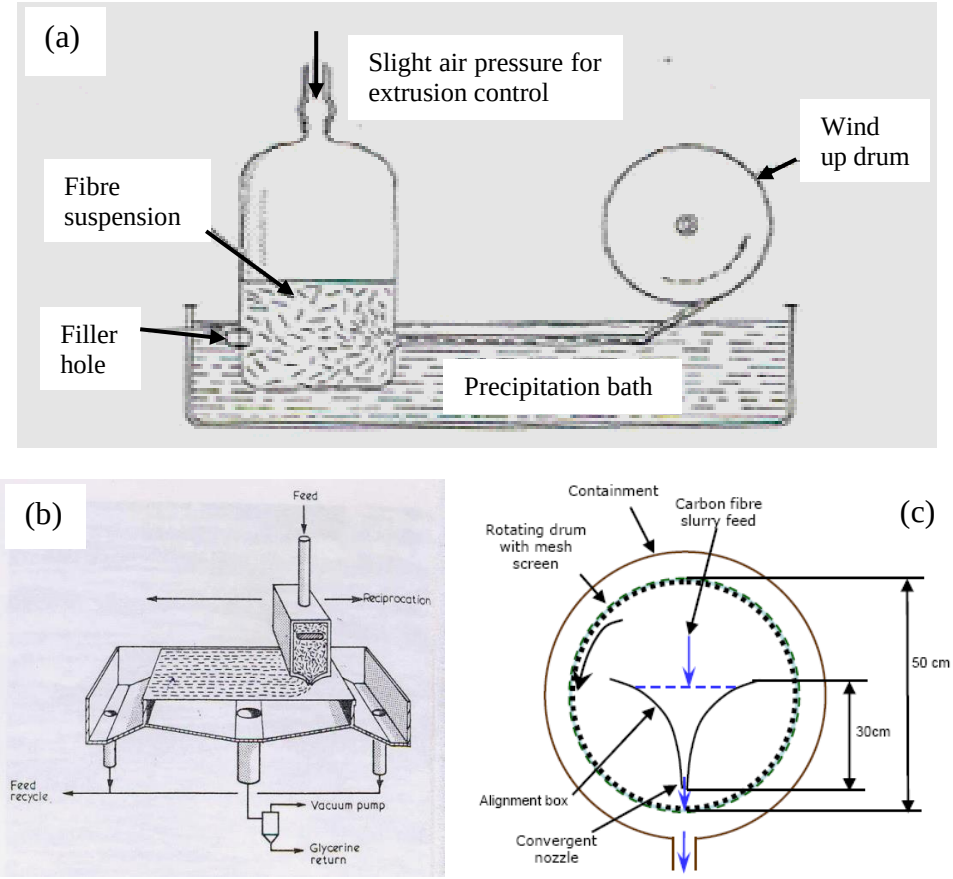


Figure 2.1 – ERDE processes: (a) Extrusion; (b) Filtration; (c) Centrifugal

In the centrifugal process, a series of circular converging nozzles was designed to instead of the slit. In addition, the conveying mesh was replaced with a rotating drum lined with a fine mesh. It was claimed that a better alignment was achieved with higher throughput rate [10].

Figure 2.2 shows the comparison of dry fibre mat compaction tests of the ERDE centrifugal and filtration processes. The data of UD fibre prepreg and random fibre mat were listed as the benchmark. Under the same compaction pressure, discontinuous fibre mats produced by the centrifugal process achieve the higher volume fraction compared to that of materials from the

filtration process. In other words, the products from centrifugal process show higher close-packed performance which is due to the better alignment quality. This is beneficial from using a circular nozzle which reduced the so-called edge effect arising from the oscillating motion of the convergent head [6].

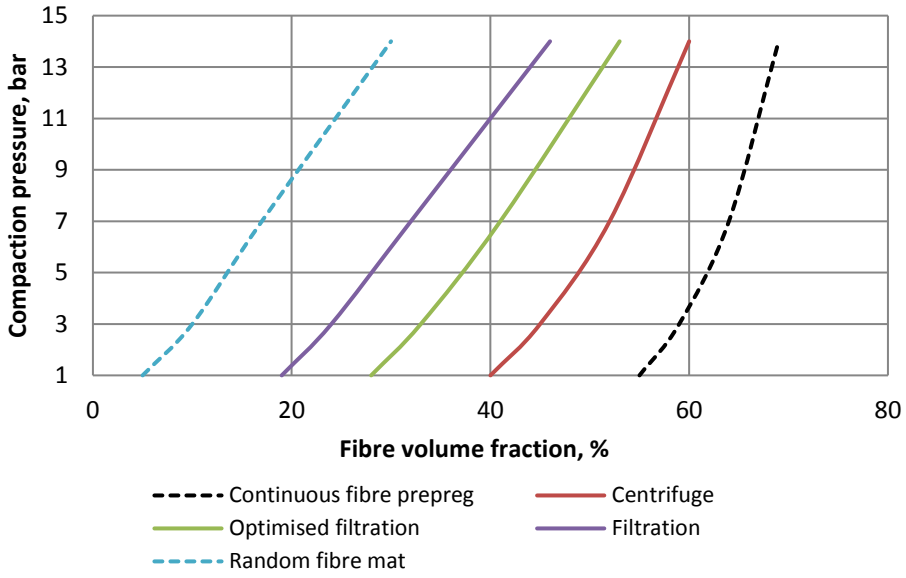


Figure 2.2 Comparison of various ERDE alignment processes with non-woven recycled fibre veil

2.1.2 Hydrodynamic alignment process for recycled carbon fibre

In the University of Nottingham, a bench-top centrifugal rig has been constructed according to the principles outlined in the ERDE work, a schematic diagram is presented in Figure 2.3. The discontinuous fibre was dispersed in glycerine to form a suspension. A good dispersion quality was obtained if there were no undispersed bundles in the bulk suspension and this could be achieved with the selection of short fibre length, low fibre loading and the presence of a high shear rate within the viscous medium. Air

entrapment should be kept to minimums fibres deviating around air bubbles that would affect the alignment quality.

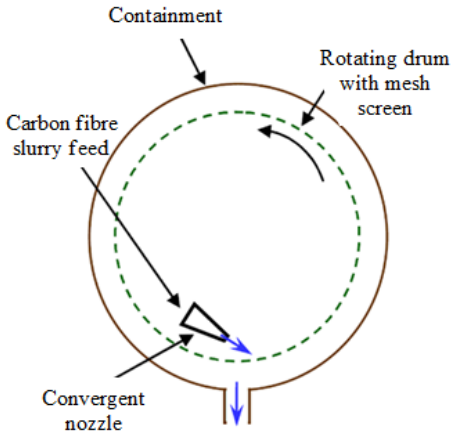


Figure 2.3 A schematic representation of the hydrodynamic alignment process

During the alignment process, the fibre dispersion is pumped into an intermediate holding tank which is pressurized to create a steady flow to a concentric conical nozzle that is located above a rotating drum. A nylon mesh positioned inside the drum is employed as a filter to separate the fibre from the dispersion medium. Vacuum suction is applied under the mesh to increase the liquid drainage rate, the mesh also serves as a pressure distribution medium. The nozzle is fixed to a linear actuator which continuously moves forward and backward to create a certain width of fibre mat. The filtered glycerine is pumped back to a storage tank for reuse. Once the target veil areal density has been met, the slurry deposition process is be halted. The mat is then washed with warm water to remove the remaining dispersion media, and an epoxy based binder is applied and post cured under 120° to maintain the aligned fibre orientation.

On the other hand, as the mat thickness increases, the alignment efficiency becomes lower due to the reduction in through-thickness permeability and the flooding flow damages the aligned fibre orientation. In order to maintain the alignment of the deposited fibres, the liquid medium has to be filtered out quickly, and measurement of through-thickness permeability can be used to calculate this removal speed.

2.2 Effect of fibre suspension jet stability on alignment quality of discontinuous carbon fibre mat

2.2.1 Liquid jet break up regime

Liquid jet research has been developed experimentally and theoretically for more than a century. Liquid jets are known to break up somewhere downstream of the nozzle because of the liquid surface tension and interfacial forces between the jet and the surrounding air. When a liquid jet is discharged into air, disturbances on the jet surface will be augmented because of the aerodynamic interactions between the jet and the surroundings. Growth of these disturbances causes the liquid column to disintegrate into droplets soon after discharge [11]. If the diameter of the droplets exceeds some critical size, they also tend to break into smaller droplets. These processes are referred to as primary and secondary breakups. When a water jet breaks up, its kinetic energy will be divided among many fine droplets and the jet loses efficient energy transfer, a pre-requisite in many applications (e.g. hydroentangling or waterjet cutting).

The most commonly accepted jet disintegration classification in fluid mechanics literature was developed by Ohnesorge [12] who combined the

Reynolds and Weber numbers and proposed a dimensionless Ohnesorge number Z (or Oh) [13].

$$Z = \frac{\mu_L}{\sqrt{\rho_L \sigma d_j}} = We_L^{0.5} Re_L^{-1} \qquad \text{Equation 2.1}$$

$$We_L = \frac{\rho_L V^2 d_j}{\sigma} \qquad \text{Equation 2.2}$$

$$Re_L = \frac{\rho_L V d_j}{\mu_L} \qquad \text{Equation 2.3}$$

Where, We_L is the Weber number of the liquid, Re_L is the Reynolds number of liquid, ρ_L is the density of the liquid, σ is the surface tension of the liquid, μ_L is the viscosity of liquid, V and d_j are the jet velocity and the liquid jet diameter at the nozzle exit. Based on Ohnesorge's work, Reitz suggested that there are four liquid jet breakup regimes which are presented in Figure 2.4 and Table 2.1[13] and Derby stated that the criterion for a drop to possess sufficient kinetic energy to be ejected from the nozzle is $We_{crit} \geqslant 4$ or $Re \leqslant 2/Z$ [14]. Therefore, a stable jet can be developed when $4 \leq We_L < 8$.

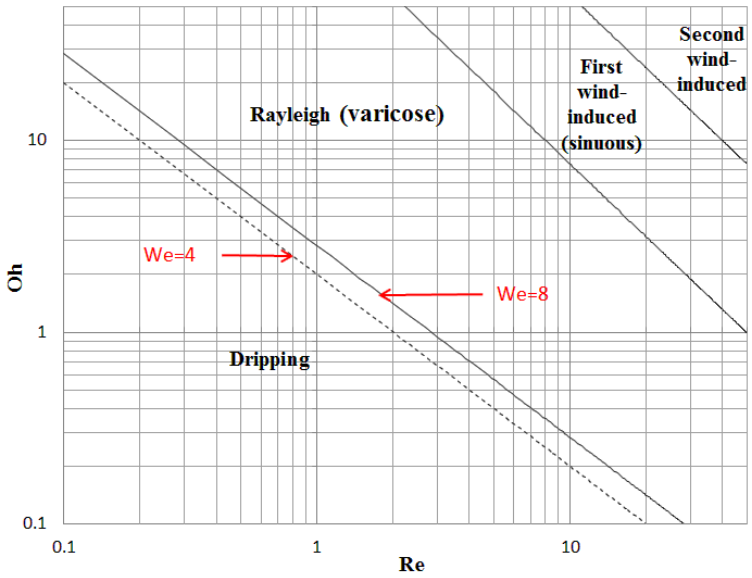


Figure 2.4 Classification of the modes of liquid jet disintegration [12]

The research work on jet stability have not considered the fibre suspension situation. However, the hydrodynamic interactions between the fibres may change the boundary conditions of liquid jet break-up regime. This will be evaluated by experiment in Chapter 3.

Table 2.1 Expressions for breakup regimes [13]

Regime	Range
Rayleigh (varicose)	$We_L \geqslant 8$ and $We_g < 0.4$
First wind-induced (sinuous)	$1.2+3.41Z0.9 < We_g < 13$
Second wind-induced	$13 < We_g < 40.3$
Atomization	$We_g > 40.3$

2.2.2 Influences of nozzle design on the jet stability behaviour

Figure 2.5 shows four jets in which the Weber number, Ohnesorge number, Reynolds number are approximately constant. However, the increasing nozzle aspect ratio from left to right causes these jets to display various break-up phenomena, though they are represented by the same point on Ohnesorge's graph [13].

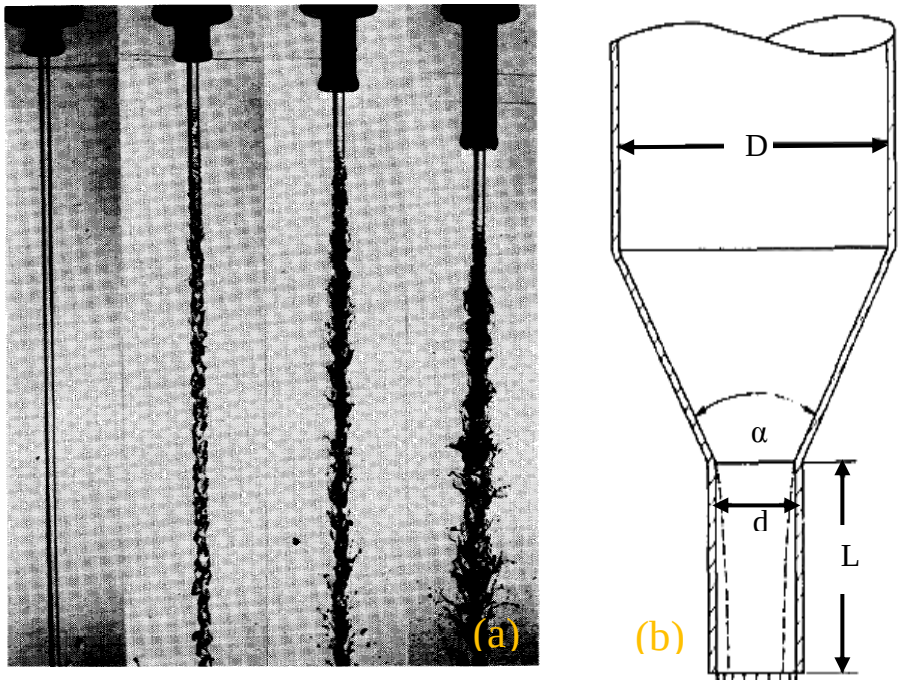


Figure 2.5 Different nozzle aspect ratios affect the stability of glycerol-water jets [15]. (a) Experimental work by Derby [15] validated that increasing the aspect ratio of nozzle will change the jet break up behaviour. (b) A description of nozzle geometry properties (nozzle contraction ratio = d/D, nozzle aspect ratio = L/d, contraction angle = α).

Researchers have tended to consider improving the jet stability through adjusting nozzle design. McCarthy and Molloy [15] investigated the characteristics of a wide range of liquid jets and presented expressions relating to their stability for conditions ranging from laminar to the fully turbulent flow regime. The main conclusions from this work defined the major requirement of a nozzle as being the efficient conversion of potential energy to kinetic energy which can be best achieved by a sudden, smooth contraction of the flow area from the supply line to the desired nozzle diameter; the nozzle aspect ratio L/d has a highly significant effect on the initial jet velocity profile and subsequent jet surface shape up to L/d values where the shear stress and static pressure gradient are fully developed. In fact, the variability of L/d offers a means of control of the jet surface roughness over a considerable range. Theobald [16] pointed out that a concave nozzle

featuring a sudden smooth contraction in flow area from the inlet to the outlet consistently produced the best jet in terms of stability. For straight-sided profiles, one which approached the axis at 30° formed the best all round jet of a series of profiles and can exhibit better stability than that of the fire hose nozzle designed by Rouse [17].

Although the jet generated from a concave nozzle presents the best stability behaviour, there is a lack of observation referring to the effects on fibre orientation. Thus, in the following section, reviews will focus on the influencing factors from nozzle design on fibre motions in suspension.

2.3 Fibre orientation in a jet of fibre – liquid suspension

2.3.1 Jeffery's orbit and orientation tensors

The best way to learn about fibre motion is first to analyse how a single fibre behaves in a flowing suspension. A fibre, immersed in a flowing fluid, is controlled by the local velocity gradients in the fluid. Under the velocity gradients, deformations of fluid elements, such as rotation and stretching, will occur. Even though a fibre will rotate with the deformation of the flow, the length of the fibre will not change. A disturbance field will form in a suspension around an immersed fibre. Within the area of disturbance, the motion of the fibre will be affected by the presence of another fibre or a wall. The fibre shape and the local rheological properties of the suspending fluid will affect the hydrodynamic force and torque of the fibre which determine the rotational and translational velocities of the fibre [18].

Initially, most of theoretical models were built to predict the motion of a single particle. However, the effect of interaction of rod-like fibres on the qualitative behaviour was observed and those theories mentioned above have a limitation in predicting the motion of multiple particles when interaction between particles is considered. Therefore, it is necessary to understand the mechanics of fibre-fibre interactions to be able to quantify this effect and investigate its impact on the structure of a flowing suspension. In general, fibre suspensions are classified into three concentration regimes, shown in Figure 2.6, according to the fibre volume fraction, ϕ_v, and fibre aspect ratio, r_f (length l versus diameter d).

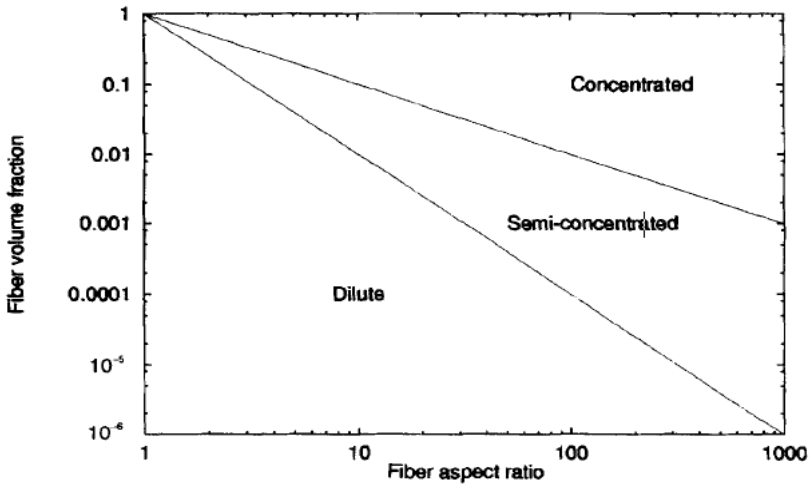


Figure 2.6 Classification of fibre suspensions [18]

In the dilute region, Jeffery's theory [19] can be used to model the fibre rotations, because the spacing between the fibres is greater than their length and the fibres can move and rotate freely, such that hydrodynamic interactions between the fibres are negligible. In semi-concentrated suspensions the spacing between the fibres is less than fibre length but greater than the diameters and hydrodynamic interactions can be felt. In the concentrated region (the spacing between fibres is of the order of fibre diameter), some

physical collisions between fibres, non-hydrodynamic effects, should be considered, as they have a significant influence on predicting the motion and rotation of the fibres. Therefore, the physics of the angular motion of particles in dilute and non-dilute (semi-concentrated regime plus concentrated regime) suspensions is vastly different.

Ignoring Brownian motion, Jeffery [19] described the rotation of a neutral ellipsoid in a Newtonian fluid by using a coordinate system shown in Figure 2.7. The origin is the centroid of the ellipsoid with a certain aspect ratio r_e, and vector p indicates the major axis of the ellipsoid. The two angular velocities of the ellipsoid in a simple shear flow $v_x = \dot{\gamma} y$ are given as follows:

$$\dot{\theta} = (\frac{r_e^2 - 1}{r_e^2 + 1}) \frac{\dot{\gamma}}{4} \sin 2\theta \sin 2\emptyset \qquad \text{Equation 2.4}$$

$$\dot{\emptyset} = \frac{-\dot{\gamma}}{r_e^2 + 1} (r_e^2 \sin^2 \emptyset + \cos^2 \emptyset) \qquad \text{Equation 2.5}$$

where $\dot{\gamma}$ is strain rate. From Figure 2.7, it can be noticed that $\dot{\emptyset}$ is maximum when the ellipsoid is vertical to the flow, while $\dot{\emptyset}$ is minimum when the ellipsoid is parallel to the flow. Therefore, the two equations above can be rewritten as:

$$\tan \emptyset = \frac{1}{r_e} \tan[\frac{-\dot{\gamma} t r_e}{r_e^2 + 1} + \tan^{-1}(r_e \tan \emptyset_0] \qquad \text{Equation 2.6}$$

$$\tan \theta = \frac{C r_e}{r_e^2 \sin^2 \emptyset + \cos^2 \emptyset} \qquad \text{Equation 2.7}$$

where C is orbit constant and $\emptyset_0$ is the value of $\emptyset$ at t=0. Furthermore, the period, T, of the orientation of the ellipsoid is derived and shown as follows:

$$T = \frac{2\pi}{\dot{\gamma}}\left(\frac{r_e^2 + 1}{r_e}\right) \qquad \text{Equation 2.8}$$

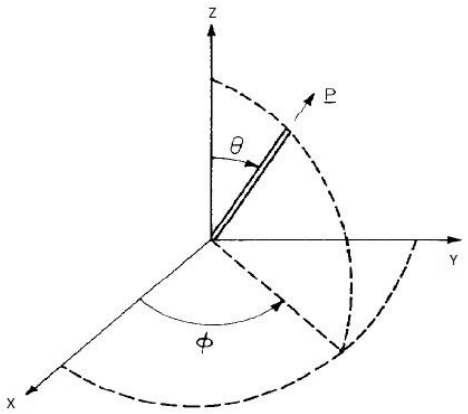


Figure 2.7 The coordinate system used in Jeffery's theory

After that, slender body theory was proposed by Burgers [20] to describe the rotation of particles with a large aspect ratio. Then by applying this theory, many researchers investigated the drag on a slender particle with different shapes in different flow types [21][22][23].

Apart from the investigation of single fibre motion, the movement and rotation of multiple fibres, which is a more practical situation, were also investigated [18]. Thence, a distribution function, ψ(θ,ϕ), was proposed. This function is developed to define the probability of finding a fiber between angles θ and θ + dθ and ∅ and ∅ + d∅ is given by ψ(θ,ϕ)sinθ dθ d∅. For this function, two physical conditions needed to be satisfied. One is that there is no distinction between two ends of a fibre. Another one is that all possible fibre orientations must equal unity. These two conditions can be presented by functions as follows:

$$\psi(\theta, \emptyset) = \psi(\pi - \theta, \emptyset + \pi) \qquad \text{Equation 2.9}$$

$$\int_0^{2\pi}\int_0^{\pi}\psi(\theta,\emptyset)\sin\theta\, d\theta d\emptyset = 1 \qquad \text{Equation 2.10}$$

However, the calculation for this distribution function is troublesome. For the convenience of calculation, orientation tensors are introduced. The second and fourth order tensors are a_{ij} and a_{ijkl} respectively and defined as:

$$a_{ij} = \langle p_i p_j \rangle \qquad \text{Equation 2.11}$$

$$a_{ijkl} = \langle p_i p_j p_k p_l \rangle \qquad \text{Equation 2.12}$$

Where, "< >" stands for:

$$< g >= \int_0^{2\pi}\int_0^{\pi} g\psi(\theta,\emptyset)\sin\theta\, d\theta d\emptyset \qquad \text{Equation 2.13}$$

Where **p** is a unit vector. In addition, fibre diffusion was considered and modelled. The following equation presents the angular velocity of a fibre.

$$\dot{\mathbf{p}} = -\frac{1}{2}(\omega\cdot\mathbf{p}) + \frac{1}{2}\lambda(\dot{\gamma}\cdot\mathbf{p} - \dot{\gamma}:\mathbf{ppp}) - Dr\frac{1}{\psi}\frac{\partial\psi}{\partial\mathbf{p}} \qquad \text{Equation 2.14}$$

Where, ω is the vorticity tensor, $\lambda = (r_e^2 - 1)/(r_e^2 + 1)$, $\dot{\gamma}$ is the rate of strain tensor. According to Folgar and Tucker [24], Dr, a diffusion coefficient which is used to model the effect of fibre-fibre interactions on their angular velocity and is defined as:

$$Dr = C_I[\dot{\gamma}] \qquad \text{Equation 2.15}$$

where $[\dot{\gamma}]$ is strain rate tensor and C_I is a dimensionless number, also known as the interaction coefficient which is used to model the effect of the suspension parameters on the strength of the interactions. For a given suspension, the C_I number is assumed as a constant which is independent od

the orientation state. It should be noticed that the equation above is only valid for dilute suspensions. Subsequently, Advani and Tucker [25] developed the model and the changes of the second and fourth orientation tensors (a_{ij} and a_{ijkl}) were expressed with some simplification to describe the orientation state of fibre suspension:

$$\frac{Da_{ij}}{Dt} = -\frac{1}{2}\left(\omega_{ik}a_{kj} - a_{ik}\omega_{kj}\right) + \frac{1}{2}\lambda\left(\dot{\gamma}_{ik}a_{kj} + a_{ik}\dot{\gamma}_{kj} - 2\dot{\gamma}_{ik}a_{ijkl}\right) + 2Dr(\delta_{ij} - \alpha a_{ij}) \quad \text{Equation 2.16}$$

$$\frac{Da_{ijkl}}{Dt} = -\left(\omega_{im}a_{mjkl} - a_{ijkm}\omega_{ml}\right) + \lambda\left(\dot{\gamma}_{im}a_{mjkl} + a_{ijkm}\dot{\gamma}_{ml} - 2\dot{\gamma}_{mn}a_{ijklmn}\right) + Dr[-\beta a_{ijkl} + 2\{a_{ij}\delta_{kl} + a_{ik}\delta_{jl} + a_{il}\delta_{jk} + a_{jk}\delta_{il} + a_{jl}\delta_{ik} + a_{kl}\delta_{ij}\}] \quad \text{Equation 2.17}$$

where δ is a unit vector in polar coordinates, α is 3 for three-dimensional orientation and is 2 for planar orientation, β is 20 for three-dimensional orientation and is 16 for planar orientation. From these two equations, there is a fourth order tensor in the former equation, and similarly there is a sixth order tensor in the latter one, indicating that the change of a tensor with certain order always has a higher order tensor component. Therefore, a closure approximation for the higher order tensor must be made. Hand [26] proposed a closure approximation for higher fourth and sixth order tensors, known as linear closure and shown as follows:

$$\widehat{a_{ijkl}} = -\frac{1}{35}\left(a_{ij}\delta_{kl} + a_{ik}\delta_{jl} + a_{il}\delta_{jk}\right) + \frac{1}{7}(a_{ij}\delta_{kl} + a_{ik}\delta_{jl} + a_{il}\delta_{jk} + a_{kl}\delta_{ij} + a_{jl}\delta_{ik} + a_{jk}\delta_{il}) \quad \text{Equation 2.18}$$

For planar orientation, the numerical factors are $-\frac{1}{24}$ and $\frac{1}{6}$.

$$\widehat{a_{ijklmn}} = \frac{1}{693}\left[\delta_{ij}\delta_{kl}\delta_{mn} + \delta_{ik}\delta_{jl}\delta_{mn} + \cdots (15\ terms)\right] - \frac{1}{99}\left[a_{ij}\delta_{kl}\delta_{mn} + \delta_{ij}a_{kl}\delta_{mn} + \cdots (45\ terms)\right] + \frac{1}{11}\left[a_{ijkl}\delta_{mn} + a_{ijmn}\delta_{kl} + \cdots (15\ terms)\right]$$

Equation 2.19

For planar orientation, the numerical factors are $\frac{1}{480}$, $-\frac{1}{80}$, and $\frac{1}{10}$.

Additionally, a quadratic and hybrid closure approximation were also used by other researchers. Advani and Tucker [25] made several comparisons among the three-closure approximation mentioned above and the exact value at different conditions: flow types and C_I, for example. Based on their results, the accuracy of an approximation is different under different conditions. Linear closure provides very good approximation for transient orientation in simple shear flow when C_I is 1.0, whilst it does not work well for transient orientation in simple shear flow when C_I is 0.01. In summary, linear closure performs well when fibres are at a random state, while quadratic closure works well if fibres are highly aligned in a suspension. In terms of hybrid closure, a combination between linear and quadratic closure, works well for the whole range of orientation.

As a summary, the fibre suspensions are classified into three concentration regimes according to the fibre volume fraction, ϕ_v, and fibre aspect ratio. Fibre suspension in different regimes has a different level of hydrodynamic interaction between fibres which can be an influencing factor of fibre suspension jet stability (Chapter 3). Orientation tensors are the most common methods that have been used to predict and describe fibre orientation is

suspension. Researchers in the paper making industry developed lots of models to predict the fibre orientation in a headbox, thus, the geometry of headboxes have been optimised. The literature stated here are used as background knowledge for the flowing sections.

2.3.2 Nozzle geometry effects

In injection moulding, researchers indicated that the fibre orientation is determined and affected by the flow kinematics [5][6]. For instance, in a simple shear flow (Figure 2.8_a), the fibres tend to align along the velocity gradient. The hydrodynamic force tends the fibres located near wall to rotate until they reach an equilibrium state and become fully aligned with the velocity field. However, for those fibres located around the flow symmetry plane, the velocity gradient will decrease which results a zero hydrodynamic force and an anisotropy fibre orientation.

In a converging channel (Figure 2.8_b), the elongational flow is generated due to the flow acceleration. In the near wall region, shear flow is dominant and the fibres tend to align in the flow direction. In the core region, the shear stress decreases and the flow is extensional flow dominated, thus the fibres are flowing along the flow direction.

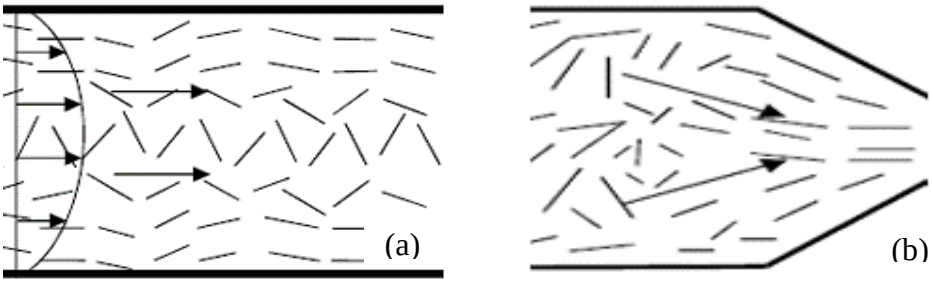


Figure 2.8 Schematic representation of (a) Simple shear and (b) Convergent flow and their influence on fibre orientation

The effect of nozzle geometry on fibre orientation has been extensively investigated in the paper manufacturing industry. Ullmar and Norman [27] investigated the geometry effect through using different contraction ratio (CR), defined as the ratio of nozzle inlet to outlet area. They concluded that, at high CR, fibres have better alignment along with the stream wise direction. Additionally, even though changing velocity of the flow induces different deviation of fibre orientation when CR is fixed, the effect is not much stronger than the effect induced by changing geometry of the nozzle.

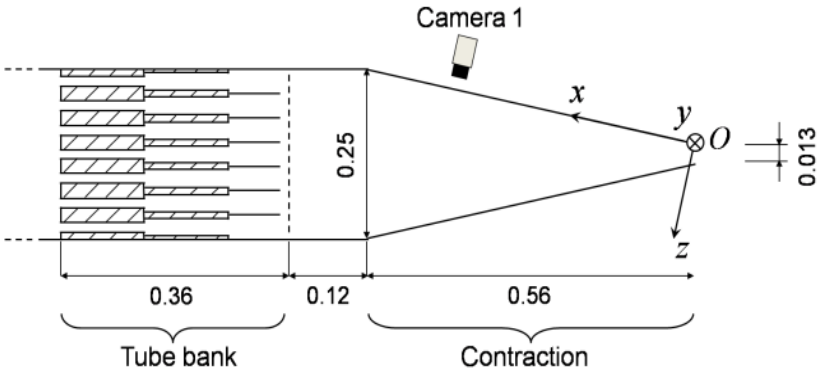


Figure 2.9 A typical structure of headbox [25] (the dimensions here are in m)

Carlsson and co-workers [28] carried out a meticulous investigation on fibre orientation near a headbox wall. As indicated in Figure 2.9, a coordinate system is set at the outlet orifice. The orientations of fibres at 15 positions on the x-z plane (3 positions on x axis and 5 positions on z axis) were recorded. Fibres preferentially align along the mean flow direction at positions near the wall, and the distribution of the fibres becomes more anisotropic along downstream direction. The authors reasoned that high shear rate and strong fluid inertial effects near the wall could be used to explain the results they observed. Based on Jeffery's theory, the authors believed that high shear rate

near the wall provided fast processing of fibre alignment along the direction parallel to the wall. In terms of inertial effect, it was expected that the fibre rotation period could be prolonged, and orientation drift towards the flow direction could also be introduced simultaneously. In addition, fibres do not tend to rotate any more once they are aligned with the wall. Many researchers found the relationship among fibre length, the fibre-wall gap and the effect near wall. Li and Ingber [29] stated that, when the fibre-wall distance is around five times less than the fibre length, the effect near wall can be observed. Whilst Bibbo et al. [30] provided an upper limitation of fibre-wall gap for the effect near wall. They concluded that the effect near wall is much less significant when the gap is approximately 1.2 times larger than the fibre length. Besides, according to Barta and Liron [31][32], the fibres having high aspect ratio (length to diameter) are easier to be influenced by the effect near wall, and if a fibre is not parallel or vertical to the wall, fibre migration occurs due to a component of force having different direction with flow movement.

Parsheh et al. [33] stated that inside the headbox acceleration of the flow makes the fibres align in the machine direction and turbulence tends to randomize the orientation. For nozzle design, the only significant effects on fibre orientation are under the assumption that the flow initial conditions at inlet are same for each case. Four contraction shapes were explored in Parsheh's [33] work, and each was characterized by constant mean rate of strain, linear rate of strain, quadratic rate of strain and the planar contraction with flat walls. The geometry of contraction shapes is shown in Figure 2.10, the nozzle length (L), inlet height (h_0), outlet height (h_{out}), inlet turbulent

intensity, fibre length (l) and inlet flow rate are all same for each case during the analysis.

To describe fibre orientation distribution, Advani and Tucker [25] showed that even-order tensors give a concise description of orientation distribution function. In Parsheh's study, the fourth order planar orientation tensor (Equation 2.18) is used to represent the orientation distribution function. The contraction with flat walls, which is widely used in industrial processes, has the worst fibre alignment at the outlet. However, the contraction with constant rate of strain gives the best fibre alignment at the nozzle exit.

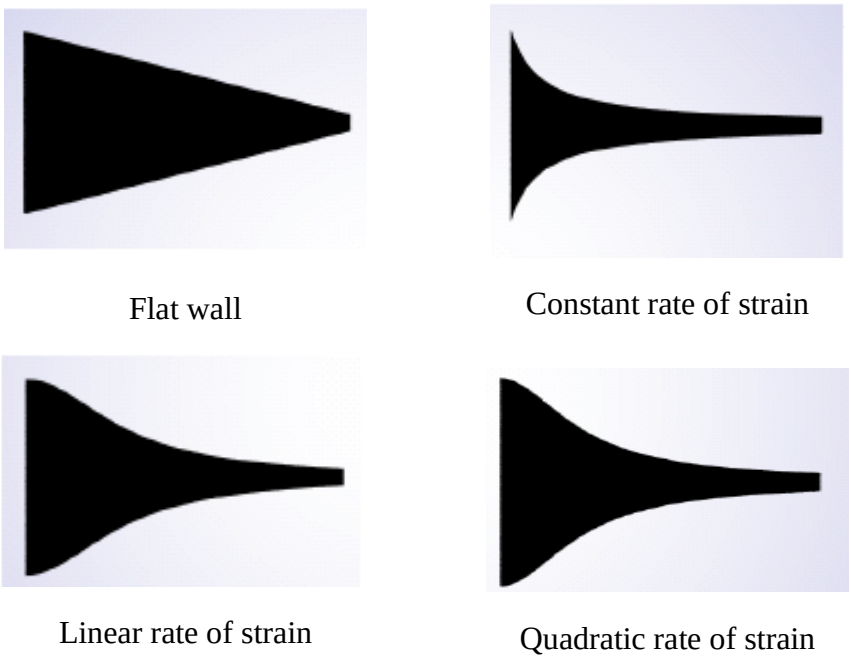


Figure 2.10 – Converging nozzle geometries

Although researchers have already undertaken lots of work on nozzle design for either improving jet stability or fibre alignment, there is still an absence of combination. In this thesis (chapter 3), the influencing from interaction in

fibre suspension on jet stability will be investigated. The optimal nozzle geometry which can improve the fibre alignment quality inside nozzle and maintain the orientation though good jet stability will explored.

2.4.1 Fibre length effects

For short fibre composite materials, the effect of fibre length on material properties has been explored by many researchers. At first, there are two definitions that need to be understood: The optimal length is the fibre length that can give the ultimate realizable performance of fibre in a composite [34][35][36], and the critical fibre length is defined as the minimum length at which the center of the fiber reaches the ultimate tensile strength, when the matrix achieves the maximum shear strength. If the fibre length is greater than the critical length, when it is under tension, tensile failure will occur rather than shear failure of the interface [37]. When the fibre length is smaller than the critical length, the fibre won't fail but the fibre will pull out of the matrix to let the crack extend [40].

It was mentioned by Jacob et al. [38] that when fibre length was reduced from 50mm to 25mm (but above the critical fibre length), the tensile strength and modulus became lower. The author pointed that the reason for this correlation could be the increased concentration of stress due to short fibres. Their study was carried out on composite plates manufactured from chopped carbon tows compression moulded with an epoxy system.

2.4.2 Volume fraction effects

It is commonly known that increasing the fibre volume fraction in composites results in improved mechanical performance. However, this rule may not be

applied on every situation. Reduction in material strength of continuous fibre composites, with increased volume fraction, has been associated with material porosity [43]. Thomason & Vlug [44] suggest that reduced modulus at high volume fractions could be related to fibre packing problems resulting in increased void content. Higher volume fractions may also require variations in the manufacturing process, e.g. increased injection pressure, which may have a significant effect on the properties of the final part [45]. Greater injection pressures can lead to movement of fibres within the mould. It should also be noted that, by adding relatively low proportions of fibre to the matrix, the composite may actually exhibit lower ultimate tensile strength than that of the matrix [46]. This is typically only seen at low volume fractions, where the addition of discontinuous fibres introduces stress concentrations at the ends.

2.4.3 Analytical models for determining mechanical properties of discontinuous fibre composites

2.4.3.1 Stiffness models

The rule of mixtures is the commonly used analytical method for estimating longitudinal stiffness in composites. It is derived by if both the fibre and matrix experience equal strain, a theory first proposed by Voigt [47]. The material is treated as if it were composed of parallel slabs of the two constituents bonded together [48]. The solution for a continuous fibre composite is stated as [49]:

$$E_c = V_f E_f + V_m E_m \qquad \text{Equation 2.20}$$

where E and V are Young's modulus and volume fraction; and the subscripts c, f, and m refer to the composite, fibres, and matrix.

Many modern analytical methods for determining stiffness in composites are based on the shear lag model, originally proposed by Cox [50], which accounts for the fibre aspect ratio. When the model is applied to resin-bonded fibrous materials, each fibre is embedded in a continuous solid medium of resin. Tensile stress transfer between the fibre and the matrix is assumed to take place through interfacial shear of the two components. The build-up of tensile stress in the fibre is determined by the distribution of the shear stress along its length [48]. The fibre axial stress is highest at the centre diminishing towards zero at the fibre ends, whereas the interfacial shear strength is maximum (negatively) at the fibre ends and falls to zero in the centre [51]. Consequently, the stiffness is related to the length and radius of the fibre,

$$E = \eta_l V_f E_f + (1-V_f)\, E_m \qquad \text{Equation 2.21}$$

$$\eta_l = \frac{1-\tanh(\frac{\varphi l}{2})}{(\frac{\varphi l}{2})} \qquad \text{Equation 2.22}$$

$$\varphi = \sqrt{\frac{2G_m}{E_f \ln(\frac{R}{r})}} \qquad \text{Equation 2.23}$$

It can be seen from the first of these equations that the rule of mixtures has been extended to account for the length of fibres using a length correction factor η_l. This is calculated using the length (l) and radius (r) of the fibre, the shear modulus of the matrix (Gm), and the fibre-packing factor (R). This model was extended by Krenchel [52] to account for the effect of fibre orientation. The Krenchel orientation factor is given by **Error! Reference source not found.**.

$$\eta o = \Sigma \alpha_i (\cos\theta_i)^4 \qquad \text{Equation 2.24}$$

Where α_i is the proportion of fibres directed in the orientation θi. For a two-dimensional random orientation of fibres, where an equal proportion of fibres are assumed to be directed in each orientation, the orientation factor evaluates to exactly 0.375. For the unidirectional fibre composite, the orientation factor is equal to 1.

Criticisms of shear-lag analysis have been related to how stress is transferred within a composite. Although the greatest shear stresses are located at the ends of the fibres, stress transfer across the fibre ends are neglected. Several authors have modified the shear-lag model to account for stress transfer across the fibre ends. Clyne [53] postulates that the fibre end stress σe is equal to the average of the peak fibre stress (neglecting fibre end stresses) and the remote matrix stress values predicted by the standard shear lag model:

$$\sigma_e = \frac{\varepsilon[E_f(1 - \operatorname{sech}(\varphi s)) + E_m]}{2} = \varepsilon E_m \qquad \text{Equation 2.25}$$

At the position x along the fibre, where 0 is the centre and ±½l are the fibre ends, the axial stress is given by

$$\sigma_f = \varepsilon[E_f - (E_f - E'_m)\cosh(\frac{\varphi x}{r})\operatorname{sech}(\varphi s)] \qquad \text{Equation 2.26}$$

For small aspect ratios ($\leqslant$10), the fibre end stress may be relatively large. The influence of axial stress across the fibre ends becomes very small as aspect ratio increases and the proportion of the fibre bearing the peak axial load becomes larger.

Starink and Syngellakis [54], who suggested a similar approach to Clyne but by considering the presence of fibre end stresses in the expression for peak fibre stress. Consequently, larger axial stresses are estimated at the fibre ends resulting in larger predictions for Young's modulus. Both models follow the

form of the shear-lag model in Eq. 2, but the length correction factor has been modified to give

$$\eta_l = 1 - \frac{(E_f - E'_m)\tanh(\varphi s)}{E_f \varphi s} \quad \text{Equation 2.27}$$

$$\eta_l = 1 - \left(\frac{1 - E_m/E_f}{2 - \operatorname{sech}(\varphi s)}\right)\left(\frac{\tanh(\varphi s)}{\varphi s}\right) \quad \text{Equation 2.28}$$

In the standard shear-lag model, there is also no consideration of stress transfer between touching fibres. The validity of the shear-lag model for random fibre networks has been examined by Räisänen et al. [55], who questioned whether the model applies to such networks. They argue that the dominant loading mode is the transfer of axial stress directly from one fibre to another at fibre crossovers. They also point out another common criticism of the shear lag model – the assumption that transverse stiffness is the same as that of matrix.

Despite these concerns, the shear lag approach continues to form the basis of many analytical models. The methods take the general Cox-Krenchel as:

$$E = \eta_l \eta_0 V_f E_f + (1 - V_f) E_m \quad \text{Equation 2.29}$$

In this thesis, the predicted tensile modulus of composite laminate is evaluated by the Equation 2.29 which was defined by Curtis et al. [38].

2.5 **Permeability measurement and prediction**

2.5.1 Darcy's law

Permeability is the ability of a porous material to be impregnated by a fluid. Darcy's law (Equation 2.30) is a commonly accepted rule for modelling fluid flow through porous media.

$$U_D = \frac{K}{\mu}\frac{\Delta P}{L}$$ Equation 2.30

Where, U_D = Volume-averaged superficial fluid velocity (m/s)

μ = Newtonian viscosity of the fluid (Pa·s)

K = Permeability tensor of the porous medium (m^2)

ΔP = Pressure drop through fibre mat (Pa)

L = Length of the sample in the microscopic flow direction (m)

This relationship is valid in the creep flow regime (Reynolds number $\leqslant$ 1). Darcy's assumptions are that the flow of fluid across the porous medium is fully saturated. In this equation, all the complicated interactions that take place between the fluid and the fibre preform structure is accounted for in K. Accurate permeability data is a critical requirement if such simulations are intended to be successfully used in the design and optimization of recycling processes. Currently, experimental measurement is the best method to determine the permeability tensor [60]. However, it has drawbacks as it requires a large number of carefully controlled experiments and has no predictive capability (i.e. each new material must be handled on a case by case basis). Thus, it is also desirable to have available analytical or computational tools for predicting permeability.

2.5.2 Analytical permeability prediction method

2.5.2.1 Kozeny-Carman equation

The earliest and most widely applied models in the composites area for predicting permeability are capillary models [61] (such as the Kozeny-Carman (KC) equation). The KC equation is applied in various fields such as ground water flow, water/oil reservoirs, chemical engineering, medicine,

biochemical and electrochemical engineering. For different media types, this equation can be modified as different forms. Based on a capillary model, it assumes that the porous media consists of tortuous capillary channels with varying cross-section. Furthermore, the flow obeys the properties of laminar flow. One of most popular modification of KC equation for fibre mat media is given by Choi et al. [62]:

$$K = \frac{r_f^2}{4C}\frac{(1-V_f)^3}{V_f^2} \qquad \text{Equation 2.31}$$

Where, K = Permeability tensor of the porous medium (m^2)

C = Kozeny constant

r_f = Fibre radius (m)

V_f = Fibre volume fraction

The Kozeny constant is an empirical constant derived from the comparison with the experimental data, it is strongly dependent on the flow direction, fibre volume fraction, and fibre packing structure [63]. As a result, it makes this model inadequate when predicting the permeability of some new materials which requires more physical data from measurement. There are several other theoretical models for predicting permeability in fibrous porous media. However, most of these methods show a satisfactory agreement at low fibre volume fractions, but fail at higher volume fractions which are of most interest in composite applications. This is because of that the interactions between fibres are not considered in these methods.

In later studies which were based on the structure of media and interactions between fibres, flow in idealized unit cell structures such as periodic arrays of cylinders or some other appropriate geometry is modelled. And as a result,

predicted permeability can be calculated. The most important requirement in formulating a model for predicting permeability in fibrous porous media is the scale analysis of media microstructure with all the relevant structural details [61].

2.5.2.2 Stokes equation and Gebart method

In general, analytical studies employ the Stokes equation for a specified domain with periodic boundary conditions [64]. Permeability can be calculated through the scale analysis of flow in the porous media. In the creeping regime, the scale velocity $\vec{V}$ is defined by Stokes equation [65]:

$$\vec{\nabla} \cdot \vec{V} = 0, \mu \nabla^2 \vec{V} = -\vec{\nabla} P \qquad \text{Equation 2.32}$$

Due to the limitations of the methods, the computational domain, which can state as building block of the pore structure, is in the form of a simplified, well-defined structure in which the grains of the porous medium are represented in the form of two dimensional obstacles, ordered sphere packing, or ordered packing of cylinders [64]. Detailed numerical simulations of flow in porous media are now feasible with the development of computing power and advanced numerical algorithms.

Recently, a geometric model which is used to predict the arrays of unidirectional aligned solid cylinders with circular cross-section was performed by Gebart [66]. Based on the Stokes equation, Gebart derived the permeability of an idealized unidirectional reinforcement consisting of regularly ordered, parallel fibres both for flow along and for flow perpendicular to the fibres. The solution for flow along fibres has the same

form as the Kozeny-Carman equation, while the solution for transverse flow has a different form as follows:

$$K = C(\sqrt{\frac{V_a'}{V_f}} - 1)^{2.5} R^2 \qquad \text{Equation 2.33}$$

Where, K = the transverse permeability

C = constant and only depends on the fibre arrangement (0.40 for quadratic or 0.23 for hexagonal arrangement)

R = the effective fibre radius

Using lubrication theory, an expression for the permeability as a function of solid spacing was performed which closely matches experimental results at high volume fractions.

Bruschke [67] introduced another predictive model for permeability of an idealized domain with regular array of cylinders. This model provides closed form relationships comprising two limiting solutions: a lubricating solution for low porosities and a cell method solution for high porosities.

The limitation of the Gebert and Bruschke models is that the physical model used to describe the system excludes the structural details of real materials. Virgin fibre products generally consist of tows or yarns, rather than of individual fibres. And the geometric arrangements of them are usually more complex than the one assumed in analytic models.

In this thesis, the through thickness permeability of aligned fibre mat will be evaluated. Due to the self-compaction behaviour, the permeability of fibre mat will change with the loading pressure. In the dewatering process, the suction pressure applied is below 0.8bar. As a result, the fibre volume fraction

of deposited mat is relatively low (below 20%). Thus, the KC equation can be applied to predict the through thickness permeability of aligned fibre mat. On the other hand, the geometrical structure of aligned fibre mat can neither be defined as 1D (unidirectional) nor 2D random. Thus, the analytical models for a specific microstructure may be not the optimal method in this thesis.

2.6 Summary of literature review

The fundamental working theories of different hydrodynamic alignment processes are introduced in Section 2.1. A bench-top alignment rig has been developed and it consist of three processes: dispersion, deposition and dewatering. This thesis focuses on understanding the behaviours of the last two. Section 2.2 stated that the Re number We number and Oh number are the variables used to define the liquid jet break up regimes. This gives the influencing factors which are needed to be investigated in determining the stability of fibre suspension jet. In addition, different kind of interactions in fibre suspension can be classified referring to the fibre suspension regime (Section 2.3). This could be another factor which can affect the stability of fibre suspension jet. After combing the influences of nozzle design on jet stability and fibre orientation (Section 2.2 and Section 2.3), the optimal nozzle geometry will be determined in this work. Section 2.5 described various factors (fibre length, fibre volume fraction and fibre orientation) can affect the performance of discontinuous fibre composites (DFC) and the analytical models used to predict the stiffness of DFC. However, all these theories are appropriate for discontinued virgin fibre composite. The analysis with recycled fibre composite will be stated in this work. For dewatering process, permeability of the deposited fibre mat is an important factor. The

permeability testing rig has been designed basing on the Darcy's law (Section 2.5). Furthermore, different permeability prediction approaches are introduced in Section 2.5. KC equation will be applied in the energy cost estimation model for the dewatering process.

References

[1]. Timbrell V 1972 J App Phys 43 4839-40.

[2]. Matthews M, Dresselhaus M, Dresselhaus G, Endo M, Nishimura Y, Hiraoka T and Tamaki N 1996 Appl Phys Let 69 430-2.

[3]. Park C, Wilkinson J, Banda S, Ounaies Z, Wise K, Sauti G, Lillehei P and Harrison J 2006 J Pol Sci Part B: Pol Phys 44 1751-62.

[4]. Seyam A, Cai Y, Wendisch B and Kim Y 2008 J Text Inst 99 375-83.

[5]. Parratt N 1968 GB 1128321

[6]. Bagg G, Dingle L, Jones R and Pryde A 1971 US 3617437

[7]. Bagg G, Cook J, Dingle L, Edwards H and Ziebland H 1977 US4016031

[8]. Kacir L, Narkis N and Ishai O 1975 Polym Eng Sci 15 525-31.

[9]. Edwards H and Evans N 1980 Econ Comput Econ Cyb 2 1620-35.

[10]. Salariya A and Pittman J 1980 Polym Eng Sci 20 787-97

[11]. Lefebvre AH (1989) Atomization and sprays. Hemisphere Publishing Corporation, New York

[12]. Ohnesorge W 1936 ZAMM – J Appl Math Mech 16 355-8

[13]. Reitz R and Bracco F 1986 Encyclopedia of Fluid Mechanics: Gas Fluid Flows 233-49

[14]. Derby B 2010 Annu Rev Mater Res 40 395-414

[15]. M. J. McCarthy, Ph.D. Thesis, Univ. of Newcastle, N.S.W., Australia, 1972.

[16]. C. Theobald, The effect of Nozzle design on the stability and performance of turbulent water jets, Fire Safety Journal, Volume 4, Issue 1, 1981, Pages 1-13, ISSN 0379-7112

[17]. H. Rouse et al., Experimental investigation of fire monitors and nozzles, Trans. Am. Soc. Civ. Eng., 117 (1952) 1147

[18]. S. Ranganathan and S.G. Advani, Fiber-fiber and fiber wall interactions during the flow of non-dilute suspensions, Journal of Rheology 35(8):1499-1522, November 1991

[19]. G.B. Jeffery, The motion of ellipsoidal particles immersed in a viscous fluid, Proc. R. Soc. London, Ser A., 102:161, 1923

[20]. J.M. Burgers, Second report on viscosity and plasticity, Technical Report, North Holland, Amsterdam, 1938

[21]. E.O. Tuck, Some methods for flows past blunt slender bodies, J. Fluid Mech., 18:619, 1964

[22]. J.P.K Tillett, Axial and transverse stokes flow past slender axisymmetric bodies, J. Fluid Mech., 44:401, 1970

[23]. R.G. Cox, The motion of long slender bodies in a viscous fluid, Part I General theory, J. Fluid Mech., 44:791, 1970

[24]. F.P. Folgar and C.L. Tucker, Orientation behaviour of fibers in concentrated suspensions, J. Reinforced Plastics Compos., 3:98, 1984

[25]. S.G. Advani and C.L. Tucker, The use of tensors to describe and predict fiber orientation in short fiber composites. J. Rheol., 31:751, 1987

[26]. G.L. Hand, A theory of anisotropic fluids, J. Fluid Mech., 13:33, 1962

[27]. M. Ullmar and B. Norman, Observation of fiber orientation in a headbox nozzle at low consistency, Engineering & Papermakers Conference, 865-874, 1997

[28]. A. Carlsson, L.D. Soderberg, and F. Lundell, Fibre orientation measurements near a headbox wall, Nordic Pulp and Paper Research Journal vol.25 no.2, 2010

[29]. J. Li and M.S. Ingber, A boundary element study of the motion of rigid particles in internal Stokes flow, In Boundary Elements XIII, eds. C. A. Brebbia and G.S. Gibson, page 149, Elsevier Applied Science, 1991

[30]. M.A. Bibbo, S.M. Dinh and R.C. Armstrong, Shear flow properties of semiconcentrated fiber suspensions, J. Rheol., 29(6):905, 1985

[31]. E. Barta and N. Liron, Slender body interactions for low Reynold's numbers Part 1 Body-wall interactions, SIAM J. Appl. Math., 48(5):992, 1988

[32]. E. Barta and N. Liron, Slender body interactions for low Reynold's numbers Part 2 Body-wall interactions, SIAM J. Appl. Math., 48(6):1262, 1988

[33]. M. Parsheh a, M.L. Brown b, C.K. Aidun c, Variation of fibre orientation in turbulent flow inside a planar contraction with different shapes, International Journal of Multiphase Flow 32 (2006) 1354–1369.

[34]. Harper, L.T., et al., Characterisation of random carbon fibre composites from a directed fibre preforming process: The effect of fibre length. Composites Part A: Applied Science and Manufacturing, 2006. 37(11): p. 1863-1878.

[35]. Kaverov, A.T., M.E. Kazakov, and V.Y. Varshavsky, Carbon Fibres, in Fibre science and technology, V.I. Kostikov, Editor. 1995, Springer.

[36]. Tucker, I.C.L. and E. Liang, Stiffness predictions for unidirectional short-fiber composites: Review and evaluation. Composites Science and Technology, 1999. 59: p. 655-671.

[37]. Matthews, F.L. and R.D. Rawlings, Composite Materials: Engineering and Science. 1st edition ed. 1999: Woodhead Publishing.

[38]. Jacob, G.C., et al., Effect of fiber volume fraction, fiber length and fiber tow size on the energy absorption of chopped carbon fiber-polymer composites. Polymer Composites, 2005. 26(3): p. 293-305.

[39]. Hithcen, S., S. Ogin, and P. Smith, Mechanical Properties and Notch Sensitivity of Short Carbon Fibre-Epoxy Composites, in Developments in the science and technology of composite materials: 6th European Conference on Composite Materials, September 20-24, B.A. R, K. A, and M. A, Editors. 1993, Woodhead Publishing: Bordeaux, France.

[40]. Cottrell, A.H., Strong Solids. Proceedings of the Royal Society of London. Series A. Mathematical and Physical Sciences, 1964. 282(1388): p. 2-9.

[41]. Allred, R.E. and D.M. Schuster, The impact toughness of discontinuous boron-reinforced epoxy composites. Journal of Materials Science, 1973. 8(2): p. 245-250.

[42]. Salkind, J., Application of Composite Materials. 1973: American Society for Testing & Materials.

[43]. Vasiliev, V.V. and E.V. Morozov, Mechanics and Analysis of Composite Materials. 2007, Oxford: Elsevier.

[44]. Thomason, J.L. and M.A. Vlug, Influence of fibre length and concentration on the properties of glass fibre-reinforced polypropylene: 1. Tensile and flexural modulus. Composites Part A: Applied Science and Manufacturing, 1996. 27(6): p. 477-484.

[45]. Olivero, K.A., et al., Effect of Preform Thickness and Volume Fraction on Injection Pressure and Mechanical Properties of Resin Transfer Molded Composites. Journal of Composite Materials, 2004. 38(11): p. 937-957.

[46]. Kaw, A.K., Mechanics of composite materials. 2nd edition ed. 2006: CRS Press.

[47]. Voigt, W., Theortische student uberdie elasticitats verhalinisse krystalle. Abh Ges Wiss Goetting, 1887. 34.

[48]. Hull, D. and T.W. Clyne, An Introduction to Composite Materials. Cambridge Solid State Science Series. 1996: Cambridge University Press.

[49]. Gay, D.G., Composite Materials: Design and Applications. 2003: CRC Press.

[50]. Cox, H.L., The elasticity and strength of paper and other fibrous materials. British Journal of Applied Physics, 1952(3): p. 72.

[51]. Kim, J.K. and Y.W. Mai, Engineered Interfaces in Fiber Reinforced Composites. 1998: Elsevier Science.

[52]. Krenchel, H., Fibre reinforcement: theoretical and practical investigations of the elasticity and strength of fibre-reinforced materials. 1964: Akademisk forlag.

[53]. Clyne, T.W., A simple development of the shear lag theory appropriate for composites with a relatively small modulus mismatch. Materials Science and Engineering: A, 1989. 122(2): p. 183-192.

[54]. Starink, M.J. and S. Syngellakis, Shear lag models for discontinuous composites: fibre end stresses and weak interface layers. Materials Science and Engineering: A, 1999. 270(2): p. 270-277.

[55]. Räisänen, V., et al., Does the shear-lag model apply to random fiber networks. J. Mater. Res, 1997. 12(10): p. 2725.

[56]. Zak, G., et al., Mechanical properties of short-fibre layered composites: prediction and experiment. Rapid Prototyping Journal, 2000. 6(2): p. 107-118.

[57]. Kelly, A. and W.R. Tyson, Tensile properties of fibre-reinforced metals: Copper/tungsten and copper/molybdenum. Journal of the Mechanics and Physics of Solids, 1965. 13(6): p. 329-350.

[58]. O'Gara, J.F., G.E. Novak, and M.G. Wyzgoski, Predicting the tensile strength of short glass fiber reinforced injection molded plastics. 2010.

[59]. Bader, M.G. and W.H. Bowyer, The mechanical properties of thermoplastics strengthened by short discontinuous fibres. Journal of Physics D: Applied Physics, 1972. 5(12): p. 2215.

[60]. Parnas, R. S. and Salem, A. Polym. Composite. 1993, 14 (5) 383

[61]. Schlichting, H. Boundary layer theory, 7th Edn. McGraw Hill. New York, 1979, Chapt 2.

[62]. M.A. Choi, M.H. Lee, J. Chang, and S.J. Lee, J. Non-Newtonian. Fluid. Mech., 79(2), 585, (1998).

[63]. Frederick R. Phelan Jr and Geoff Wiset, Analysis of transverse flow in aligned fibrous porous media, Composites Part A 27A (1996) 25-34.

[64]. Aydin Nabovati a, Edward W. Llewellin, Antonio C.M. Sousa, A general model for the permeability of fibrous porous media based on fluid flow simulations using the lattice Boltzmann method, Composites Part A 40 (2009), 860–869.

[65]. Ali Tamayol, Majid Bahrami, Transverse permeability of fibrous porous media, Physical review e 83, 046314 (2011).

[66]. B.R. Gebart, J. Compos. Mater., 26(8), 1100, (1992).

[67]. Buschke M.V., A predictive model for permeability and non-isothermal flow of viscous and fluids in anisotropic fibrous media, PhD thesis, University of Delaware, Newark, (1992).

3. Characterisation of liquid jets and nozzle design

3.1 Introduction

Significant amounts of research have been done by researchers in the paper making industry to predict and control fibre orientation in a contracting channel. However, much less attention has been paid to the influence of the stability of fibre suspension jets on fibre orientation distributions. It has been found through careful observation of the fibre suspension jet that an unstable jet (Figure 3.1 a) which splashes during deposition process will reduce fibre alignment. A varicose jet and air bubbles (Figure 3.1– b, c) can also misalign fibres. Therefore, a good jet quality is required to maintain the pre-aligned fibre orientation.

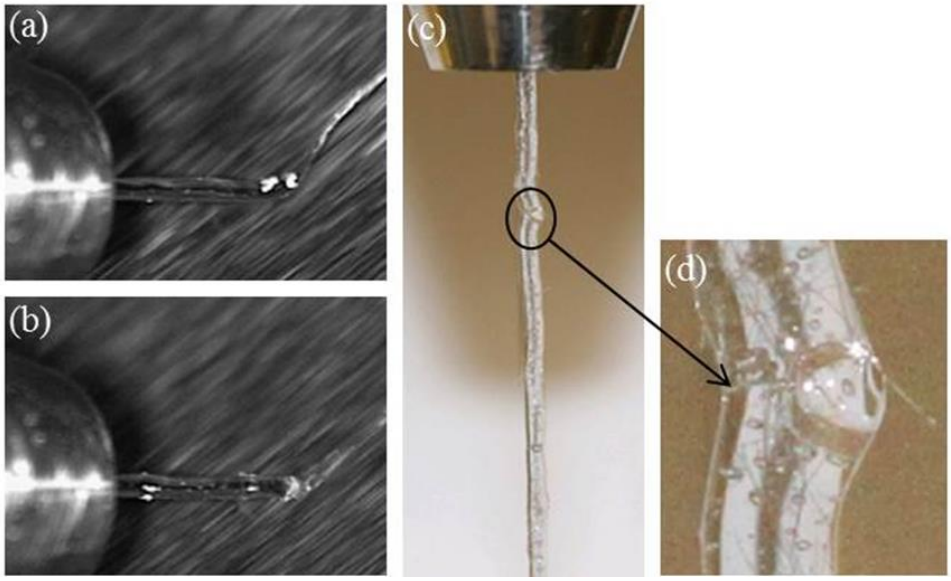


Figure 3.1 Photos of unsatisfactory fibre suspension jets – (a) unstable bouncing jet is depositing on the fibre mat which leads to an uncontrollable fibre orientation; (b) varicose jet shape may make a splashing on the mat which will damage the fibre orientation; (c) jet containing air bubbles; (d) air bubbles damage the smooth jet surface and fibres protrude at the air bubble.

As a two-phase flow, the fibre suspension jet's breakup regime is likely to be different to the pure liquid jet's phenomenon. Figure 3.2 shows that the fibre–liquid interaction and fibre–fibre interaction gives jets various types of instability although the Weber numbers are the same. The property of a fibre suspension is always described by fibre length, the viscosity of dispersion media and fibre volume concentration and these factors will affect the design of fibre suspension jet's stability test.

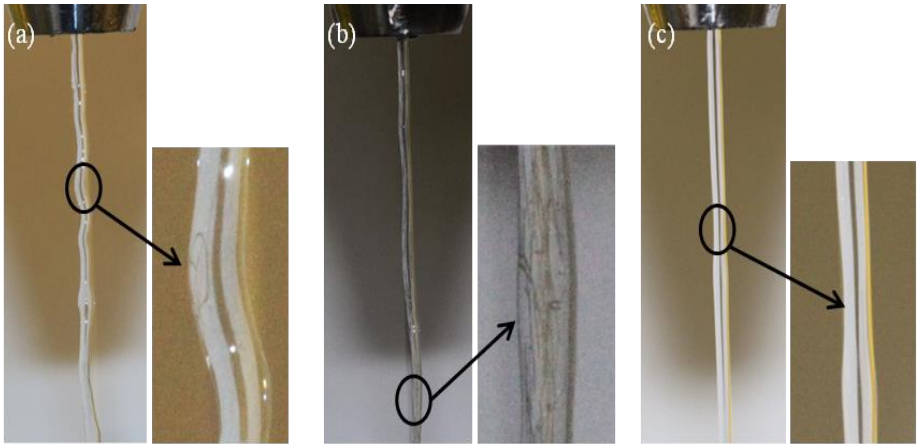


Figure 3.2 Images of fibre suspension jets and glycerine/water jets all at the same Weber number: (a) 12mm length fibre_0.05% volume fibre concentration jet – the fibre becomes disturbed in the wavy jet; (b) 3mm length_0.15% volume fibre concentration - fibre suspension jet and fibres are aligned with flow direction; (c) glycerine/water solution jet behaves slightly varicose.

Although researchers have already undertaken lots of work on nozzle design for either improving jet stability or fibre alignment, there is still an absence work on the combination of these effects. Experimental work with platen nozzles will therefore be used to validate whether the convex nozzle offers the best alignment quality compared to a straight sided nozzle and large aspect ratio straight sided nozzle. Furthermore, the fibre alignment performance of a concave nozzle will be explored in this chapter, and CFD simulated shear rate profile is involved in describing the reason for good stability behaviour of the concave nozzle.

3.2 Materials and methods

3.2.1 Jet stability test

A Stability test of a glycerine/water solution jet has been undertaken to validate the liquid jet breakup regime. Oleon Glycerine 4810 with glycerol content ⩾99.5% was supplied by Univar UK. The glycerine was diluted with different percentage weights of tap water to achieve various viscosities. A

Brookfield LVDVII viscometer was used to measure the viscosity, and the temperature was also noted. The properties of the jet tested are listed in Table 3.1. The glycerine/water solution was fed into a pressure pot which has a convergent nozzle attached at the bottom (Figure 3.3). By adjusting pressure level, the liquid jet was generated with different velocities and exhibited various jet break-up regimes. For each test, 50 jet images were captured continuously by a camera to record the jet motion.

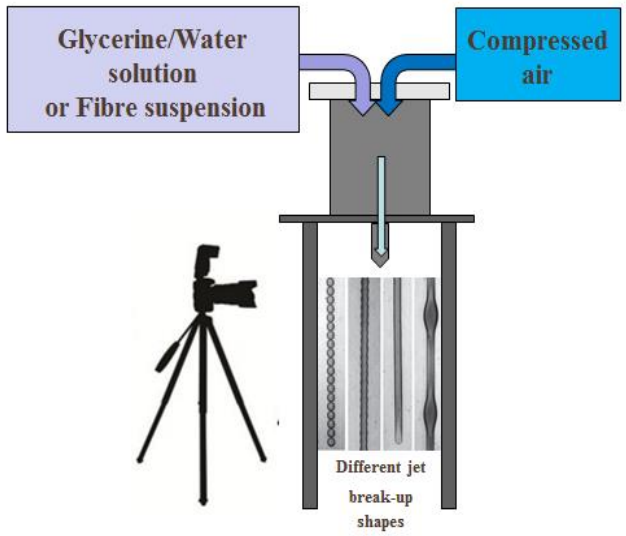


Figure 3.3 The experimental settings of jet break-up regimes test

Table 3.1 The calculated properties of glycerine/water solution in pure liquid jet test

Glyc. % Wt.	Viscosity	Temperature	Glyc./Water Solution Density
%	mPa·s	°C	kg/m^3
97.1	1250	15.9	1258.8
96.8	830	19.9	1255.4
94.4	560	17.6	1246.7
86.1	185	14.7	1221.7

Table 3.2 Fibre suspension properties

Fibre length	Fibre volume concentration	Viscosity	T*	$\frac{1}{\text{Fibre aspect ratio}}$	Fibre suspension concentration regime
mm	%	mPa·s	°C	/	/
3	0.05	2450	4.5	0.0023	Semi-concentrated
	0.1	350	43.5	0.0023	Semi-concentrated
		1350	21.8		
		2445	6.5		
12	0.05	1550	20.2	0.00058	Semi-concentrated
		380	43.5		
		2355	4.5		
		1585	20.8		

T* – Temperature

For the fibre suspension jet stability tests, glycerine/water solution was used as dispersion media. Tenax®-A HT C124 carbon fibre strips coated with a water-soluble sizing, was supplied by Toho Tenax Europe GmbH. The fibre lengths were 3 mm and 12 mm. The fibre volume concentrations are listed in Table 3.2. The viscosities of the suspension were controlled by changing the temperature rather than the weight percentage of water in suspension, as changing the water content will lead to an effect on fibre concentration. The Brookfield LVDVII viscometer was used to measure the viscosity of fibre suspension. The stability test of fibre suspension jet followed the pure liquid jet testing procedure as described before. Furthermore, three aligned fibre

mats were made with jets in the different breakup regimes (We_L<4 – dripping jet, We_L=6 – stable jet and We_L=10 – varicose jet) to validate the influence of suspension jet stability on fibre alignment quality.

3.2.2 The effects of nozzle geometries on fibre alignment

The profiles of the nozzles examined are shown diagrammatically in Figure 3.4 as they fall into two groups, the first consisting of straight-sided profiles with different nozzle aspect ratios. The second group of curved nozzles consisted of a venturi-shaped nozzle [1] and a prototype concave profile based on modified design criteria for wind tunnel applications [2]. All these nozzles have a 70mm inlet and 10mm outlet which means they had been designed with the same contraction ratio. The nozzle shapes were made by waterjet cutting, and then the thin flat nozzle was sandwiched between a machined 1mm thick aluminium plate (incorporating the inlet) and a clear acrylic window to allow observation of the internal behaviour of the nozzle. The pressure pot was filled with 3mm Tenax®-A HT C124 fibre suspension which has a 0.1% fibre volume concentration. Then constant pressure was supplied, and the suspension flowed through a pipe which is attached at the bottom of the platen nozzle. A camera was set above the nozzle and parallel to the top surface. Thus, fibre motion in the contraction region and near the nozzle exit can be observed and recorded. At the same time Ansys Fluent Computational Fluid Dynamics software (CFD Fluent) was used to create a 2-D simulation to explore the flow kinetics performances inside these nozzles.

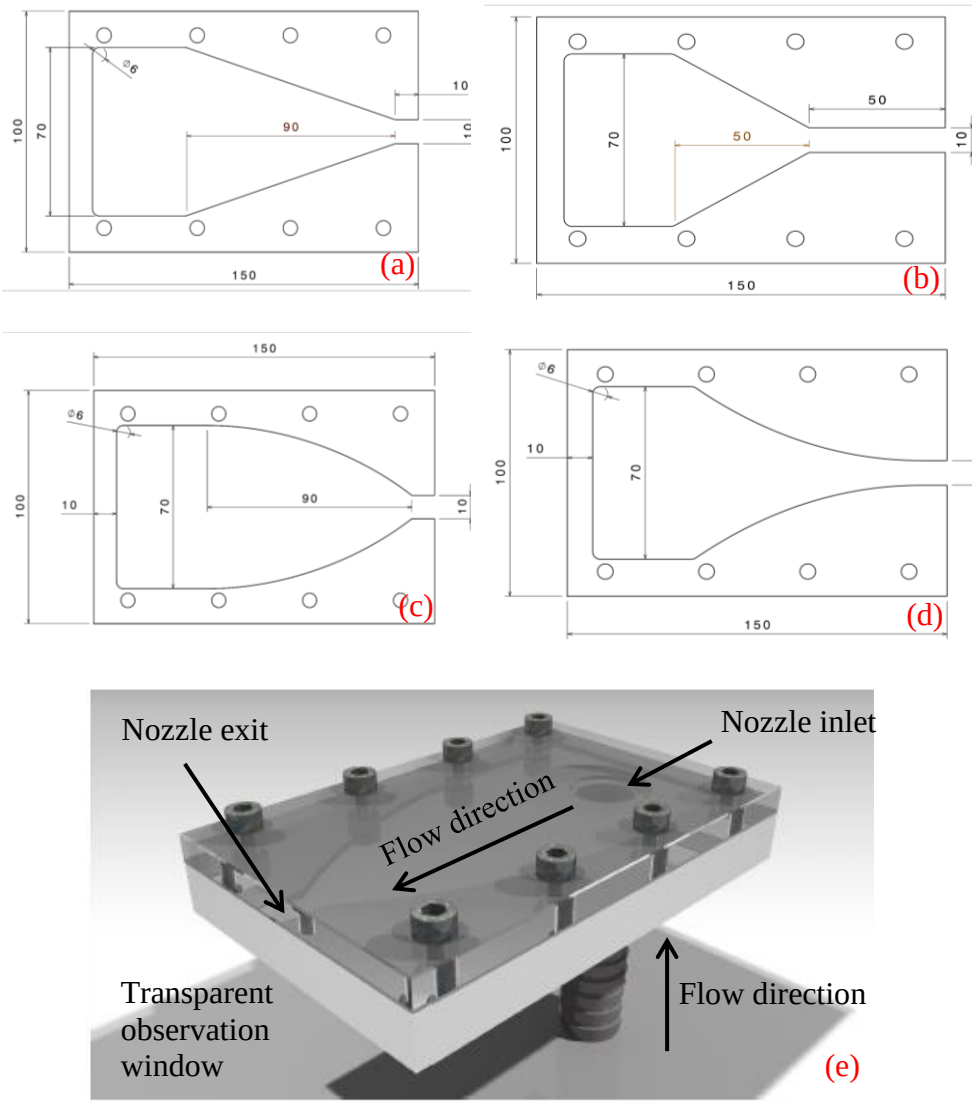


Figure 3.4 Geometries of platen nozzles and schematic diagram of the testing rig. (a) original straight sided nozzle; (b) straight sided nozzle with aspect ratio = 25; (c) concave nozzle; (d) convex nozzle; (e) schematic diagram of testing rig.

3.3 **Results and discussion**

3.3.1 Liquid jet break-up regimes validation

In hydrodynamic alignment processes, a low-speed laminar jet is required to maintain the aligned orientation of fibre before the jet is deposited on the rotating drum which has a layer of nylon mesh attached. The Re number for the jet is always below 10, and Oh number is around 4 which depends on the fibre length and fibre volume concentration. Thus, according to the liquid jet

break-up regimes, the break-up phenomenon of suspension jet is in the varicose regime but close to the boundary of dripping. Figure 3.5 shows the photo results of glycerine/water solution jet's break-up phenomenon test.

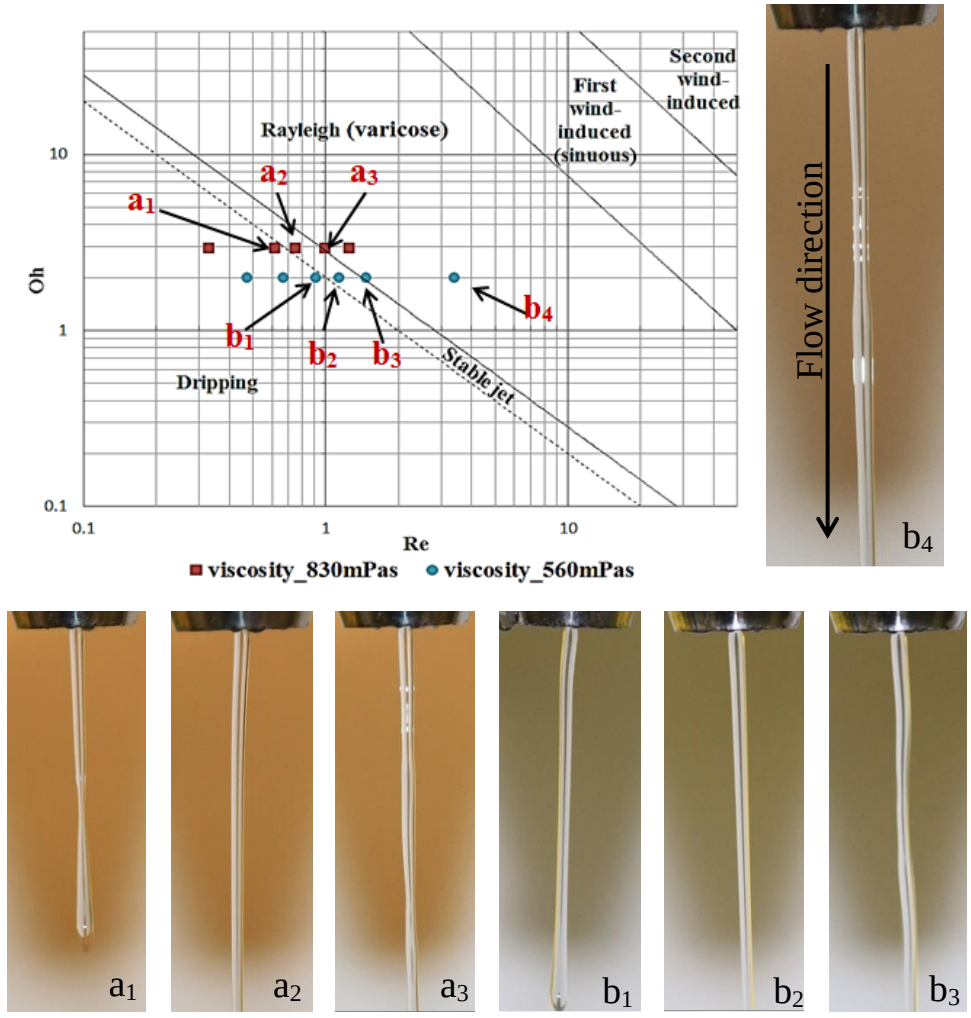


Figure 3.5 Image results of glycerol-water jet stability test

Photo a1 and b1 clearly show that the jets were dripping as the kinetic energy is not enough to generate a jet when $Re \leqslant 2/Oh$. When the liquid jet has a property, $4 \leqslant We_L \leqslant 8$, a smooth cylinder jet was achieved as shown in photo a2 and b2. As the velocity was increased, the varicose behaviour is more obvious (photo a3 and b3). When the data point is close to the midpoint between the Rayleigh regime and sinuous regime the varicose shape was clearly obtained (as shown in photo b4). These results also validate the jet

stability curve which is discussed by many researchers and summarised by McCarthy and Mollo [3]. It suggests that when the viscosity and density become constant, the jet break-up length grows with the increasing velocity [3].

3.3.2 Break-up regime exploration of short fibre suspension jet

As described in the previous sections, the liquid jet break-up regime is based on the combinations of inertia of the fluid, surface tension and aerodynamic forces acting on the jet. However, for a short fibre suspension jet, more influencing factors need to be considered. In this section, the effects of different fibre lengths, fibre suspension concentrations and fibre suspension viscosities on fibre suspension jet's break-up regimes are described.

Figure 3.6 shows that different fibre lengths can make the suspension jets behave with different stability phenomena. When the suspension viscosity is constant, the jet stability becomes worse with increasing Re number which shows the same behaviour with the pure liquid jet described by Ohnesorge's breakup regime. However, when the fibre volume concentration is constant, the fibre-fibre interaction in 12mm fibre suspension is more significant as the fibre aspect ratio is four times larger. Thus, if the fibre concentration, suspension viscosity and jet Re number are same, the use of 12mm fibre can make the jet more unstable (Figure 3.6).

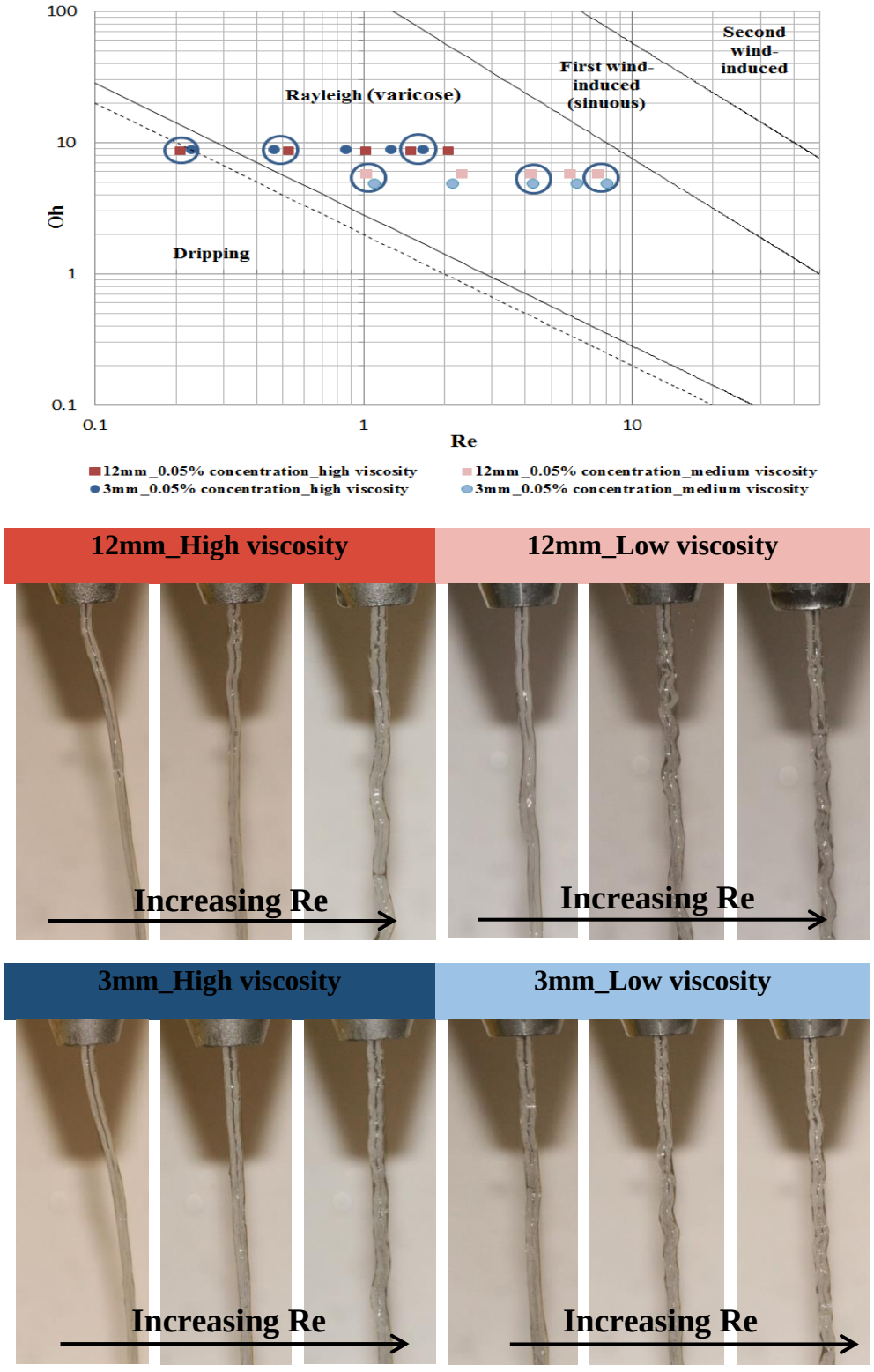


Figure 3.6 Image results of fibre suspension jets' stability test – influences of different fibre lengths

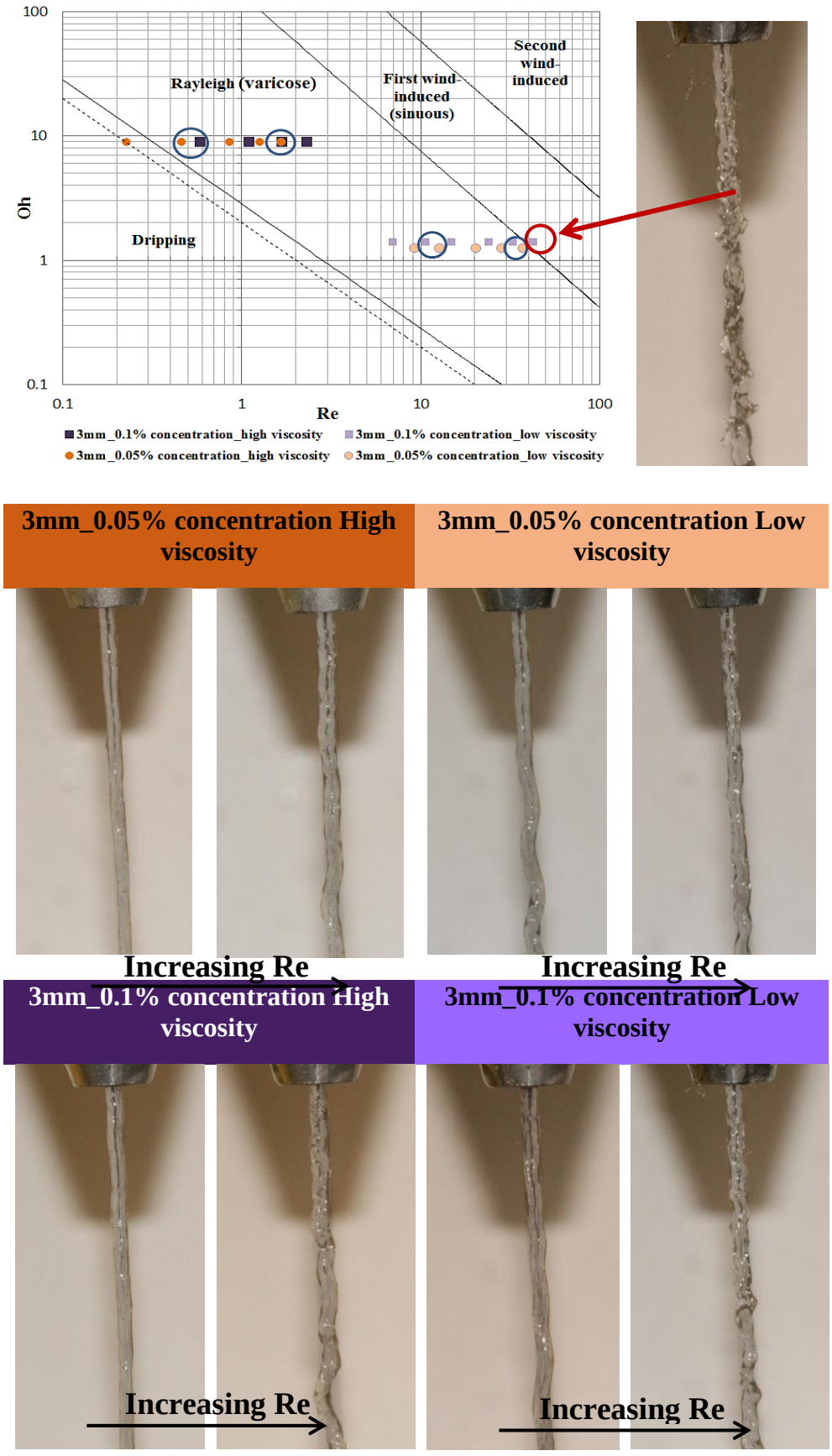


Figure 3.7 Image results of fibre suspension jets' stability test – influences of different fibre volume concentrations

On the other hand, by increasing the fibre concentration, the fibre-fibre interactions become larger although the fibre length is same. Thus, the photo results in Figure 3.7 validate that the greater the fibre-fibre interactions in the suspension, the more instability was induced.

It was mentioned by Soderberg [4] that the waves on the jet surface are more homogeneous in the flow of a fibre suspension jet compared to the flow of a water jet. Also, it was found that the strength of the break-up of the jet was lower for the fibre suspension than for the pure water jet at the same flow rate. Thus, the presence of fibres in the water clearly has an impact on the properties of the flow. Thus, it can be assumed that not only the fibres but also their orientation distribution could affect the stability of suspension jet. In Figure 3.8, the photo results show that with a certain fibre length and fibre concentration, the stability of suspension jet was improved by reducing the viscosity of dispersion media. Short fibres rotate under the shear stress field with greater ease as the viscose resistant forces become smaller. Then better alignment quality can be achieved which tends to be beneficial to the jet stability.

To validate the influences of jet stability on fibre alignment quality, three 2.5gsm mats were manufactured with 3mm Tenax®-A HT C124 carbon fibre and a fibre volume concentration in the suspension of 0.05%. The first mat (Figure 3.9_a) was made with a dripping jet ($We_L<4$), fibres were bent and became bundles inside the droplet then deposited on the nylon mesh. When $We_L=10$, the jet behaves varicose, fibre could be bent inside the jet near the varicose surface or even protrude as shown in Figure 3.10_d. At this varicose jet condition, the second mat was made, and the fibre orientation was shown

in Figure 3.9_b. The third mat in Figure 3.9_c was manufactured with a jet which has a We_L= 6. The fibre orientation is homogeneous and aligned with the flow direction.

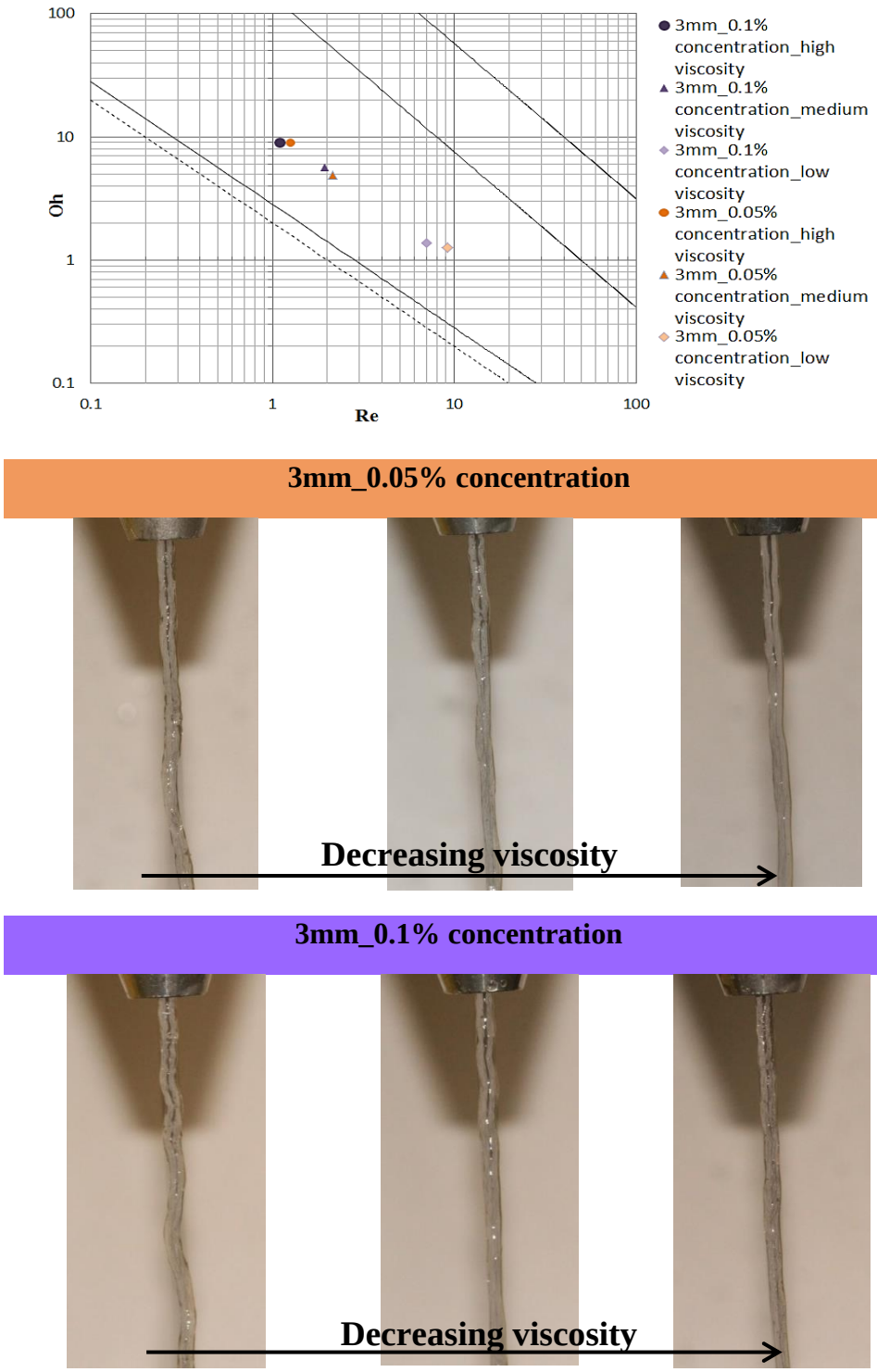


Figure 3.8 Image results of fibre suspension jets' stability test – influences of different viscosities of fibre suspensions

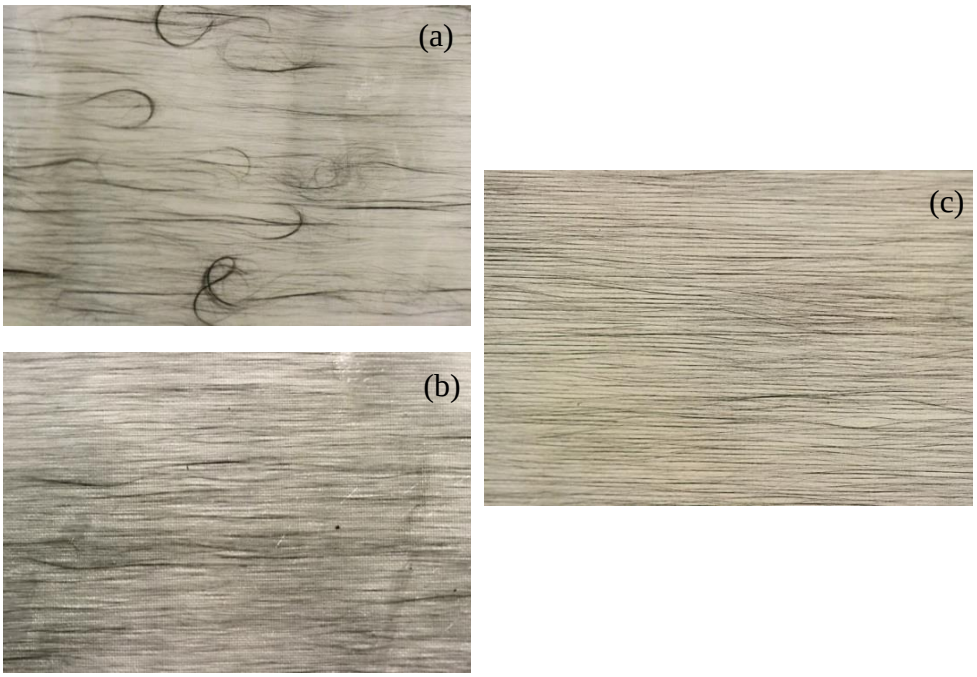


Figure 3.9 The effects of fibre suspension stability on the alignment quality: (a) mat made with dripping jet, $We_L<4$; (b) mat made with the unstable jet in the varicose regime, $We_L=10$; (c) mat made with stable jet, $We_L=6$.

Thus, it can be predicted that the stability of a fibre suspension jet will significantly affect the fibre alignment quality. Large fibre to fibre interaction in the jet will induce greater instability. On the other hand, good fibre alignment inside the nozzle can help to improve the jet stability, and this can be achieved by nozzle geometry design.

3.3.3 The effects of nozzle geometries on flow kinematics and fibre alignment

To explore the effects of different nozzle geometries on the flow kinematics, the shear flow and elongational flow profiles in four different nozzle shapes (Figure 3.11) were evaluated by CFD simulation respectively. All the nozzles have same inlet and outlet dimensions and consistent boundary conditions.

In Figure 3.12, the average shear strain rate (velocity gradient) and average elongational strain rate profiles in the original straight sided nozzle are plotted

from nozzle inlet to the exit (nozzle length is 0m at the nozzle inlet and the nozzle length is 0.077m at the nozzle exit). Both shear strain rate and elongational strain rate keep increasing from the nozzle inlet to the exit because of the linearly increasing nozzle contraction ratio.

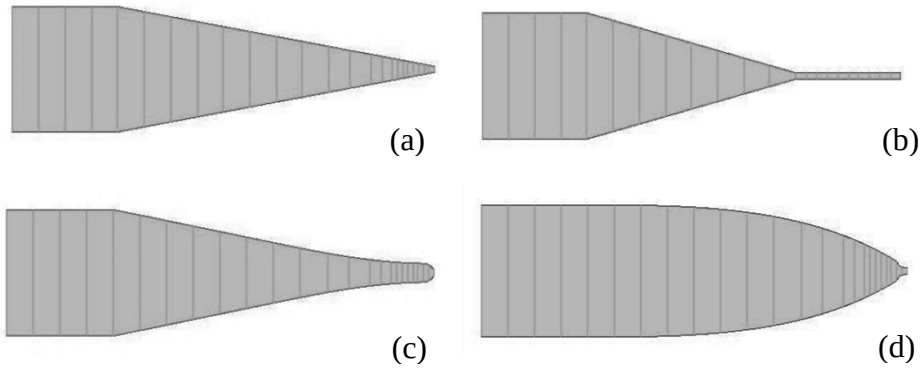


Figure 3.11 Geometries of nozzles which were applied in CFD simulation: (a) the original straight sided nozzle; (b) the straight sided nozzle with aspect ratio =25; (c) the convex nozzle; (d) the concave nozzle. (the inlet, outlet and nozzle length dimensions of all these nozzles are same respectively)

The flow characteristics in the long straight section nozzle are shown in Figure 3.13. The contraction ratio of this nozzle is 0.05 which is same as the straight sided nozzle. However, the length of the converging section is a third shorter than that of the straight sided nozzle. In the converging region (0.02<nozzle length<0.06 m), the average shear strain rate and elongational strain rate keep increasing and have a sharp growth at the boundary between the converging section and straight section (nozzle length is 0.06m). When the flow enters the straight section, the average shear strain rate becomes constant (3.17 sec^{-1}) which is same as the value at the boundary position. However, the elongational train rate presents a sharp decrease from 0.931 to 0.018 sec^{-1} and then keeps constant. Thus, the flow in the straight section is

shear flow dominated which can be considered as the simple shear flow in a pipe.

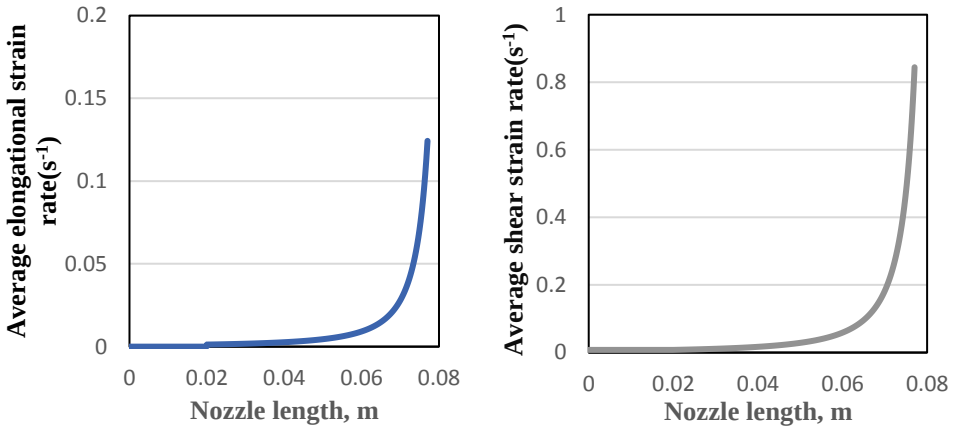


Figure 3.12 Plot of average elongational strain rate and shear strain rate at each cross section inside the original straight sided nozzle

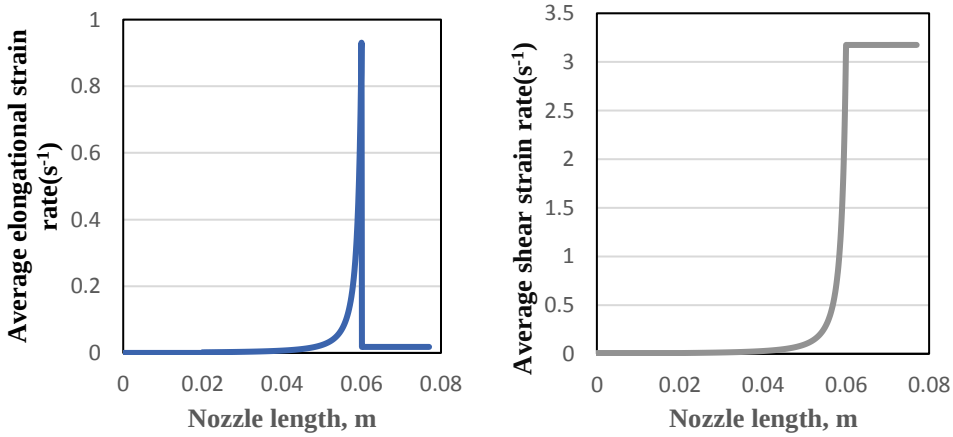


Figure 3.13 Plot of average elongational strain rate and shear strain rate at each cross section inside the straight sided nozzle with aspect ratio =25

Figure 3.14 shows the average elongational strain rate and average shear strain rate profiles inside the convex nozzle. In the initial 7cm of the nozzle, the convex profile makes the flow have higher shear strain rate compared to that of straight sided nozzle as the contraction ratio is greater. However, in the following section (0.07<nozzle length<0.077m), the contraction ratio is trending to 1 and the contraction angle is trending to 0° (for a straight pipe,

the contraction ratio is 1 and contraction angle is 0°) which leads to a reduction on flow acceleration. Thus, the flow elongational strain rate reducing gradually at the convex nozzle end region (nozzle length is between 0.07m and 0.077m) and the average shear strain rate is smaller than that of the straight sided nozzle.

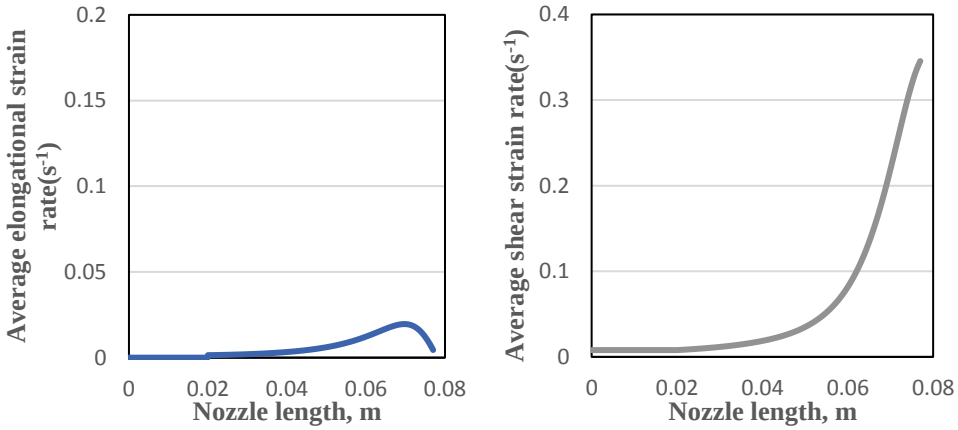


Figure 3.14 Plot of average elongational strain rate and shear strain rate at each cross section inside the convex nozzle

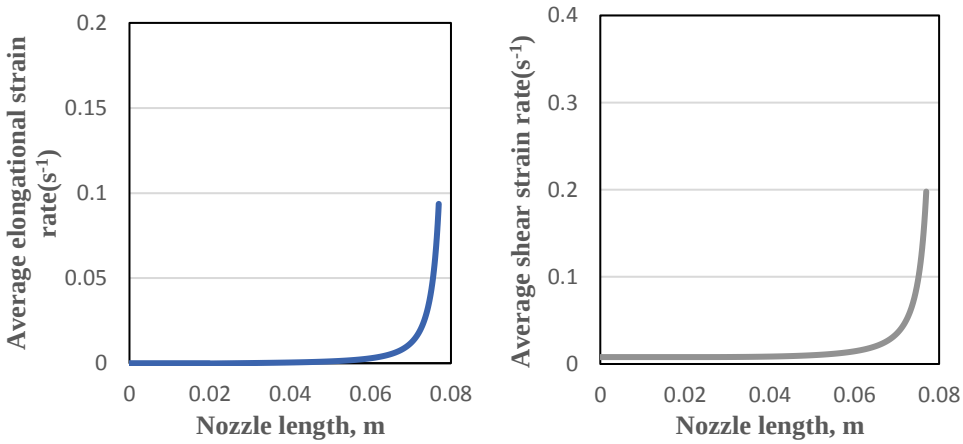


Figure 3.15 Plot of average elongational strain rate and shear strain rate at each cross section inside the concave nozzle

Inside the concave nozzle, along with the flow direction, both the average elongational strain rate and the average shear strain rate are increasing (Figure 3.15). The concave shape generates the smallest average shear strain rate at

the nozzle exit comparing to the other three nozzles (77% lower than the average shear strain rate at the exit of straight sided nozzle) and a high elongational strain rate which is only 24% smaller than the average elongational strain rate at the exit of the straight sided nozzle.

Furthermore, the ratio of average elongational strain rate and shear strain rate at these nozzles exit cross sections are plotted in Figure 3.16. The ratio of concave nozzle is more than 3 times higher than the straight sided nozzle and 20 times higher than convex nozzle. In other words, the concave geometry can make the flow at the nozzle exit strongly dominated by the elongational flow.

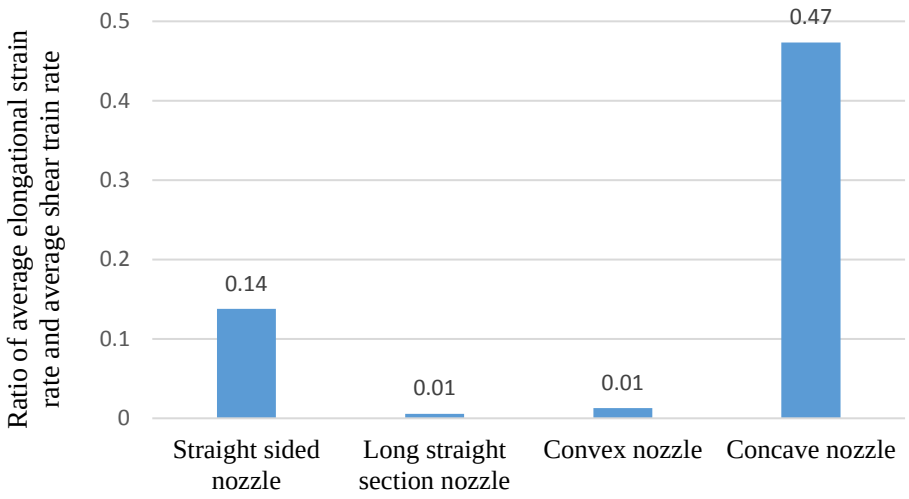


Figure 3.16 The ratio of average elongational strain rate and shear strain rate at the nozzle exit cross section

To validate the effects of flow kinematics on fibre orientation, four different nozzles (Figure 3.4) were applied in the experimental work. The fibre orientation at the nozzle exit was captured, and the images are shown in Figure 3.17. The relationship of fibre orientation quality produced by these nozzles can be concluded as:

Concave nozzle > Convex nozzle > Straight-sided nozzle > Long straight section nozzle

Thus, the simulated results indicate the concave nozzle shape with an increasing contraction angle can make the flow become elongational flow dominated at the nozzle exit and this characteristic can result a good fibre alignment quality which is validated by the experimental fibre orientation observation in 2D platen nozzle.

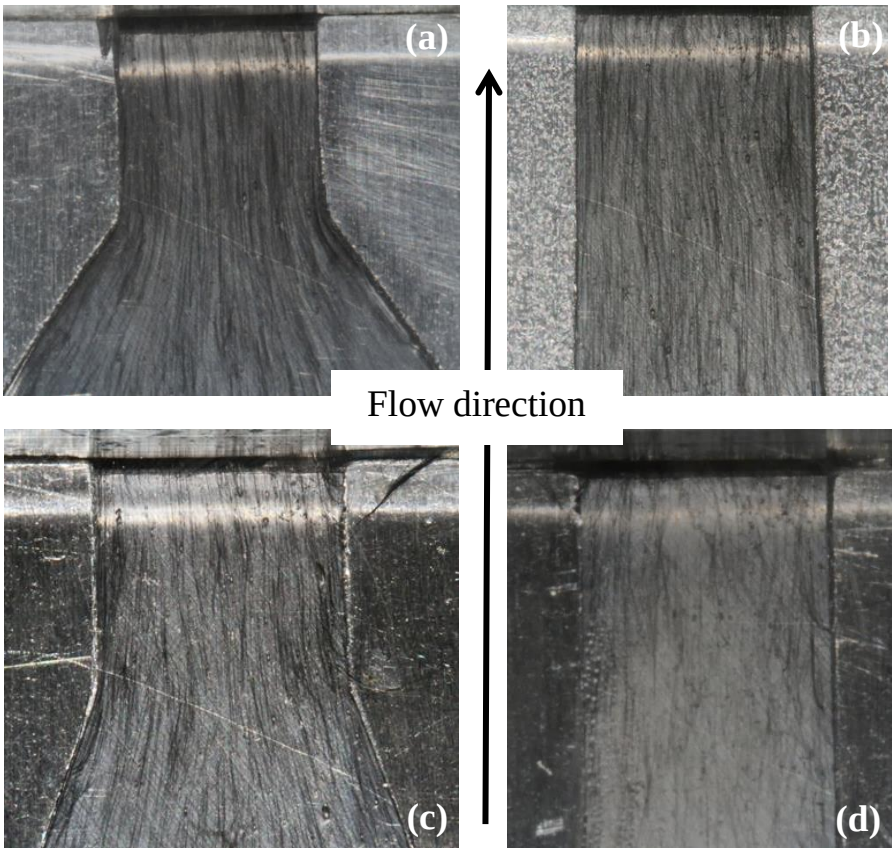


Figure 3.17 Fibre orientation distributions in different platen nozzles: (a) concave nozzle; (b) convex nozzle; (c) original straight sided nozzle; (d) straight sided nozzle with an aspect ratio=25

3.4 Conclusion

The stability of fibre suspension jets has a significant influence on fibre alignment quality in processes requiring high fibre packing efficiency. The pure liquid jet breakup regimes can be used to describe the behaviour of a

suspension jet and when $4 \leqslant We_L \leqslant 8$, a smooth cylinder jet was achieved. However, nozzle geometry, fibre to fibre interaction and fibre orientation inside the nozzle are important factors in determining jet stability. The jet which is generated by a concave nozzle profile presents higher stability as there is less influence of wall shear on the flow. Furthermore, the appropriate increment of contraction angle generates a high elongational strain rate which consequently gives good fibre alignment quality and this homogenous fibre orientation will be beneficial to maintain the stability of jet.

References

[1]. C. Theobald, The effect of Nozzle design on the stability and performance of turbulent water jets, Fire Safety Journal, Volume 4, Issue 1, 1981, Pages 1-13, ISSN 0379-7112

[2]. L. G. Whitehead, L. Y. Wu and M. H. L. Waters, Contracting ducts of finite length, Aeronaut. Q., 2 (1951) 254 - 271

[3]. M. J. McCarthy and N. A. Molloy, Review of stability of liquid jets and the influence of nozzle design, Chem. Eng. J., 7 (1974) 1 - 20.

[4]. Soderberg, L. D. 1999, A comparison between the flow from a paper machine headbox and a low Reynolds number water jet. In Tappi Engineering Conference, Anaheim

[5]. Bay, R.S., 1991. Fiber orientation in injection molded composites: A comparison of theory and experiment. Ph.D Thesis, Department of Mechanical Engineering, Urbana-Champaign, USA

[6]. Sadabadi, H. and M. Ghasemi, 2007. Effects of some injection molding process parameters on fiber orientation tensor of short glass fiber polystyrene composites (SGF/PS). J. Reinf. Plast. Compos., 26: 1729-1741

4. Characterisation of aligned mats and composites

4.1 Introduction

A bench-top centrifugal alignment process has been devised for converting discontinuous random recycled carbon fibre into mats with a highly-aligned orientation. This allows composites with high fibre content to be manufactured at lower moulding pressures with the added benefit of minimum degradation of fibre length. With further improvements in processing factors it is possible to manufacture a composite achieving 46% fibre volume fraction under 7 bar moulding pressure in an autoclave, exhibiting good mechanical properties with almost 100 GPa tensile modulus and over 800 MPa tensile strength.

The capability of the rig was investigated in the present chapter via a 2-level full factorial experiment design to provide a better insight into the effect of operating conditions on alignment quality. The five factors under consideration were fibre length, fibre volume concentration in suspension, dewatering vacuum level, relative speed between the rotating drum and lastly the slurry deposition rate. Orientation of the fibre within the aligned mat was measured via image analysis of both the fibre elliptical cross-sectional geometry and in plane fibre orientation geometry. As observed by Wong [1], a higher level of alignment means that the fibres are more tightly packed and result in a high fibre volume fraction under the same compressing pressure. Dry mat compaction testing was used to evaluate the fibre volume fraction in aligned mats under different loading pressures and these data were used as an output response to assess the effect of changes from the four input factors. The results of the test allowed the determining of the best operating conditions

for aligning recycled carbon fibre. Finally, tensile testing was used to evaluate the mechanical properties of aligned discontinued carbon fibre moulded laminates.

4.2.1 Materials

Tenax®-A HT C124 carbon fibre staples coated with a water-soluble sizing, was supplied by Toho Tenax Europe GmbH. The fibre lengths were 3 mm and 12 mm and the individual fibre nominal diameter is 7 μm. Fibre sizing was removed by placing the staples inside an ashing furnace at 550 ° C for 15 mins. Oleon Glycerine 4810 with glycerol content ≥99.5% was supplied by Univar UK. The glycerine was diluted with tap water until a viscosity of around 400 mPa·s was measured at room temperature (15 ℃) using a Brookfield LVDVII viscometer. The diluted glycerine was used as a dispersion medium. The fibre suspension tank and glycerine/water solution tank are all covered by the lids to avoid glycerine absorbing water from the atmosphere. A cooling system in the suspension tank was designed to help keeping the viscosity of suspension as a constant by controlling temperature.

Table 4.1 Details of full factorial DoE

Fibre length, mm	Fibre volume concentration in suspension, %	Wire/ Jet velocity ratio	Dewatering vacuum level	Number of replicates
3	0.05	1.5	Low	2
12	0.15	5	High	

A 2-level full factorial experimental work plan was designed to explore the effects of processing factors on alignment quality of discontinuous carbon fibre in a hydrodynamic alignment process. Details of the factors and levels are listed in Table 4.1. The 'Wirer/Jet velocity ratio' can be explained as when the drum tangential speed is 1.5 or 5 times higher than the suspension flow velocity at the nozzle exit.

4.2.2 Dry fibre mat compaction testing

A compaction test rig for measuring carbon fibre mat thickness (used to determine the average fibre volume fraction) under different compression pressure is shown in Figure 4.1.

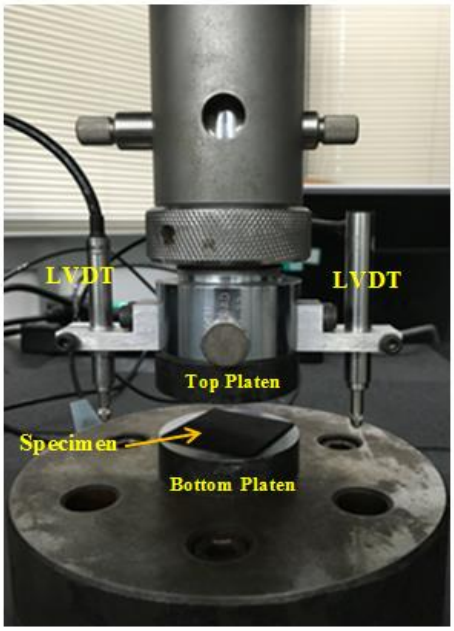


Figure 4.1 Dry fibre mat compaction testing apparatus

The rig essentially contains two flat platens; the bottom platen is fastened to the base of a 5969 universal testing machine from Instron; the upper platen is connected to a 50 kN load cell, which is mounted to the machine crosshead. The system compliance of the entire rig was first determined by closing the

two platens together at a crosshead speed of 1mm/min until a compression pressure of 10 bar was registered by the load cell. The crosshead location was automatically logged by the machine's control software during the test. The data was used to measure the distance between the two platens. Two linear variable differential transformers (LVDTs) were also mounted on the top platen to provide accurate readings of the distance between the platens. To measure the thickness and volume fraction of the mats, square test specimens with an edge length 35mm were obtained by stamping carbon fibre mat using a cutting template. Each mat was weighed before the test. Then 4 samples were stacked together and carefully transferred to the bottom platen and were compressed at 1 mm/min until 10 bar pressure was attained. The compliance of compaction test system was measured by two LVDT units when 10 bar pressure was applied on the bottom platen and no specimen was placed on it. The thickness and fibre volume fraction of the mats were determined by taking the average of the readings from the two LVDT units after the compliance was subtracted. The fibre volume fraction of the dry fibre mat (V_f) can be calculated by:

$$V_f = \frac{Dry\ fibre\ mat\ areal\ density}{\rho_f t_{mat}} \qquad \text{Equation 4.1}$$

Where, ρ_f is the density of fibre and t_{mat} is the thickness of the dry fibre mat under certain compressing load.

4.2.3 Glycerine washing methods

To explore whether the glycerine residue will lead to a reduction in composite mechanical properties, two kinds of composite specimens were manufactured

from continuous unidirectional virgin fibre mats with different post processing.

- Dry mat composite laminate: epoxy binder was applied on the dry continuous unidirectional virgin fibre mats. Then the mats were placed in the oven at 120 °C for 2 hours to cure the binder. The composite laminate was made with these fibre mats and resin films.
- Glycerine wetted mats composite laminate: the fibre mats were wetted with a glycerine/water solution and washed three times with warm water (each wash takes 40s). The mats were dried in the oven. Binder and resin films were applied following the same procedure to make composite specimens.

Tensile tests were undertaken to measure the mechanical properties, the details of specimen properties are listed in Table 4.2.

Table 4.2 Specification of dry and glycerine wetted unidirectional continuous virgin fibre preforms and composite samples

Specimen	Fibre mat areal density	Fibre volume fraction	No. of layers fibre mat	Tensile testing specimen dimensions	No. of specimens
	gsm	%	/	l × w × t (mm)	/
Dry mats composite laminate	100	62	20	250×25.03×2.21	3
Glycerine wetted mats composite laminate	100	62	20	250×25.1×2.04	3

To find out the most effective method, four different washing methods were tried on aligned fibre mats which were made with 3mm virgin fibre. To explore whether different fibre length will affect the washing efficiency, 12mm fibre mat was involved in the 3 times and 6 times hot water washing tests. The details of experimental design are listed in Table 4.3. Finally, the FTIR (Fourier transform infrared spectroscopy) technique was used to obtain the glycerine absorption in fibre mats after different washing processes.

Table 4.3 Experimental design of different washing methods

Washing methods	Fibre length	Experimental procedures
Washing up liquid foam washing	3 mm	• Gently applying the wash up liquid foam on the mat to avoid the damage of fibre orientation. • After 5 mins, washing the mat with hot water for three times.
Acetone washing	3 mm	• A layer of fine nylon mesh was placed on the top of fibre mat which is used to protect the fibre orientation when sparing acetone/water solution on fibre mats. • Repeat the sparing after 2 mins, As the acetone is volatile. • Washing the mat with hot water for three times.
3 times hot water washing	▪ 3 mm ▪ 12 mm	▪ Washing the mat with hot water for three times.
6 times hot water washing	▪ 3 mm ▪ 12 mm	▪ Washing the mat with hot water for six times.

4.2.4 Manufacture of aligned fibre composite in an autoclave and tensile testing

Laminates were made from discontinuous aligned fibre mats (details given in Table 4.4). Not only short virgin fibres (Tenax®-A HT C124_3mm and

12mm, Toray_T800_7mm), but also recycled fibre was introduced in this work. End life carbon fibre composites were supplied by ELG Carbon Fibre Ltd, and had been shredded and recycled by the Fluidised Bed at the University of Nottingham. The effective number average fibre length is 1.15mm. MTM57 resin films were supplied by Cytec Industrial Materials, UK. The materials were vacuum bagged to remove trapped air and the compacted materials were then moulded at 120 °C, 7 bar pressure, for 1 hour. Finally, it was cooled down to around 60 °C under pressure before demoulding.

Table 4.4 Specification of aligned preforms and composite samples

Fibre length	Fibre type	Fibre mat areal density	Fibre volume fraction	No. of layers fibre mat	Tensile testing specimen dimensions	No. of specimen
mm	/	g/m^2	%	/	l × w × t (mm)	/
3	Tenax®-A HT C124	152	46	2	250×25.17×(0.37±0.14)	3
12	Tenax®-A HT C124	99	40	3	250×25.22×(0.43±0.12)	3
7	Toray_T800	58	42	3	250×25.06×(0.23±0.03)	3
1.15	ELG recycled	131	38	3	250×25.03×(0.56±0.02)	3

Tensile tests were performed with a 250 kN load cell which was attached to the crosshead (Figure 4.2), and a test speed of 1 mm/min was applied for all specimens, i.e. 4 specimens from each laminate. The thickness of each

specimen was measured at 6 different positions along the fibre direction by a ball micrometre. An extensometer was attached on each specimen to record strain. Micrographs were used to view and analyse the cross-section of the laminates.

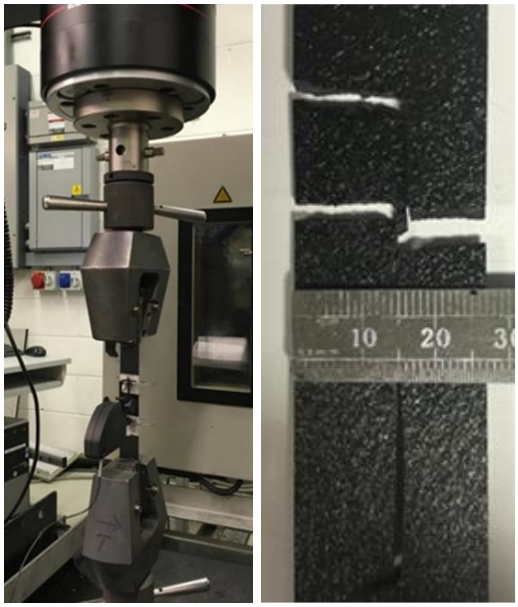


Figure 4.2 Tensile testing setup and fracture cross section of 3mm fibre laminate composite specimen

4.2.5 Fibre orientation determination

To explore the in-plane fibre orientation, the surfaces of polished composite specimens were analysed. The composite sample was prepared by placing in a thermoplastic container filled with potting epoxy resin (Prime20LV, Gurit, UK) then the hardened epoxy containing the sample was polished to expose the whole length of each fibre. All sample images were taken by an optical microscope. Then the images were imported into CAD software and the centre line of each fibre was drawn over the images manually. The data file contains angles of the lines was exported to a spreadsheet for further processing. For each case, around 5000 carbon fibres were used to identify

orientations using 5 microscope images of different surfaces. Figure 4.3 shows images of the middle surface of the aligned composite samples used for in plane fibre orientation analysing. Finally, the fibre orientation distribution results of 3mm fibre composites and 12mm fibre composites were obtained in Figure 4.10.

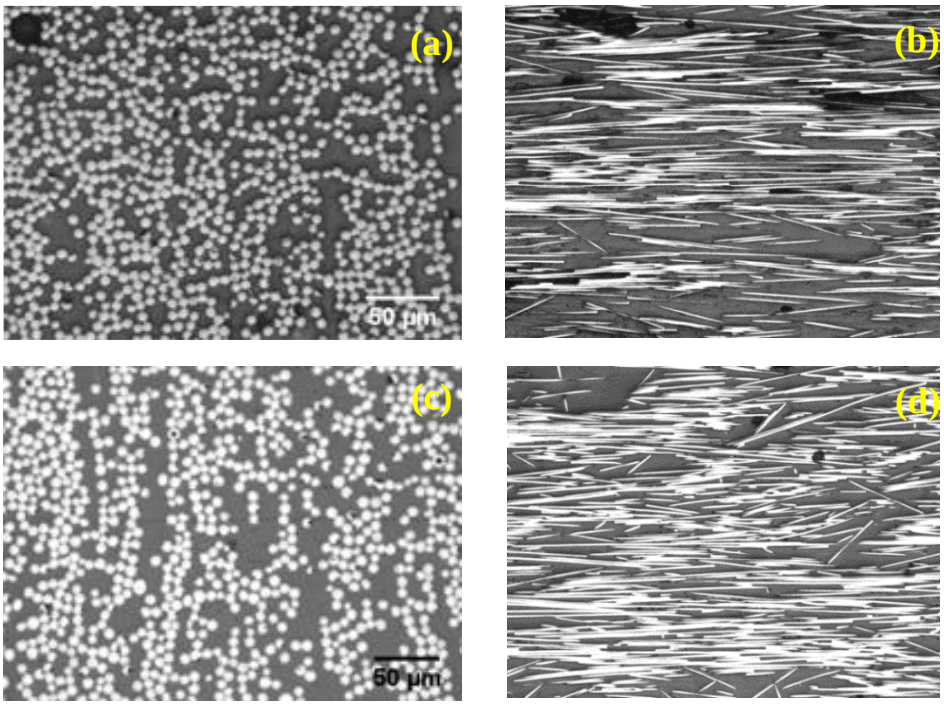


Figure 4.3 Micrograph of aligned composite cross section and in-plane view: (a)(b)3mm_46% fibre volume fraction; (c)(d)12mm_43% fibre volume fraction

4.3 Results and discussion

4.3.1 Dry fibre mats compaction results

In the previous research work, with 10 bar compaction pressure, 3mm fibre aligned mat has been shown to achieve 47.7% fibre volume fraction and 12mm fibre aligned mat obtained 32.5% fibre volume contain [2]. To improve the process efficiency and achieve higher fibre volume faction, the processing factors influencing alignment quality are explored in this paper. The

compaction test results of the fibre mats which are manufactured following the 2-level full factorial experimental design were listed in Table 4.5. Based on the compaction test results of the full factorial test, the main effects plots for fibre volume fraction are shown in Figure 4.4

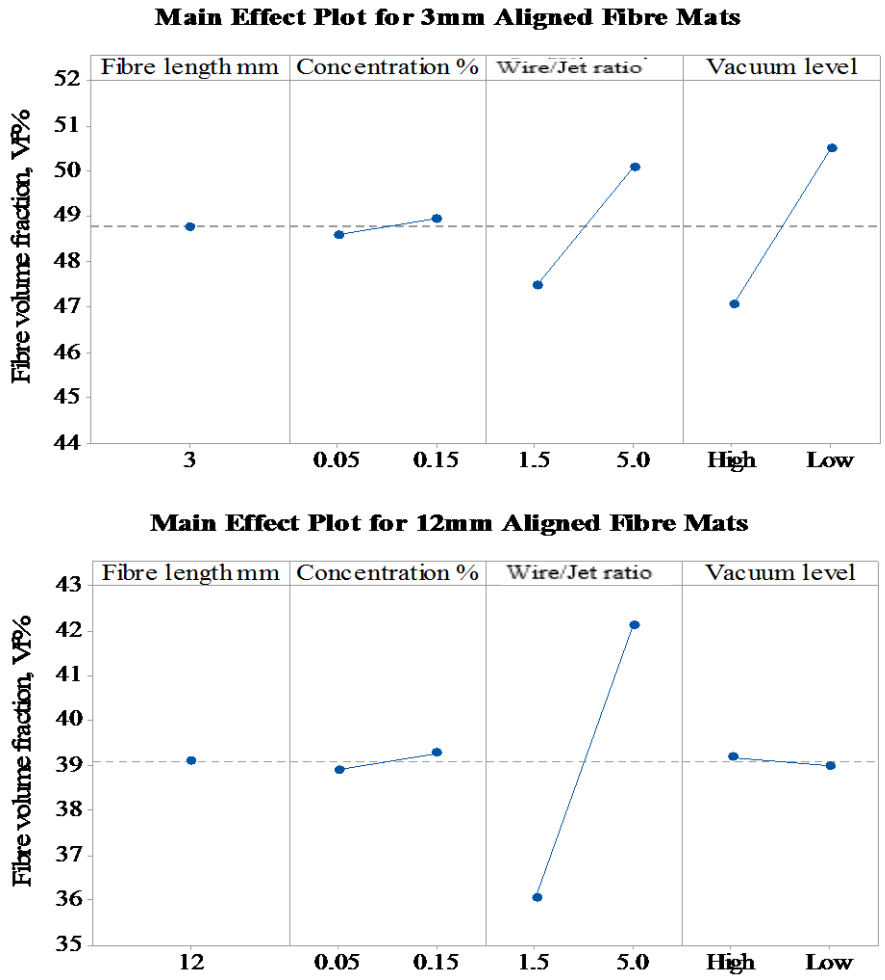


Figure 4.4Main effect plots of compaction test results from full factorial DoE

Fibre volume concentration in the suspension is not a main effect for aligning 3mm fibre and 12 mm fibre which is due to the improved dispersion process where the fibres were distributed more homogenously in the suspension. Higher wire/jet velocity ratio is beneficial to the fibre alignment for both 3mm and 12 mm fibres, as it can drive fibres along the flow direction and avoid fibre bending as it is deposited on the nylon mesh. The vacuum level applied

around the rotating drum is another important factor, as it can affect dewatering efficiency. If High vacuum level was applied, short fibres will move along the glycerine flow direction during dewatering process and the pre-aligned orientation will be damaged. Thus, lower vacuum level is required for 3mm fibre to maintain aligned fibre orientation which is validated by DoE results plotted with Minitab in Figure 4.4

The compaction result curves are plotted in Figure 4.5. This includes two benchmarks: a 2D planar random mat and a unidirectional continuous fibre (UD) mat as well as two aligned mats from the full factorial test which are made by 3mm and 12mm Tenax®-A HT C124 virgin fibres respectively. These obtained the highest fibre volume fraction in the compaction test results based on their fibre length group. Under 10bar compaction pressure, the fibre volume fraction of UD mat is 68% where the random mat can only give 18% fibre volume content at the same pressure. This clearly indicates that an aligned fibre orientation improves fibre packing efficiency. With 3mm fibre, the mat exhibits 52% fibre volume fraction under 10bar compaction pressure. The manufacturing conditions are 0.15% fibre volume concentration suspension, 5 times drum to jet speed ratio and low dewatering pressure. For 12mm fibre mat, 41% fibre volume fraction was achieved and the processing factors are 0.15% fibre volume concentration suspension, 5 times wire to jet speed ratio and high dewatering power. A 3 mm fibre aligned mat can achieve a 27% higher volume fraction than the 12 mm fibre mats. This is attributed to having a better fibre suspension quality, which is free of fibre bundles for the shorter fibre.

Table 4.5 Processing factors in DoE and compaction test results

run order	Fibre length	Fibre volume concentration	Wire/Jet velocity ratio	Dewatering vacuum level	Fibre volume fraction	Fibre volume fraction SD
	mm	%			%	%
1	3	0.05	5	Low	50.9	0.14
2	3	0.15	5	High	50.5	1.05
3	3	0.15	1.5	High	42.4	1.78
4	12	0.05	5	High	41.7	0.54
5	3	0.05	1.5	High	42.6	0.63
6	3	0.05	1.5	Low	48.3	0.25
7	3	0.05	1.5	High	49.1	1.53
8	12	0.05	1.5	High	36.6	0.61
9	3	0.15	1.5	Low	50.8	0.59
10	3	0.15	5	Low	49.3	0.78
11	3	0.05	5	High	48.8	1.62
12	3	0.05	1.5	Low	51.8	1.06
13	12	0.15	1.5	High	37.6	0.74
14	3	0.15	1.5	Low	51.2	1.16
15	12	0.05	5	High	44.9	3.42
16	12	0.05	1.5	Low	32.6	1.62
17	3	0.05	5	Low	49.4	2.24
18	12	0.15	1.5	Low	36.3	2.26
19	3	0.15	5	Low	52.3	1.56
20	12	0.15	1.5	Low	37.7	5.72
21	3	0.15	5	High	51.6	1.77
22	3	0.15	1.5	High	43.5	2.93
23	12	0.15	5	Low	45.5	4.10
24	12	0.15	5	High	37.8	2.08
25	12	0.15	5	Low	39.2	2.88
26	3	0.05	5	High	47.9	3.17
27	12	0.15	5	High	40.0	0.65
28	12	0.05	1.5	Low	32.9	1.66
29	12	0.15	1.5	High	40.2	1.41
30	12	0.05	5	Low	43.8	5.19
31	12	0.05	1.5	High	34.7	3.26
32	12	0.05	5	Low	44.1	1.78

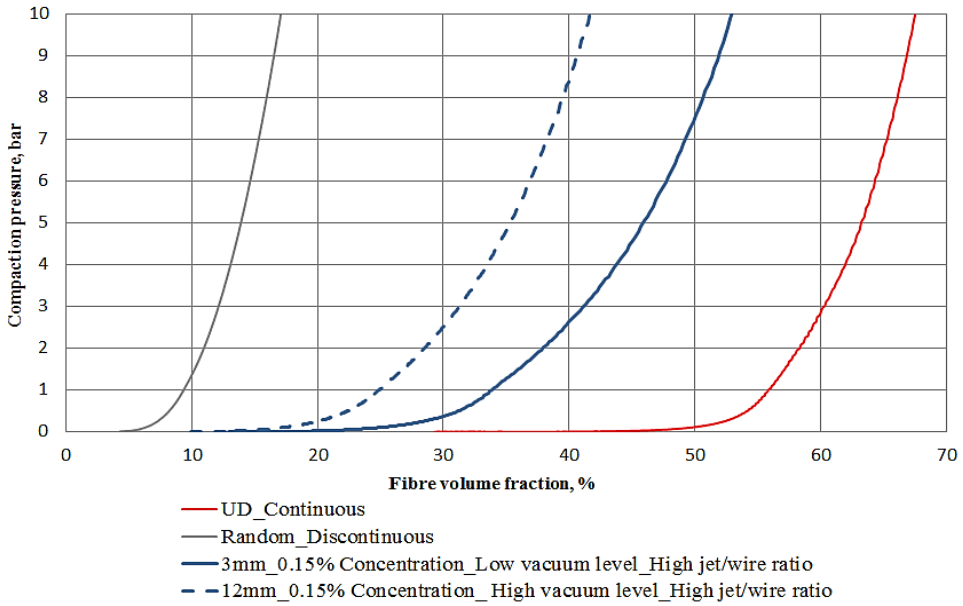


Figure 4.5 Dry fibre mat compaction test results

4.3.2 Self-compaction behaviour of aligned fibre mats

According to Figure 4.5, under 0.5bar compaction pressure, the UD fibre mat, aligned short fibre mat and random fibre mat, they all showed a fast increasing fibre volume fraction, and the reason could be explained as reducing the distance between the fibres. Thus, when the compaction pressure is raised to 0.5bar, the flexible distance between fibres become zero and fibres are just touching with each other. When the compaction pressure is developed from 0.5bar to 10bar, the fibre volume fraction of UD fibre mat is increased by 10% and the same situation is obtained from the compaction results of random fibre mat. Although random and unidirectional are two different orientation, they both have a uniform fibre orientation. Thus, it is easy to achieve an equilibrium between compaction stress and elastic resistance stress from fibre which will make the fibre volume fraction finally becomes a constant.

However, for the aligned fibre mat, its hybrid structure contains both unidirectional and misaligned fibres. Figure 4.6 presents the compaction behaviour of aligned fibre mat. After fibres are touching with each other, the misaligned fibre still can provide a lot resistance by changing its shape. In addition, the end of misaligned fibre will produce even more complicated effects on the interaction with aligned fibres. Thus, the compaction results curve of aligned fibre mat obtained a gradually increased power law which indicates that fibres are self-organising to achieve equilibrium.

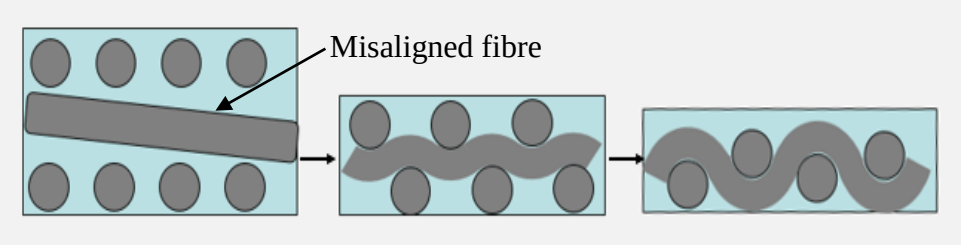


Figure 4.6 Cross section schematic diagram – compaction behaviour of aligned fibre mat

4.3.3 Glycerine washing methods results

Figure 4.7 shows that the tensile modulus of dry continuous virgin is 140 Gpa. However, with the same fibre volume fraction, the specimens which are manufactured with glycerine wetted mats can only obtain 118 Gpa tensile modulus, thus, there is a 15.7% reduction. Furthermore, as the fibre properties, fibre length, orientations are same, the reason of this reduction should be the glycerine residue in the mat after the washing process. To improve the washing efficiency, the influencing factors (washing times and various types of detergent) were investigated in the further experimental work.

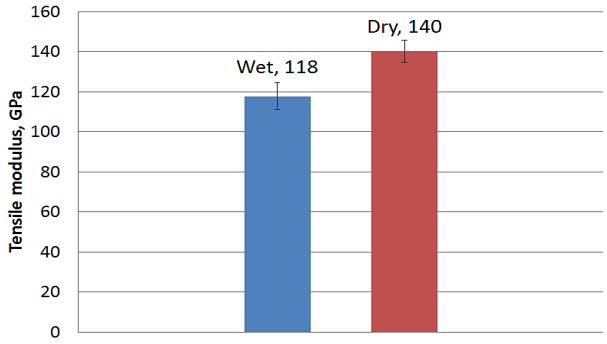


Figure 4.7 Experimental tensile properties: the blue column indicates the result of glycerine wetted mats laminar composite; the red column obtains the result of dry mats laminar composite.

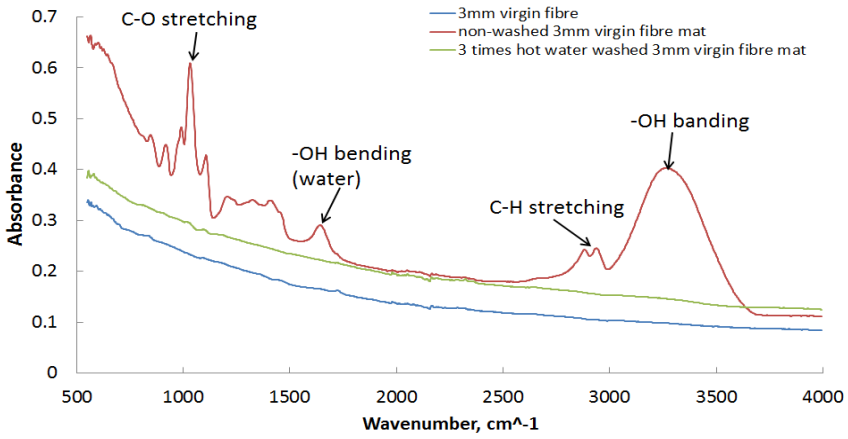


Figure 4.8 FTIR spectra of virgin carbon fibre, non-washed 3mm virgin fibre mat and 3 times hot water washed 3mm virgin fibre mat

Fourier transform infrared spectroscopy (FTIR) is used to obtain the infrared spectrum of absorption of the glycerine residue in the fibre mat. The blue line in Figure 4.8 shows the FTIR spectra of 3mm Tenax®-A HT C124 fibre (without sizing). The red line indicates the spectra of glycerine wetted aligned 3mm virgin fibre mat. The glycerol structure contains primary and secondary alcohols. At 3270cm^{-1} wavenumber, the spectra obtains broad and strong multi-association -OH stretching vibration peaks. At 1130 – 1000cm^{-1}, there

is C-O stretching vibration of glycerol. The characteristic absorption peak of water is at 1580 – 1780cm^{-1} and this strong absorption peak of water does not cover the C-O stretching vibration of glycerol. After the washing and drying process, the glycerol/water solution content in the mat is reduced. Thus, the green line in Figure 4.8 indicates the spectra of fibre mat which has been washed by hot water for three times and all the absorption peak heights drop down, peak areas reduced. The traditional washing method (3 times hot water washing) has achieved a remarkable effect on reducing glycerine residual and it's FTIR spectra present a similar shape compared with the desized virgin fibre spectra (the blue line in Figure 4.8). However, improving the washing efficiency is still important as mechanical property reduction is shown in Figure 4.7.

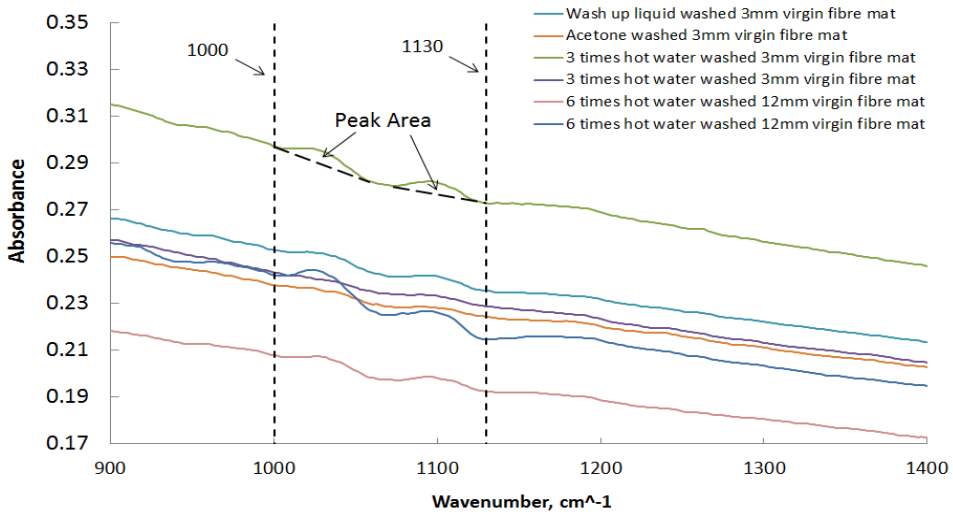


Figure 4.9 FTIR spectra of aligned 3mm and 12mm virgin fibre mat after different washing methods

Figure 4.9 is used to describe the FTIR spectra of aligned 3mm and 12mm virgin fibre mat after different washing methods. The peak at 1130 – 1000

cm^{-1} indicates C-O stretching of glycerol and the peak area measurements from different washing methods' spectra are listed in Table 4.6. Among these four washing methods, the 6 times hot water washing is the most effective one for 3mm fibre mat, as it has the smallest C-O stretching peak area. Furthermore, with same washing method, 12mm fibre mat contain more glycerine residual (larger C-O stretching peak area). The reason can be explained as the 12mm fibre always has lower fibre volume fraction. Thus, before the washing process, the glycerine content inside 12mm fibre mat is more than that of the 3mm fibre mat which could lead to more glycerine residue.

Table 4.6 C-O stretching's peak area measurements from different washing methods' spectra.

Washing methods	Fibre length	C-O stretching peak area, Absorbance/cm
Wash up liquid foam washing	3 mm	913
Acetone washing	3 mm	523
3 times hot water washing	3 mm	1290
	12 mm	1963
6 times hot water washing	3 mm	438
	12 mm	1042

4.3.4 Fibre orientation evaluation

In the previous research work, 70% of the fibres were in the range of ±4° misalignment angle in a rotating vacuum drum filtration process [3], and 90% of the fibres were in the range of ±15° in the filtration method developed by ERD [4]. However, based on the fibre orientation distribution results in

Figure 4.10, there are 93% of fibres in the range ±10° and 59% of fibres are in the range of ±3° in 3mm fibre composite samples which have 46% fibre volume fraction. 88% of fibres in the range ±10° and 54% of fibres were in the range of ±3°in 12mm fibre composite samples which have 43% fibre volume fraction. The fibre alignment quality of the cured composite samples was slightly worse following the post processing operations – residual glycerine washing, applying binder and laminating.

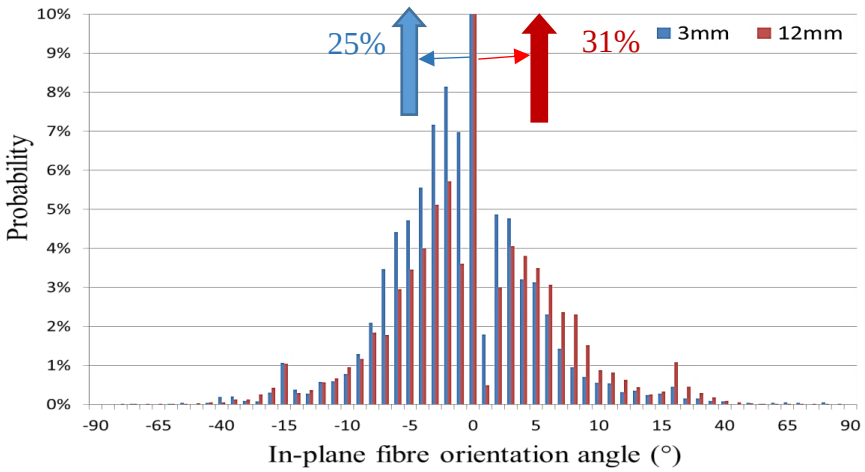


Figure 4.10 In plane fibre orientation distribution for composite specimens made by 3mm fibre (fibre orientation distribution factor η_0 = 0.987) and 12mm fibre (fibre orientation distribution factor η_0 = 0.950)

4.3.5 Mechanical properties

In Table 4 the results from tensile test are listed which include the average fibre volume fraction of each kind of specimen, mean values and standard deviations of modulus and strength. As the fibre lengths used in this work are longer than the critical fibre length, fibre breakage occurs and leads to complete rupture rather than slip between the fibres and the matrix. Thus, extensive fibre pull-out was not been observed at the fracture surface of both virgin fibre specimens and recycled fibre specimens. The fracture surface

images were obtained by Scanning Electron Microscopy JEOL 6060LV and are listed in Figure 4.11.

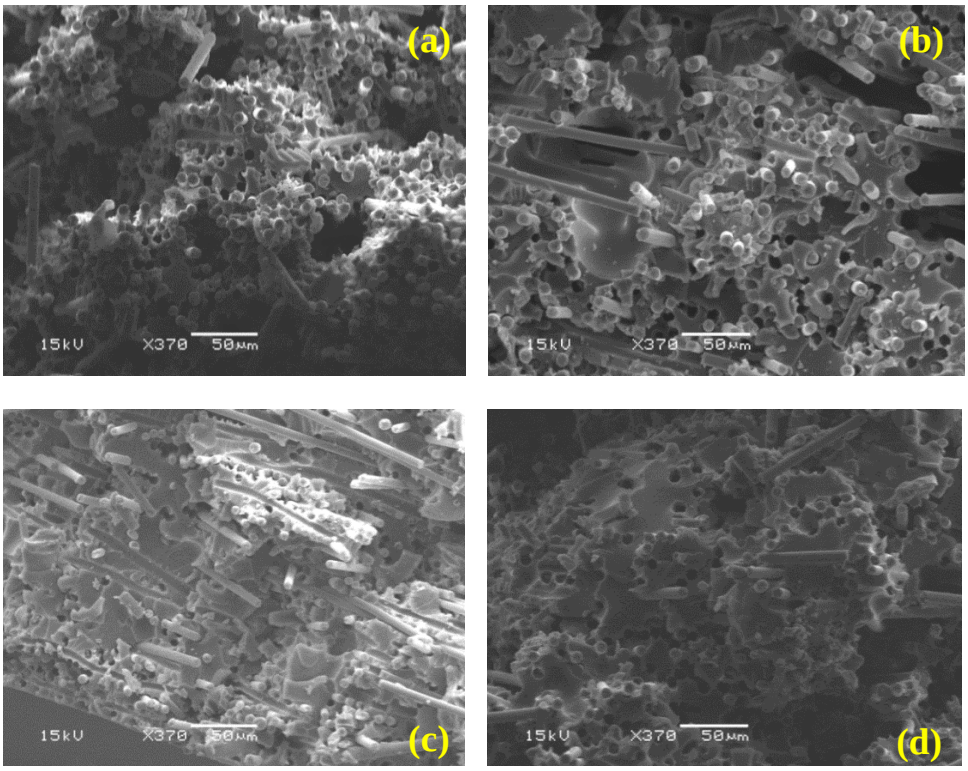


Figure 4.11 Fracture surface images obtained by SEM: (a) 3mm fibre specimen; (b) 12mm fibre specimen; (c) recycled fibre specimen; (d) 7mm_T800 fibre specimen

Table 4.7 Tensile test results

Fibre type	Fibre volume fraction	Tensile modulus	Modulus SD	Tensile strength	Strength SD
	Vf%	GPa	GPa	MPa	MPa
Tenax®-A HT C124 3mm	46	98	2.58	826	71.94
Tenax®-A HT C124 12mm	40	62	3.02	458	202.85
Toray_T800 7mm	42	87	0.67	1417	135.56
Recycled 1.15mm	38	60	4.48	322	25.55

For comparison, a modified rule of mixtures for modulus [5][6][7] was used in analytical modulus calculation. The expression is given by:

$$E_c = \eta_0 \eta_1 V_f E_f + V_m E_m \qquad \text{Equation 4.2}$$

Where, E_c = the composite Young's modulus in the fibre direction

E_c = the Young's modulus of matrix

V_f = the fibre volume fraction in the composite

V_m = the volume fraction of matrix in the composite

η_0 = fibre orientation distribution factor

η_1 = fibre length distribution factor

The fibre orientation distribution factor can be calculated using Krenchel's equation [8]:

$$\eta_0 = \sum_{i=0^\circ}^{180^\circ} V_{fi} (\cos \theta_i)^4 \qquad \text{Equation 4.3}$$

Where, θ is the measured fibre orientation angle.

η_1 can be estimated from shear lag theory (Cox[7]) which is described by:

$$\eta_1 = 1 - \frac{\tanh(\alpha l / d_f)}{\alpha l / d_f} \qquad \text{Equation 4.4}$$

$$\alpha = \sqrt{\frac{-3E_m}{2E_f \ln V_f}} \qquad \text{Equation 4.5}$$

Where, d_f is fibre diameter.

The values of η_0 and η_1 are listed in Table 4.8.

For comparison, the theoretical predictions and experimental results are plotted in Figure 4.12. Although the moulding pressure is only 7 bar which is not as high as that of typical compression moulding processes (5–10 MPa), the composites made by the developed hydrodynamic alignment process

showed a high degree of fibre packing efficiency due to the high fibre alignment level.

Table 4.8 Theoretical prediction of composites mechanical properties

Fibre type	Fibre volume fraction	η_0 *	η_1 *	Predicted tensile modulus	$\left\|\frac{(E_{Expt.} - E_{Predict})}{E_{Predict}}\right\| \times 100\%$
	Vf%			GPa	%
Tenax®-A HT C124-3mm	46	0.976	0.987	103	5
Tenax®-A HT C124-12mm	40	0.950	0.997	87	28
Toray_T800-7mm	42	0.960	0.995	121	28
Recycled-1.15mm	38	0.941	0.965	79	24

*η_0 – Fibre orientation distribution factor.

$*\ \eta_1$ – Fibre length distribution factor

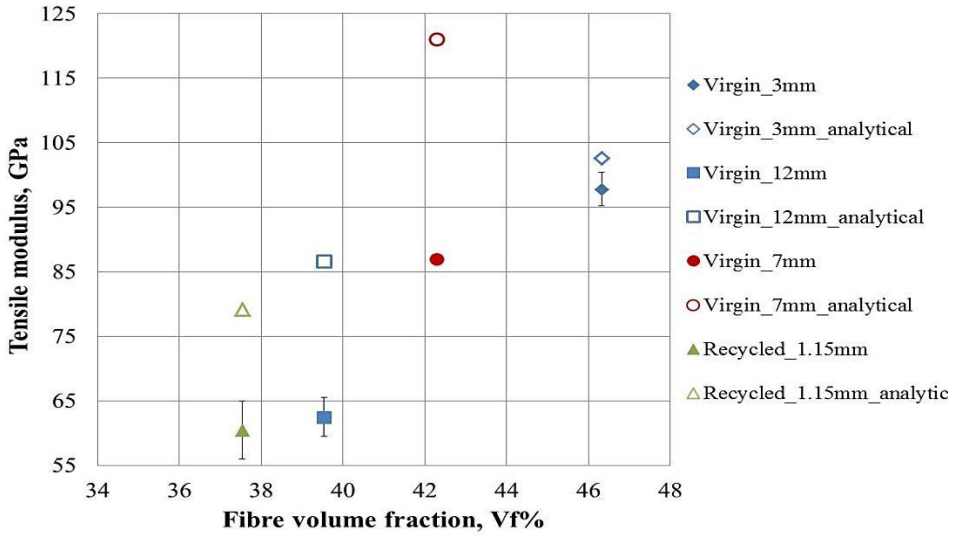


Figure 4.12 Experimental and predictive tensile properties of composites reinforced with 3mm,7mm and 12mm aligned fibre mats and 1.15mm aligned recycled fibre mats

As a result, a high tensile modulus and strength was achieved. With 46% fibre volume fraction, the 3mm fibre laminate composite gave a 98 GPa tensile modulus which achieves the closest agreement with the predicted value. This indicates that good fibre alignment has been achieved and the aligned fibre structure can make a significant improvement to the mechanical properties. With the same curing pressure (7 bar), the laminate made with 12mm fibre can only achieve 40% fibre volume content and obtained 62 GPa tensile modulus which is 28% lower than the predicted value (Table 5). The reason can be concluded as the 12mm fibre mat has a higher porosity compared to that of 3mm fibre aligned mat. Thus, during dewatering, the through thickness pressure difference of 12mm fibre mat is lower when the mat is not fully covered by glycerine which leads to the glycerine residue not being efficiently removed. However, the same washing method was applied for both 12mm and 3mm fibre mats and 12mm mat still contains glycerine residue after washing which is due to the higher initial glycerine content. Then the glycerine residue will affect material property during curing process. The T800 fibre has a smaller diameter (5μm) and when the fibre suspension has a same fibre volume concentration, the actual number of fibre filaments will be greater than with 7μm diameter fibres. Thus, the fibre to fibre interaction will be more significant and tend to reduce the alignment quality. As a result, T800_7mm fibre laminates exhibit 42% fibre volume fraction which is 8% lower (4% fibre volume fraction in difference) than that of 3mm fibre laminates. Due to this lower fibre content, the glycerine residual issue can affect its mechanical properties as well. Therefore, the experimental tensile modulus is 87 GPa which is 28% lower than the analytical value. The

recycled fibre has a 1.15mm fibre length on average. But 35% of the fibre is shorter than the average (1.15mm). Furthermore, 3% of fibre have a length smaller than the critical fibre length of 0.38mm. It is difficult to keep the aligned orientation of these short fibres during deposition process. Therefore, a 38% fibre volume fraction and 60GPa tensile modulus are obtained by the composite made by short recycled fibre. These specific properties are greater than alternative competing structural materials with the exception of carbon fibre composites and this shows the potential of fibre alignment for the manufacture of high value composites from recovered carbon fibre.

In other researchers' work, the properties of the aligned composites were also evaluated. By the conventional wet process, Piggott [5] manufactured aligned carbon/epoxy composites with 2mm long fibre which had 35% fibre volume fraction, these materials achieved 60 GPa tensile modulus and 650 MPa tensile strength. With 12mm long recycled fibre, Wong and Turner [1][10] manufactured carbon/epoxy composite samples with 45% fibre volume fraction and obtained 80 GPa tensile modulus which is 23% lower than the predicted value 103 GPa. This is due to the glycerine residual washing problem. HiPerDiF method was developed by Yu [11] to align short virgin fibre. In this process, water was used as dispersion media which can avoid any issues related to residual glycerine. On the other hand, the viscosity of water may not offer enough shear in dispersing longer fibre and fluffy recycled fibre. Composite samples were manufactured with 3mm carbon fibre to evaluate the mechanical properties. A calculated value of 21.5 bar pressure was applied to the prepregs during the curing process and 55% fibre volume

fraction was achieved. A 115GPa tensile modulus and a 1509MPa tensile strength was quoted for the small specimen size evaluated.

Nonwoven mats with aligned discontinuous fibres allow significantly better mechanical properties to be achieved, through higher fibre volume fractions in the composite and reduced fibre breakage during the moulding processes. A hydrodynamic process for achieving high levels of fibre alignment has been developed, based on existing technology, and the effects on alignment quality from processing factors have been explored and analysed. The composite laminates were made with 3mm carbon fibre under 7 bar curing pressure and had a tensile modulus of 98GPa and tensile strength of 826 MPa with a fibre volume fraction of 46%. Recycled fibre was also introduced in this work, a tensile modulus of 60GPa and tensile strength of 322 MPa was achieved by 1.15mm mean fibre length recycled fibre laminate composites with a fibre volume fraction of 38%. Demonstrating the potential of fibre alignment for the production of high value composites that give specific mechanical properties better than other widely used low cost metallic (i.e. aluminium alloy) and composite materials and approaching those of virgin carbon fibre composites.

4.4 Conclusion

Future work must now focus on developing alignment processes to a cost effective and commercially viable process. Further increase the potential of recycled fibre products in composites manufacturing industry and high value application market.

[1]. Wong KH, The potential for fibre alignment on the manufacture of polymer composites from recycled carbon fibre. In: Proceedings of SAE international journal of Aero space, 2009. p. 225–31.

[2]. Bagg G, Evans M and Pryde A 1969 Comps 1 97-100

[3]. Liu Z, Wong K, Thimsuvan T, Turner T and Pickering S 2015 20th International Conference on Composite Materials, Copenhagen Denmark

[4]. Richter H. Single fibre and hybrid composites with aligned discontinuous fibres in polymer matrix. In: Proceedings of ICCM-3. Paris, France, 1980.

[5]. A.K. Salariya, J.F.T. Pittman, Preparation of aligned discontinuous fiber pre-pregs by deposition from a suspension, Polym Eng Sci, 20 (12) (1980), pp. 787–797

[6]. A.R. Sanadi, M.R. Piggott, Interfacial effects in carbon–epoxies. 1. Strength and modulus with short aligned fibers, J Mater Sci, 20 (2) (1985), pp. 421–430

[7]. J.N. Coleman, U. Khan, W.J. Blau, Y.K. Gun'ko, Small but strong: a review of the mechanical properties of carbon nanotube–polymer composites, Carbon, 44 (9) (2006), pp. 1624–1652

[8]. Krenchel H. Fibre reinforcement: Theoretical and practical investigations of the elasticity and strength of fibre-reinforced materials. Copanhagen: Akademisk Forlag; 1964

[9]. H.L. Cox, The elasticity and strength of paper and other fibrous materials, Br J Appl Phys, 3 (March) (1952), pp. 72–79

[10]. Turner TA, Pickering SJ, Warrior NA. Development of high value composite materials using recycled carbon fibre. In: Proceedings of SAMPE, Baltimore, MD, USA, 2009.

[11]. H. Yu, K.D. Potter, M.R. Wisnom, A novel manufacturing method for aligned discontinuous fibre composites (High Performance-Discontinuous Fibre method), Composites Part A: Applied Science and Manufacturing, Volume 65, October 2014, p. 175-185,

5. Characterisation of through thickness permeability

5.1 Introduction

In paper making industry, the fibre suspension flows through the headbox to form a moist sheet and the moisture content is reduced in forming section (vacuums and aerofoils are used to drain the water), press suction and drying section (steam entering the stainless steel rolls is used to dry the sheet). The proportion of energy consumption and wt% of removed water in these sections are presented in Figure 5.1.

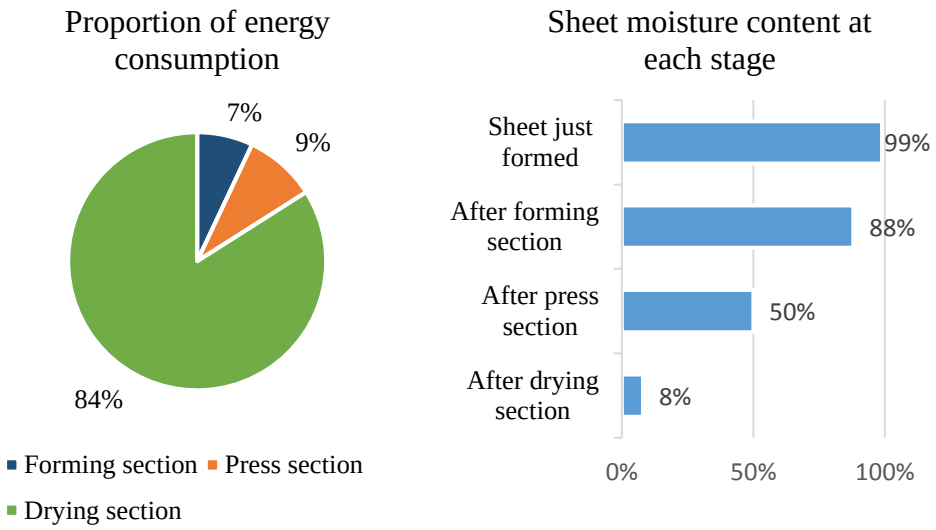


Figure 5.1 Plot of the proportion of energy consumption and sheet moisture content in forming section, press section and drying section of paper making process [1].

The dryer costs 84% energy to make the sheet moisture content be reduced from 50% to 8wt%. To reduce the energy costs, one of the advanced process control methods is maximising the removed moisture content entering the dryer to reduce need of steam. A 1% reduction in sheet moisture entering the dryer results in a 4% reduction in dryer steam demand [1]. The fundamental principles of deposition process and oven dry section in the hydrodynamic alignment process are similar to the forming section and drying section in the

paper making process. However, optimizing the vacuum draining process is not only to reduce the energy costs but also to maintain the aligned orientation of the deposited fibres.

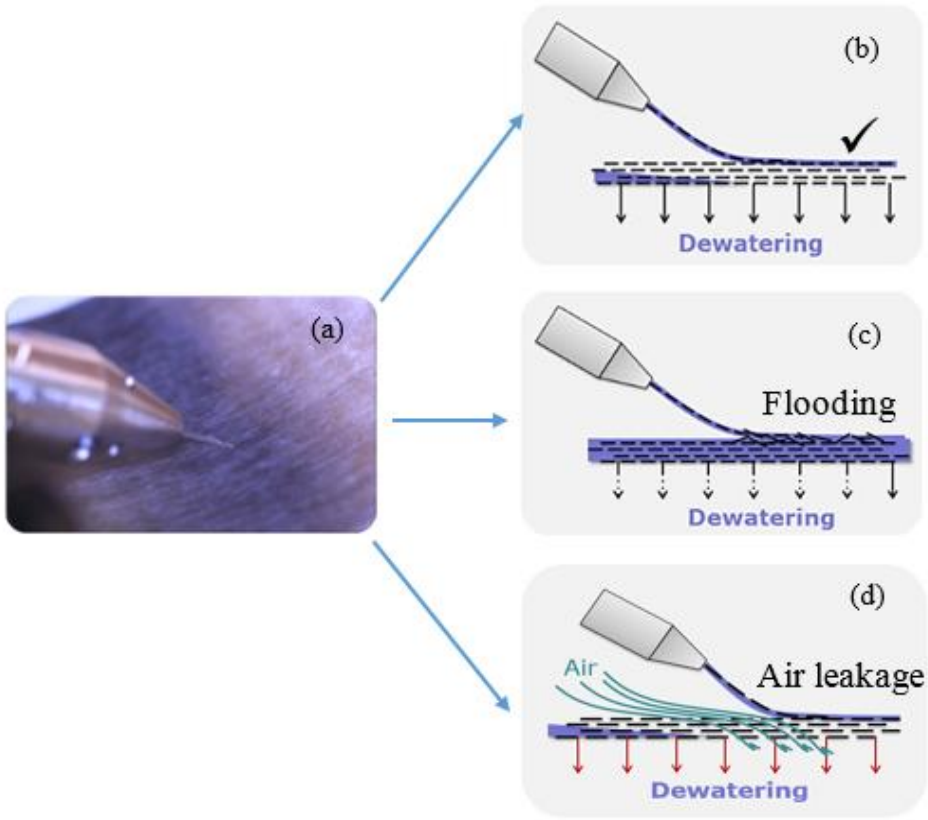


Figure 5.2 Dewatering situations in the deposition process. (a) depositing fibre suspension jet; (b) glycerine solution has been filtered out just before the next layer of mat is deposited; (c) low dewatering rate leads to flooding on the mat's top surface and the fibre orientation become flexible; (d) air flow through the fibre mat due to the excessive dewatering rate which will lead to extra energy cost to maintain the vacuum level.

Three dewatering conditions are shown in Figure 5.2. Ideally, the deposited glycerine has been filtered out just before the next layer of fibre is deposited. If the dewatering rate is smaller than the jet flow rate, flooding will be observed which leads to a reduction in alignment quality. However, if the dewatering rate is much higher than the deposition flow rate, air will flow though the dry mat. Therefore, more energy is required by the vacuum pump

to maintain the suction pressure required to maintain the through thickness liquid flow rate. In addition, leakage at the joint between the rotating drum and the containment vessel will cause further challenges in maintaining the suction pressure.

Permeability is identified as one of the key factors to determine how fast the liquid medium can be removed through the porous media. To explore the permeability of aligned fibre mat, both experimental and analytical prediction methods have been applied. The basic reference theory for experimental method is Darcy's Law which is commonly used to model the fluid flow through porous media. In this equation, all the complicated interactions which take place between the fluid and the fibre preform structure are accounted for in the permeability value. It requires many carefully controlled experiments and it has no predictive capability. Consequently, the prediction methods have been developed to speed up the design and measuring process. The Kozeny-Carman equation is the earliest and most widely used permeability prediction equation and has performed well in prediction work with low fibre volume fractions. The Kozeny-Carman equation is a kind of semi-empirical model based on correlation of experimental data. In this work, the through thickness permeability of aligned carbon fibre mat was measured and predicted. With predicted transverse permeability, the suction pressure required for dewatering the fibre mat with a target areal density can be calculated. Based on this suction pressure demand, vacuum pump selection and energy cost estimation are explored by an analytical model.

5.2.1 Design of permeability testing rig

Based on the Darcy's Law, the developed permeability rig is designed to measure the pressure drop through the fibre bed cross section and the mass flow rate of liquid under a constant supplied pressure.

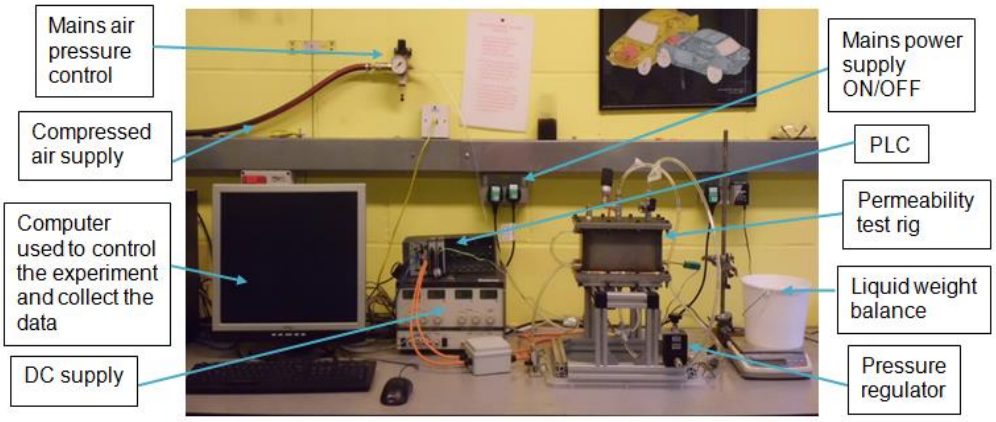


Figure 5.3 Permeability test rig and its main auxiliary components

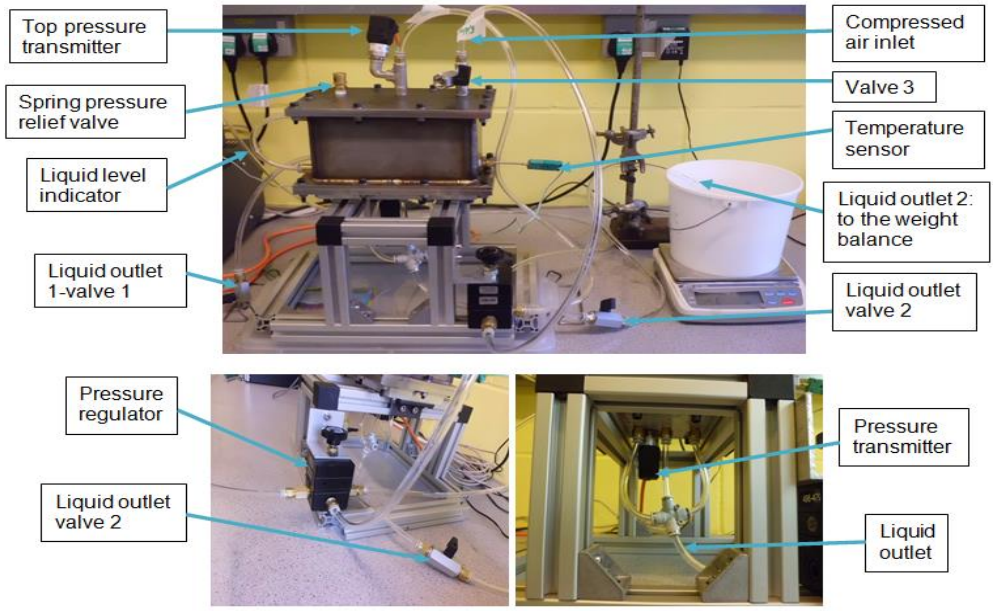


Figure 5.4 Permeability test rig

As shown in Figure 5.3 and Figure 5.4, the permeability testing is completed in cooperation with the test rig and its main auxiliary components. During the test, the rig tank is fed with glycerine solution before the tank cover has been affixed in place. After opening valve 2, liquid flow run through the sample,

the mass flow rate can be measured by the mass balance at the outlet. Together with liquid cross section area, the superficial velocity U_D is calculated. In addition, the pressure difference between top and bottom face of sample can be read from two pressure transmitters. Then the pressure drop gradient can be calculated with the mat thickness from separate compaction tests.

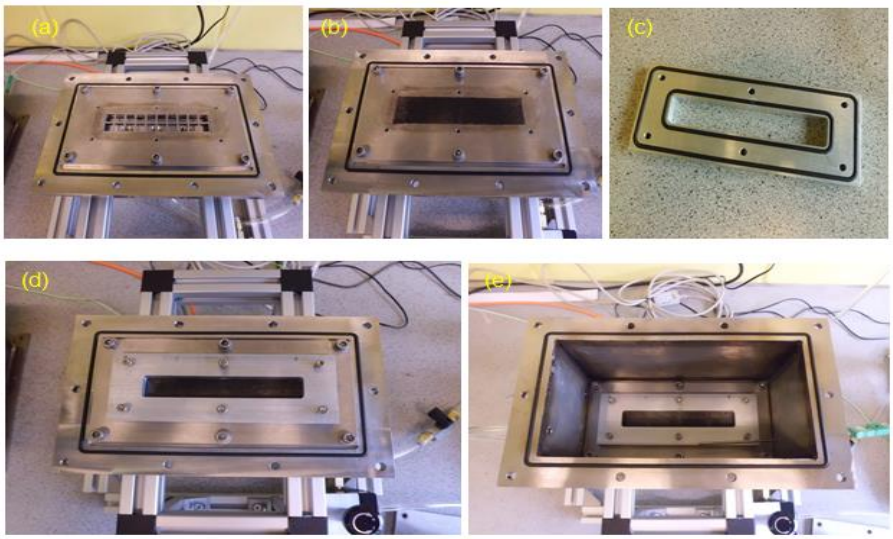


Figure 5.5 Photo of test rig inside and specimen laying procedure: (a) sample holder; (b) aligned carbon fibre mat lying on the mesh; (c), (d) sample fixed on the holder by the cover; (e) fixing the liquid tank;

Before the specimen laying procedure, the part below the sample holder should be filled with glycerine solution (87wt% glycerine) keeping the liquid level in the liquid outlet 2 the same as the height of the sample holder. The photo of the test rig inside and the specimen laying procedure is shown in Figure 5.5.

5.2.2 Testing material

To investigate the relationship between fibre orientation and the permeability of the mat, aligned short fibre, random short fibre and unidirectional

continuous fibre mats were employed in this experimental work. The material properties are listed in Table 5.1.

Table 5.1 Specification of fibre mat samples in permeability testing

Mat description	Fibre length	Fibre type	Fibre diameter
	mm		μm
30gsm aligned	3	Toray T700H	7
60gsm aligned	3	Toray T700H	7
100gsm aligned	3	Toray T700H	7
150gsm aligned	3	Toray T700H	7
100gsm random	6	Toray T600SC	7
100gsm unidirectional	*	Pyrofil TR50S	7

* unidirectional continuous carbon fibre

The measured density of the glycerine/water solution is 1105kg/m^3 and the viscosity is 145mPa*sec which is fixed by adjusting the weight percentage ratio of glycerine. A DV-II+ Pro viscometer manufactured by Brookfield company was used to measure the viscosity of glycerine and spindle S62 is recommended.

5.2.3 Permeability testing experimental design

Due to a limitation in material quantity, repeat tests have only been conducted for 30gsm, 60gsm and 100gsm mats. The details for the experimental procedure are listed below and some explanation points are also included. As a single layer of 30gsm aligned mat is thin and the fibre orientation is easily damaged by a high flowrate flow, the experiment starts from two layers of mat. For a porous media, the permeability is a pressure independent property.

However, the fibre mat configuration will change under different pressure levels which is defined as self-compaction behaviour. To explore the effects of self-compaction on permeability, various pressure levels were applied in the permeability test with 60gsm aligned short fibre mat.

Table 5.2 Material testing methods and experimental conditions

Sample	Number of layers	Pressure applied, bar	Number of tests
30gsm aligned fibre mat	2, 4, 6	0.3, 0.5	2 tests for each number of layers
60gsm aligned fibre mat	1, 2, 3	0.4, 0.35, 0.3, 0.2, 0.175, 0.15, 0.125, 0.12	
100gsm aligned fibre mat	1, 2, 3	0.3, 0.5	
150gsm aligned fibre mat	1, 2	0.3	1 tests for each number of layers
100gsm random discontinuous fibre mat	1, 2		
100gsm unidirectional continuous fibre mat	1, 2		

5.2.4 Permeability prediction

In the permeability testing, the fluid mass flowrate and pressure difference across fibre mat can be measured. Furthermore, the fibre mat thickness under different pressures can be measured through the compaction testing. The permeability of the fibre mat can then be calculated using Darcy's Law. Fibre volume fraction of the aligned mat can be worked out by the mat thickness, areal density and fibre density. Therefore, the Kozeny-Carman constant, C, can be obtained and be used in further permeability prediction and

comparison with the experimental results. The schematic diagram of the Kozeny-Carman permeability prediction procedure is stated in Figure 5.6.

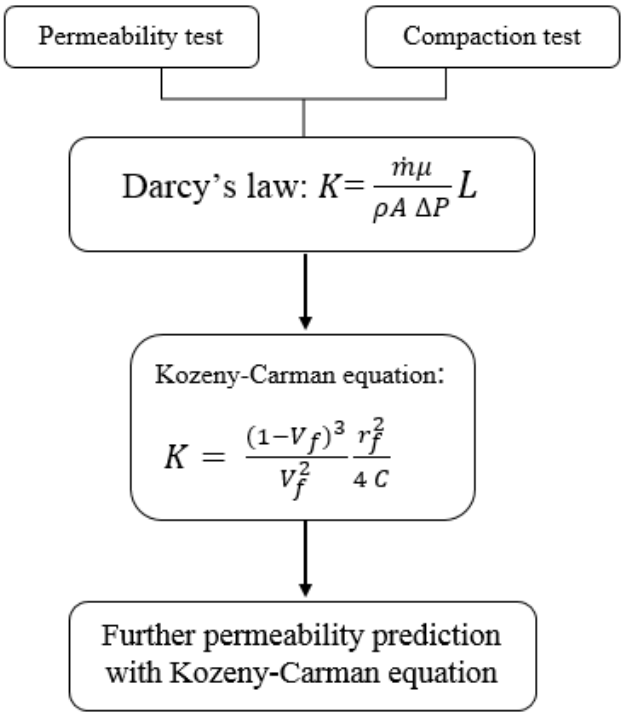


Figure 5.6 Methodology of permeability prediction with Kozeny-Carman equation

5.2.5 Fan performance analytical model

In the deposition process, glycerine solution is dewatered through the fibre mat by the vacuum suction around the rotating drum. As described in Figure 5. (b), if glycerine solution has been filtered out just before the next layer of mat is deposited, the vacuum suction plate is always fully covered by glycerine and the air flow rate should be a lot less than that of air leakage situation. In this case, the dewatered glycerine flow rate is equal to the depositing flowrate, and the required total suction pressure can be calculated following the pressure in Figure 5.7.

For a target areal density mat, the required dewatering pressure difference across the fibre mat can be stated as a function of fibre volume fraction which is based on the Kozeny – Carman equation and Darcy's law. In addition, the relationship between fibre volume fraction and compaction pressure can be observed from the compaction test results through curve fitting. Following Poiseuille's law, the head loss through the vacuum slots can be calculated. Then, the total pressure difference, in another word, the suction pressure required for dewatering a fibre mat with target areal density can be calculated.

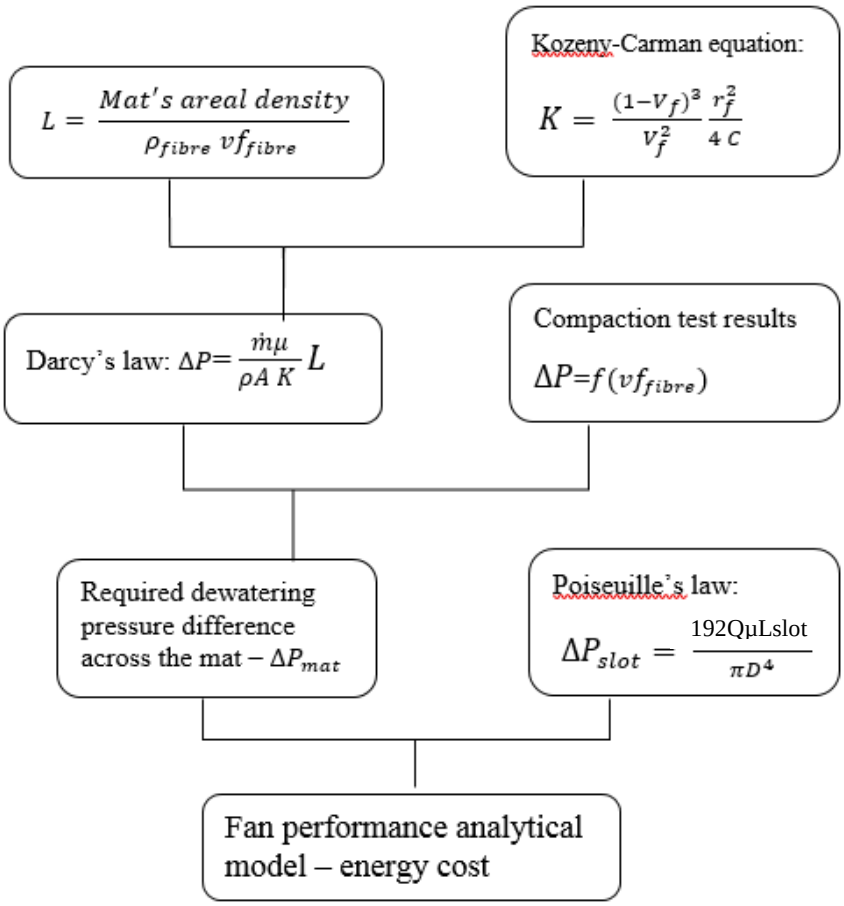


Figure 5.7 Estimating required dewatering pressure difference across the mat

The detailed information of variables is listed in Table 5.3. As described in Chapter 3, a stable suspension jet can be achieved when the Weber number is

in the range 4 to 8. In this analytical model, A slot type vacuum platen is used, the dimensions can be found in Table 5.3:

Table 5.3 Variables applied in analytical model

Fibre mat length	924mm	Suspension density	1250 kg/m^3	Vacuum slot length	150mm
Fibre mat width	150mm	Suspension viscosity (15°C)	0.5 Pa*s	Vacuum slot width	0.5mm
Fibre density	1800 kg/m^3	Suspension jet mass flow rate	0.12 kg/s (We=8)	Vacuum slot depth	5mm
			0.085 kg/s (We=4)	Number of slots	180

A fan selection analysis was undertaken to optimise the relationship between energy cost and dewatering rate, especially for the air leakage case. In this case, air is flowing through the suction box which leads to a significant reduction of vacuum level as the fan power is finite and the energy cost will be increased significantly. Various kind of pumps were investigated and their performance curves at 11kw are shown in Figure 5.8. The benchmark curve describes the behaviour of "perfect fan" which has a constant efficiency 60% under all conditions. In the current process, a liquid ring pump has been used, as it can maintain very high suction pressure (0.99bar) but only when the air flowrate is below 0.4 m^3/s. When the leakage air flowrate is above this boundary, the liquid ring pump is not able to maintain any vacuum. Thus, a pump selection was undertaken in this work. As shown in the figure below, the medium pressure radial blower can provide 0.1bar suction pressure even the air flowrate is 3 m^3/s. The 2-stage side channel blower and high pressure radial blower curves are in the middle range.

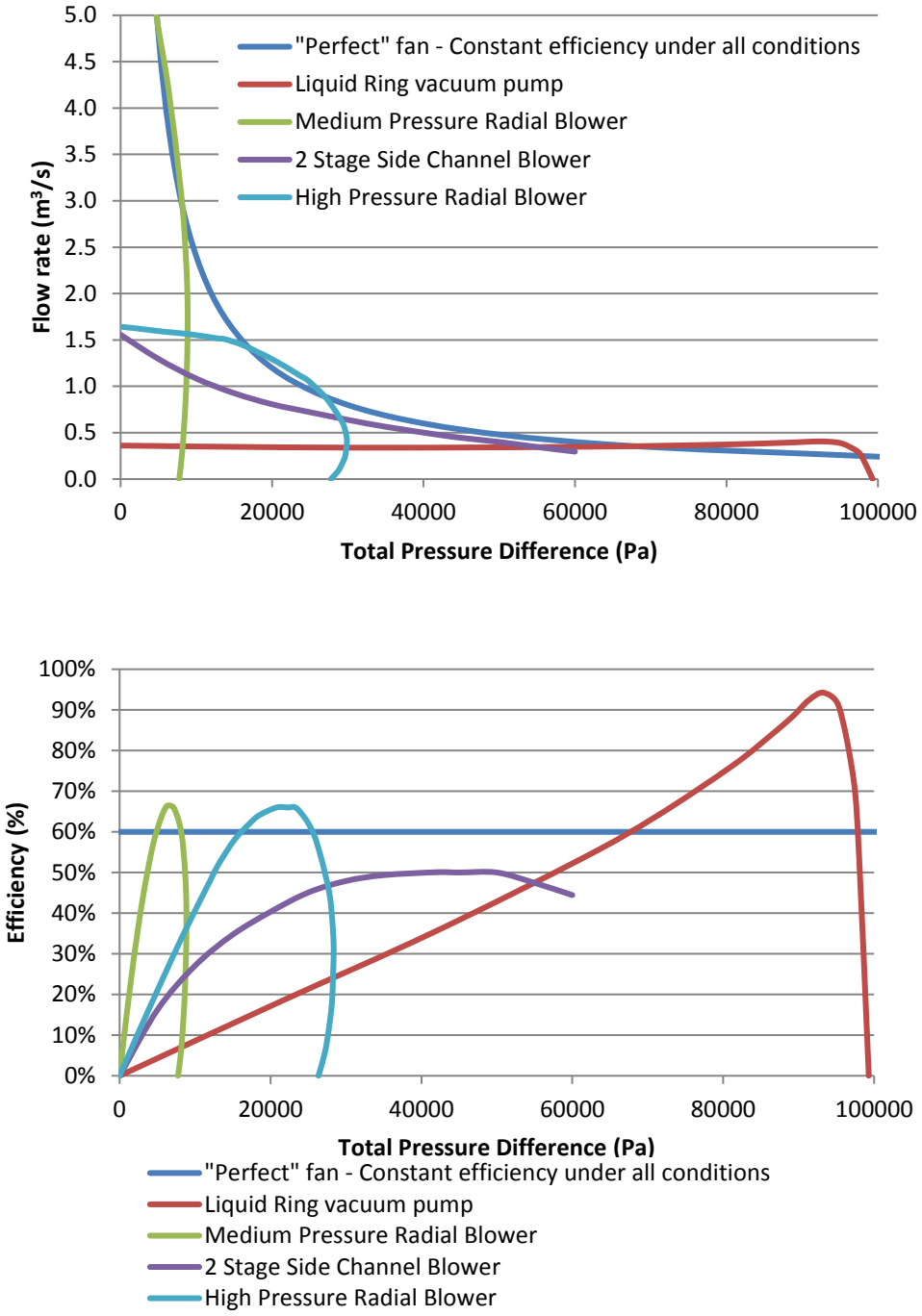


Figure 5.8 Fan performance curves

Figure 5. 5.9 describes the calculation procedure of evaluating the maximum suction pressure can be achieved when the rig has a certain leakage level.

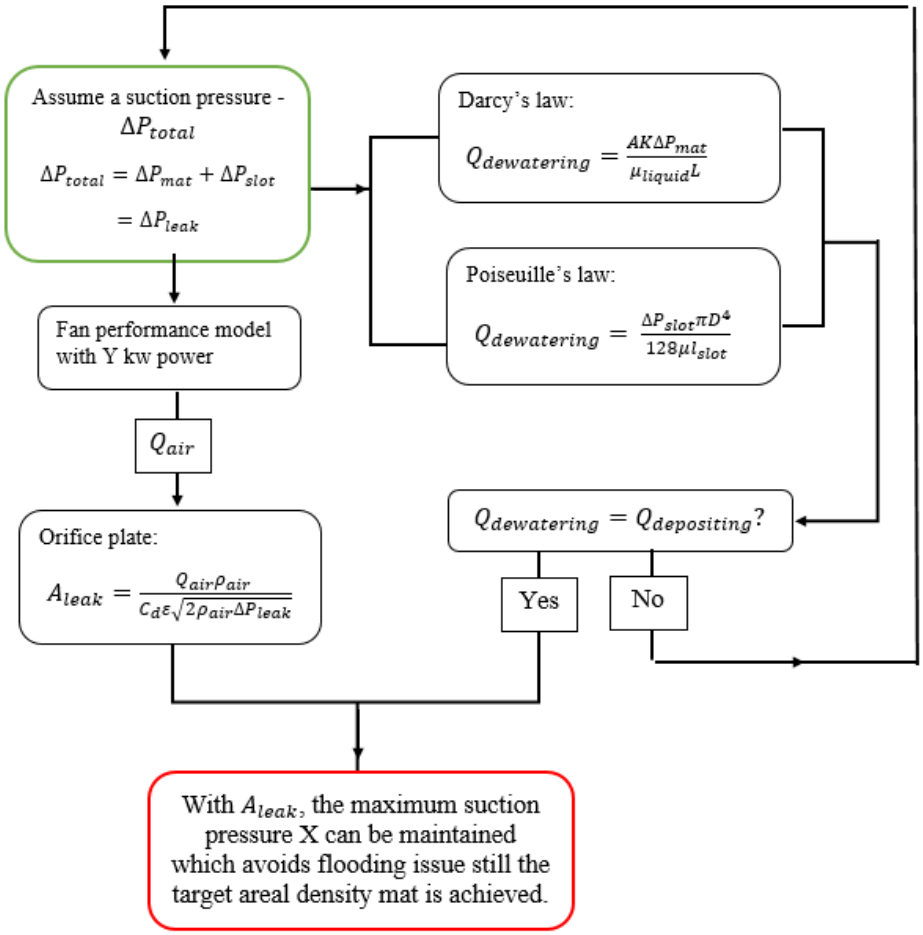


Figure 5.9 Estimating the maximum suction pressure can be achieved with a certain leaking area

5.3 **Results and discussion**

5.3.1 Effects of fibre orientation on fibre mat permeability

In three permeability tests, 0.3 bar pressure was applied on the top of the material (unidirectional continuous virgin fibre mat, aligned 3mm virgin fibre mat and random 6mm virgin fibre mat) respectively. All these specimens have same total areal density – 200gsm. The permeability results are listed in Figure 5.10. According to the highly packed unidirectional fibre orientation, there is a 0.23bar pressure loss across the UD fibre mat and resulting a 51% fibre volume fraction. Although the aligned fibre mat can finally achieve 50% fibre volume fraction when 10bar pressure was applied in the compaction test,

only 14.72% fibre volume fraction is observed in this permeability test. However, the fibre volume fraction in random fibre mat is 6% which indicates there is only a 9% reduction comparing to that of the aligned fibre mat. As a conclusion, under the same pressure, the fibre volume fraction of aligned fibre mat is close to the random short fibre mat, as the misaligned fibres make the close packed configuration is difficult to achieve. However, although the fibre volume fraction is low, the interstices between fibres could have been blocked (referring to the fibre orientation) which results a low permeability value and close to the UD fibre mat's property. This behaviour will be explained with a schematic diagram in the next sub-section.

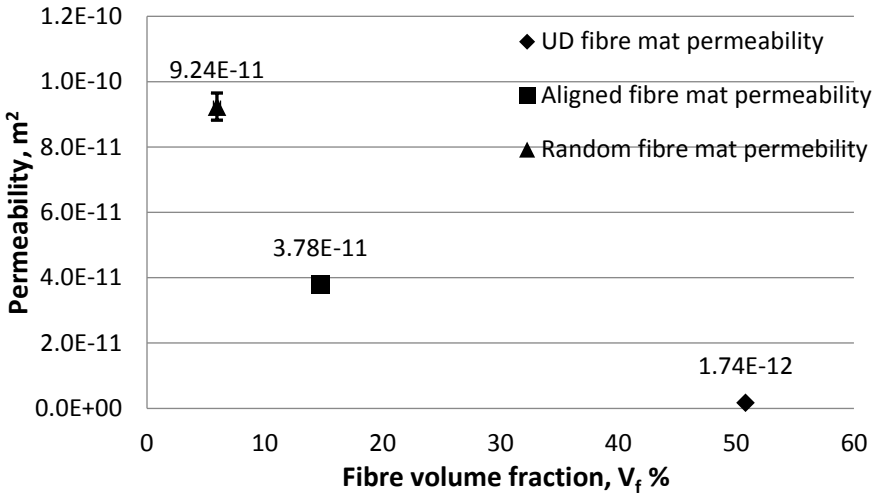


Figure 5.10 Permeability results of fibre mats with different fibre orientation – unidirectional continuous virgin fibre mat, aligned 3mm virgin fibre mat and random 6mm virgin fibre mat

5.3.2 Aligned fibre mat permeability prediction

To evaluate the self-compaction effects on aligned fibre mat permeability, 60gsm/layer, 3mm aligned fibre mats were used in the permeability test. Various pressure levels (below 0.1bar) were applied on the mat to achieve different fibre volume fraction value. The permeability results are shown in

Figure 5.11, and Kozeny-Carman constant, C, is 10.92 which is evaluated from the Kozeny-Carman equation.

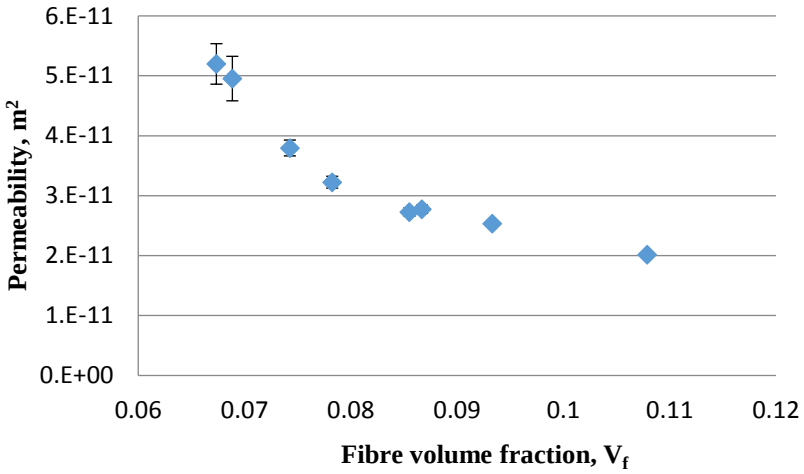


Figure 5.1 Permeability results of 60gsm/layer_ 3mm aligned fibre mat with different fibre volume content

The effects of fibre mat self-compaction behaviour on permeability (Figure 5.11) can be explained with the schematic diagram in Figure 5.12. Initially, the fibre volume fraction is low (0.65%), and liquid can easily flow through the interstices between fibre which indicates a high permeability. Under increasing load, the gap size is reduced and the permeability decreased rapidly (6.5% < vf% < 9%). After the fibre-fibre gaps have closed, it is more difficult for liquid to travelling through the fibre mat, but the space between fibres (especially between aligned and misaligned fibres) can be compacted to even smaller size. This behaviour can be observed in the permeability results as well. When fibre volume fraction is higher than 9%, the reduction of permeability becomes more gradual.

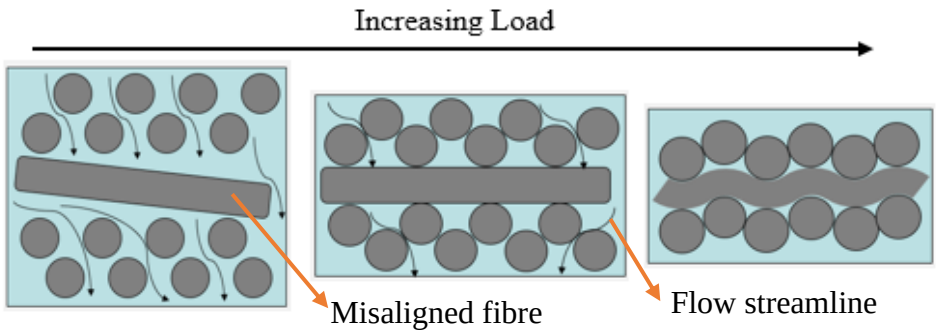


Figure 5.12 Cross section schematic diagram of aligned mat – self-compaction behaviour affects the permeability

The experimental permeability results of 3mm aligned fibre mats are shown in Figure 5.13and detailed specimen properties are listed in Table 5.4. The calculation procedures were described in the previous section. When the pressure across the mat is higher than 0.02bar, the predicted and experimental permeability achieved a good agreement. However, when the pressure difference is lower than 0.02bar, the experimental results have a large standard deviation which may be due to the measuring sensors being less accurate in this range.

Table 5.4 Properties of the specimens involved in experimental and predicted permeability comparison

Sample	Number of layers	Pressure applied, bar
30gsm aligned fibre mat	2, 4, 6	0.3, 0.5
60gsm aligned fibre mat	1, 2, 3	0.3, 0.5
100gsm aligned fibre mat	1, 2, 3	0.3, 0.5
150gsm aligned fibre mat	1, 2	0.3

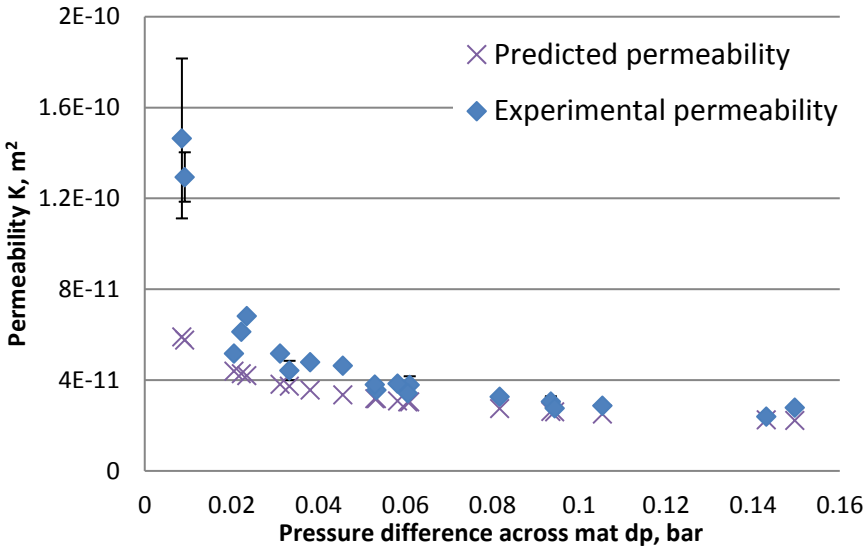


Figure 5.2 Experimental and predicted permeability results for 3mm aligned fibre mat

5.3.3 Fan selection and energy cost analytical model

The required suction level for dewatering an aligned fibre mat with target areal density is calculated and plotted in Figure 5.14. In order to maintain the stability of the suspension jet, the We number of the jet should be limited in the range of 4 to 8. Thus, for the physical size of deposition area currently modelled, the flow rate of jet needs to be controlled in 0.085 kg/s and 0.12kg/s. Using this flow rate range in the calculation, the boundary of dewatering suction level for the target areal density is marked with grey colour in Figure 5.. For example, if the target areal density is set as 500gsm, the required dewatering suction pressure is between 0.35bar to 0.54bar. In this region, the higher the vacuum level can be provided, the greater the production rate can be achieved (due to the larger depositing flow rate).

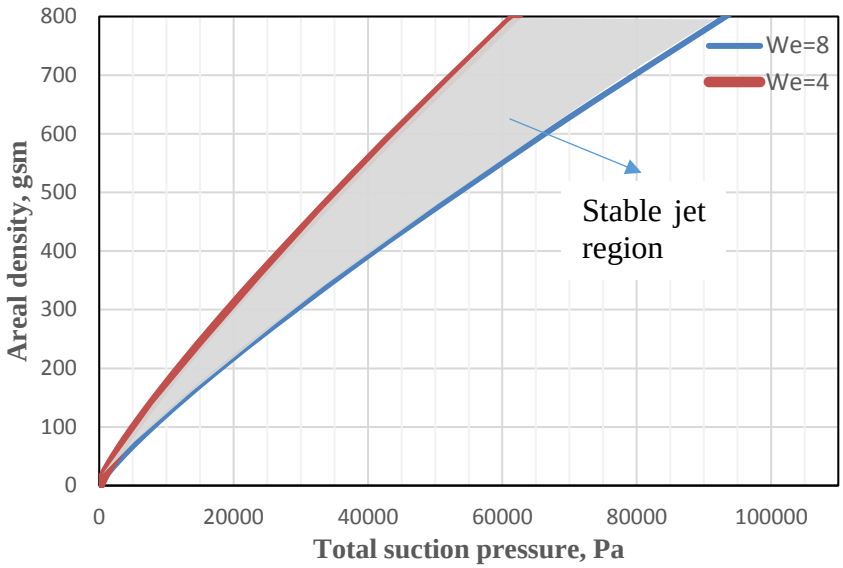


Figure 5.3 The suction pressure value is required to avoid flooding issue when dewatering an aligned fibre mat.

Three different pumps are investigated here. If there is no air leakage, a high pressure radial blower, 2-stage side channel blower and liquid ring pump can maintain 0.12bar, 0.6bar and 0.99bar suction pressure, respectively (Figure 5.). The leaking area ratio is defined as percentage of leakage area divided by the depositing area (mat area).

The current target mat areal density and power requirement by liquid ring pump is 100gsm and 11kw. In dewatering, a suction pressure between 0.5 and 0.8 bar is required. If the leaking area ratio is over 2.5%, a high pressure radial blower should be employed. As it can provide 0.084bar which is higher than the pressure from a 2-stage channel blower with the same energy cost (6kw). In addition, the liquid ring pump is not able to maintain 0.05bar vacuum level, although 11kw power is used. However, when the leaking area ratio is lower than 2.5%, a 2-stage channel blower is the best choice due to the reduced energy cost.

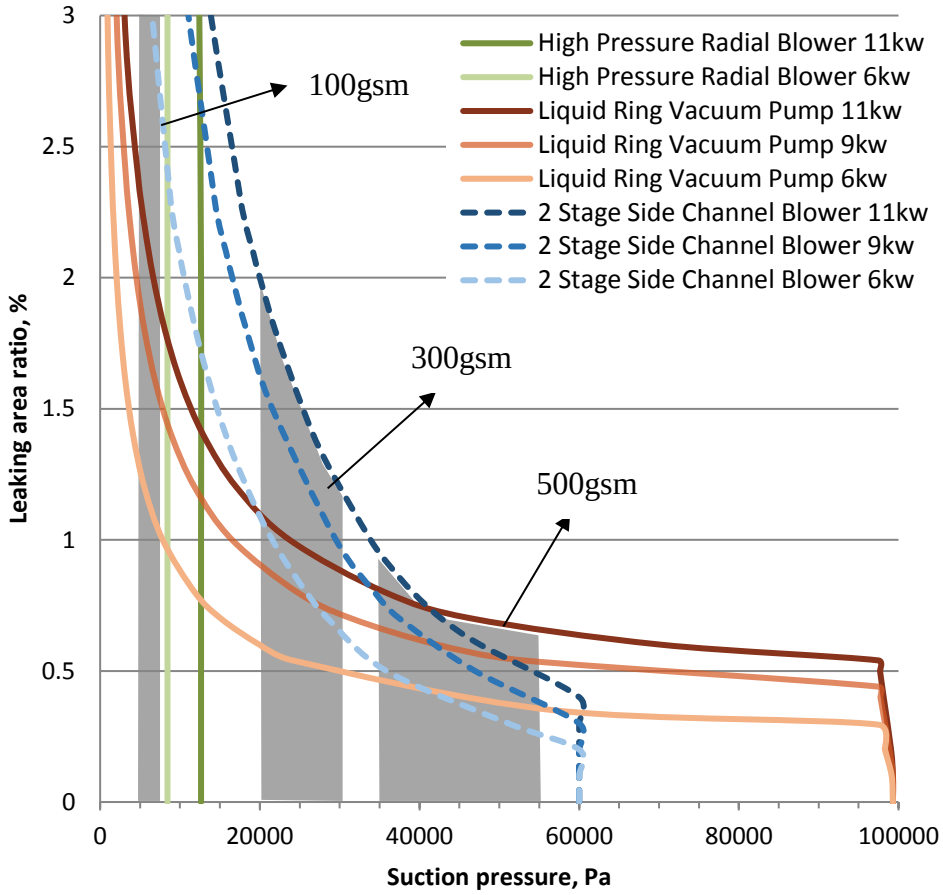


Figure 5.4 With different input power, suction pressure provided by different pump referring to various leaking area ratio.

When the target areal density is set as 300gsm, a suction pressure between 0.2 and 0.3bar is required. The leaking area ratio needs to be lower than 2% otherwise the energy cost will be higher than 11kw. The modelled high pressure radial blower is not able to achieve this pressure range (unless the energy input is permitted to increase). Comparing with the liquid ring pump, a 2-stage channel blower is the optimal option, as it can maintain a higher vacuum level with a lower energy cost. Setting 500gsm as the target area density, the suction pressure is expected in the range of 0.35 to 0.55bar. As observed in Figure 5., if the leaking area ratio is limited below 0.74%, liquid ring pump should be chosen, and the high suction pressure can be provided

under low energy cost. Thus, a higher production rate can be achieved through a larger depositing flowrate. If the areal density of the mat is expected to be above 800gsm, only a liquid ring pump is sufficient. In addition, the restriction of leaking area ratio is strict, and the maximum allowance is 0.65%.

5.4 Conclusion

A permeability testing rig was designed based on the Darcy's law. Materials with different of fibre orientation were applied in permeability testing. Unidirectional continuous fibre mat (UD fibre mat) has the smallest permeability. In addition, the permeability of aligned fibre mat is much closer to the UD fibre mat although a relatively low volume fibre volume fraction of 14.72% was observed. Based on the experimental permeability results, the Kozeny-Carman constant, C, is defined as 10.92 for the aligned fibre mat. Thus, the Kozeny-Carman equation was applied to predict the permeability value in the subsequent analytical model related to vacuum pump selection and energy cost consumption. For the current deposition process, the target fibre mat areal density is set as 100gsm. A liquid ring pump has been applied in the current experimental work and it is an appropriate choice when an extremely thick mat is expected (more than 500gsm). However, the leaking area ratio is strictly restricted to below 0.75%. If the leaking area ratio is above 2.5%, a high pressure radial blower is the optimal choice, it can maintain 0.084bar suction pressure under 6kw energy cost and high production rate (We=8) become achievable. A 2-stage channel blower is preferred when the target areal density if 300gsm, but the leaking area ratio should be limited to below 2%. The analytical model described in this chapter

can be used to optimise the current process and be considered as a design guideline for process scale up.

References

[1] Austin, Paul, Reducing energy consumption in paper making using advanced process control and optimisation, Engineering for a Low Carbon Future Seminar, University of Cambridge, London. Vol. 3. 2010.

6. Characterisation of dewatering behaviour

6.1 Introduction

In deposition process, glycerine is filtered out though the vacuum slots on the rotating drum. The main objectives here are to identify the best dewatering opening geometry for the deposition drum and explore the best combination of pressure distribution media. A high pressure difference across the fibre mat itself is preferable as it accelerates drainage. In addition, the pressure difference should be applied evenly throughout the deposition region i.e. to have homogeneous through-thickness flow. For example, if two adjacent openings are too far apart, a wet region may be left between them during the dewatering state. A dry patch appears at the opening area, and air is flowing through (Figure 6.1). This will reduce the suction pressure which lead to an extra energy cost. In addition, the inevitable lateral flow that this causes will degrade the alignment quality. In order to understand the flow behaviour and to identify an optimum opening design, a series of tests have been implemented.

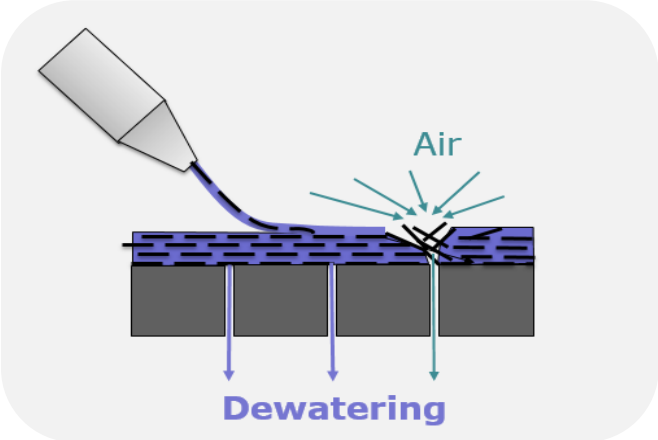


Figure 6.1 Dry patch appears at the opening area which lead to a reduction of suction pressure and affects the aligned fibre orientation

6.2.1 Vacuum plate dewatering test

A schematic drawing of the dewatering test is shown as Figure 6.2, and the experimental setup is shown in Figure 6.3. Solid walls of height 60mm were built around the suction plate and sealing tape was applied along the joining edges to form a leak-free container (approximate dimensions 136mm×170mm×60mm). One layer of fine nylon mesh was placed between the fibre mat and the suction plate (Figure 6.2). The length and width of 100gsm random fibre mat and nylon mesh match those of the suction plate. A pressure gauge was used to measure the vacuum level inside the bottom outlet plenum. An orifice plate was connected to the outlet pipe to measure the air mass flow rate. For each test, the experimental procedure was recorded by a camera for later analysis.

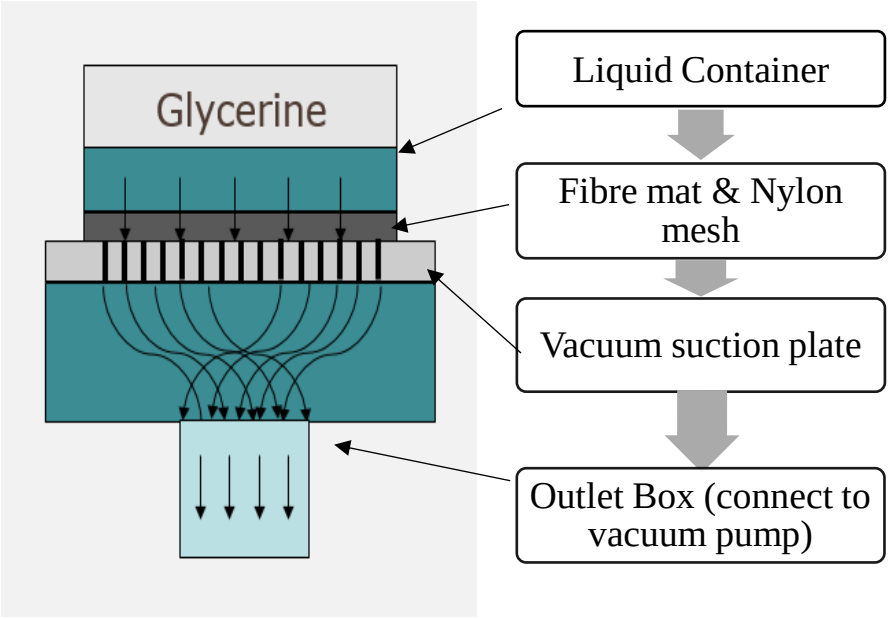


Figure 6.2 Dewatering test with vacuum suction plate



Figure 6.3 Experiment set up of vacuum suction plate dewatering test – glycerine was feeding manually before the dewatering process started.

Table 6.1 Dimensions of vacuum plates

Slot plate					
Plate name	Slot width		Slot length		Adjacent space
3 slots plate	0.5mm		150mm		50mm
5 slots plate	0.5mm		150mm		25mm
21 slots plate	0.5mm		150mm		5mm
Perforated plate					
Diameter	Spacing		Number of Rows		Number of holes
	Axial	Radial / Row	Axial	Radial / Row	
0.5mm	7.5	10.8	19.5	122	357

Four vacuum plates were manufactured from 3.5mm thick aluminium plate and each has a different configuration of opening design. They can be grouped in to either slot or hole configuration. The dimensions of the plates are shown in Table 6.1. For the slot design, the width and length of slot are 0.5mm and 150mm respectively. The perforated plate was designed basing on the filtration plate, the hole diameter is 0.5mm and there are 357 holes in total.

6.2.2 Nylon mesh selection

Nylon mesh was placed around the deposition drum, in order to achieve a uniform pressure distribution across the plate. Thus, the aligned fibre orientation won't be damaged during the depositing and dewatering processes. If the wire size is too fine, it will lead to flooding because of the high flow resistance. On the other hand, a coarse mesh would cause unwanted deformations in the deposited fibres.

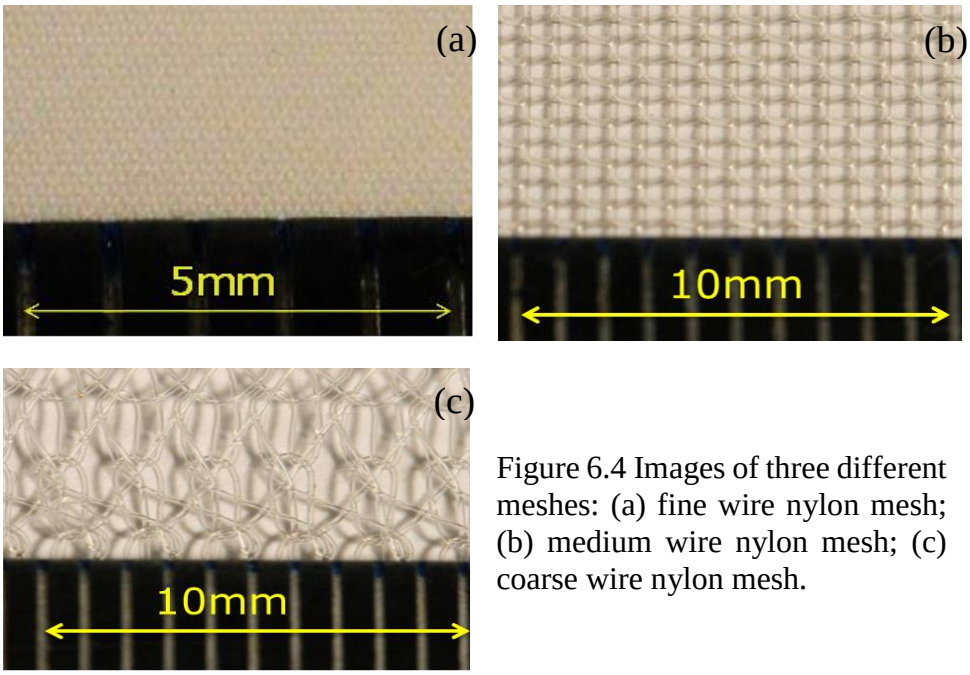


Figure 6.4 Images of three different meshes: (a) fine wire nylon mesh; (b) medium wire nylon mesh; (c) coarse wire nylon mesh.

To select the optimum configuration mesh selection testing was undertaken prior to fibre mat manufacture. A permeability testing was used to measure the flow resistance of different nylon meshes, and aligned fibre mats were manufactured to identify the influences of pressure distribution on fibre orientation. The permeability testing procedures were described in the previous chapter, and Figure 6.4 presents the close-up images of

pore size for the three different nylon meshes. The design of permeability test is listed Table 6.2.

Table 6.2 Nylon mesh selection – Permeability test design

Test No.		Coarse mesh	Medium mesh	Fine mesh
1	Number of mesh layers	1	*	*
2		*	1	*
3		*	*	1
4		2	1	*
5		3	1	*
6		2	2	*
7		2	2	1
8		1	1	1

6.3 **Results and analysis**

6.3.1 Slot vacuum plate dewatering behaviour

Photo a, b and c in Figure 6.5 were taken when the first dry patches were observed on two layers of 100gsm random fibre mat during the dewatering behaviour test with the 3 slot, 5 slot and 21 slot vacuum plate.

For the 3-slot and 5-slot plate, the first dry patch appeared around the slots, although glycerine still covers the mats area between two slots. With the 21-slot design, the localised dry patches are almost invisible due to the higher open area density and smaller solid space between slots. Thus, the pressure difference across the suction plate and mat is more evenly distributed.

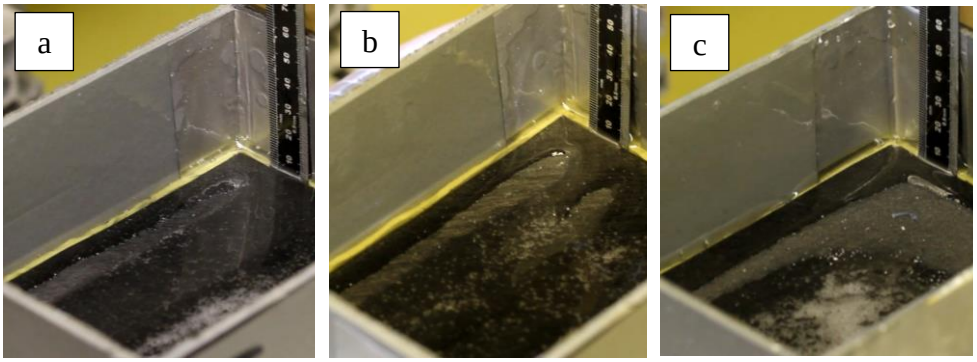


Figure 6.5 Dewatering test – slot type plates with two layers 100gsm random fibre mats: 3 slots plate (a), 5 slots plate (b), 21 slots plate (c).

The pressure difference across fibre mats and slots plate were measured and plotted with solid lines in Figure 6.6. The dashed lines indicate the air mass flow rate through the fibre mat which is measured by orifice plate flow meter. The orange marker on each pressure drop line shows the time when the top surface of the mat was totally dry (by visual observation). In each case, when air leakage appeared, there was still glycerine remaining in the mat surface. This indicates the pressure difference is not even. The shorter time it takes from the appearance of the first dry until the top surface is totally dry, the more uniform pressure difference distribution has been achieved. Although over 0.8 bar pressure difference can be achieved with all these three plates, it will suddenly drop to lower than 0.2 bar after the first air leakage appeared which will reduce the dewatering efficiency. This due to the limited air flow capacity of the vacuum pump used.

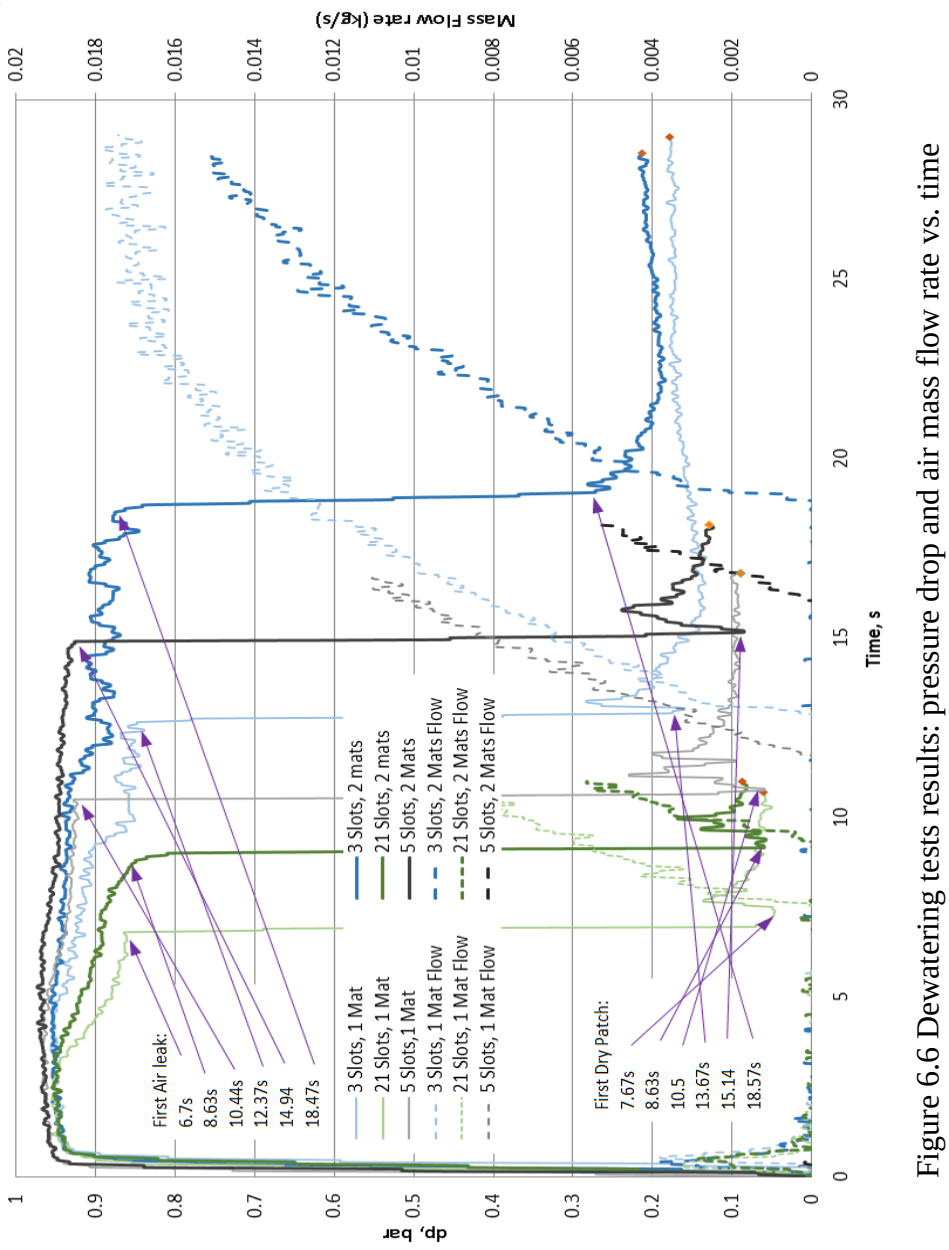


Figure 6.6 Dewatering tests results: pressure drop and air mass flow rate vs. time

6.3.2 Perforated plate dewatering behaviour

Figure 6.7 shows the photos from the perforated plate dewatering tests. Even before dry patches appeared there was evidence of some black marks, There were some black marks appearing on the fibre mat before dry patches present. these marks indicate that the liquid flow was concentrated in the region around the holes. However, because of the reduced liquid thickness the

pressure distribution issue was improved when the perforated plate design was used. In this case the dewatering was more homogeneous; small circular dry patches were not observed after the appearance of the first dry patch.

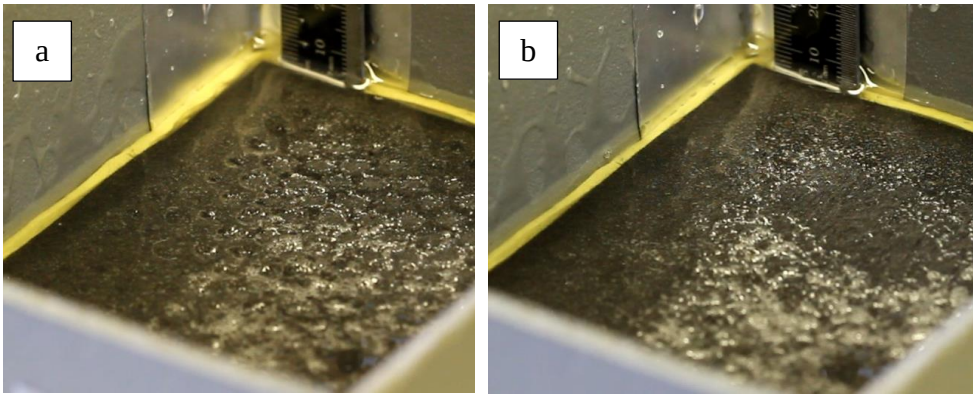


Figure 6.7 - Perforated plate dewatering tests: (a) & (b) with two layers of fibre mats, photos for before and after the dry patches appeared.

Figure 6.8 shows the pressure difference across the fibre mats and vacuum plate with orange solid lines and orange dashed lines indicating the air mass flow rate through fibre mat which is measured by an orifice plate flow meter. The red markers on the pressure drop line indicate the time point at which the top surface of the fibre mat was totally dry. Between the appearance of the first air leakage and a dry top surface, the pressure drop doesn't rapidly reduce to the minimum level (around 0.55bar). In addition, the mat is still evenly saturated as there is no significant air mass flow rate at this time. As the result of the reduced open area, the perforated plate was seen to maintain the pressure drop above 0.5 bar even after the mat was completely dry. Following this testing a new deposition rig was made with the drum design according to the perforated plate pattern in order to achieve a higher dewatering rate by making a more even pressure difference distribution and thus better use of the available pumping power.

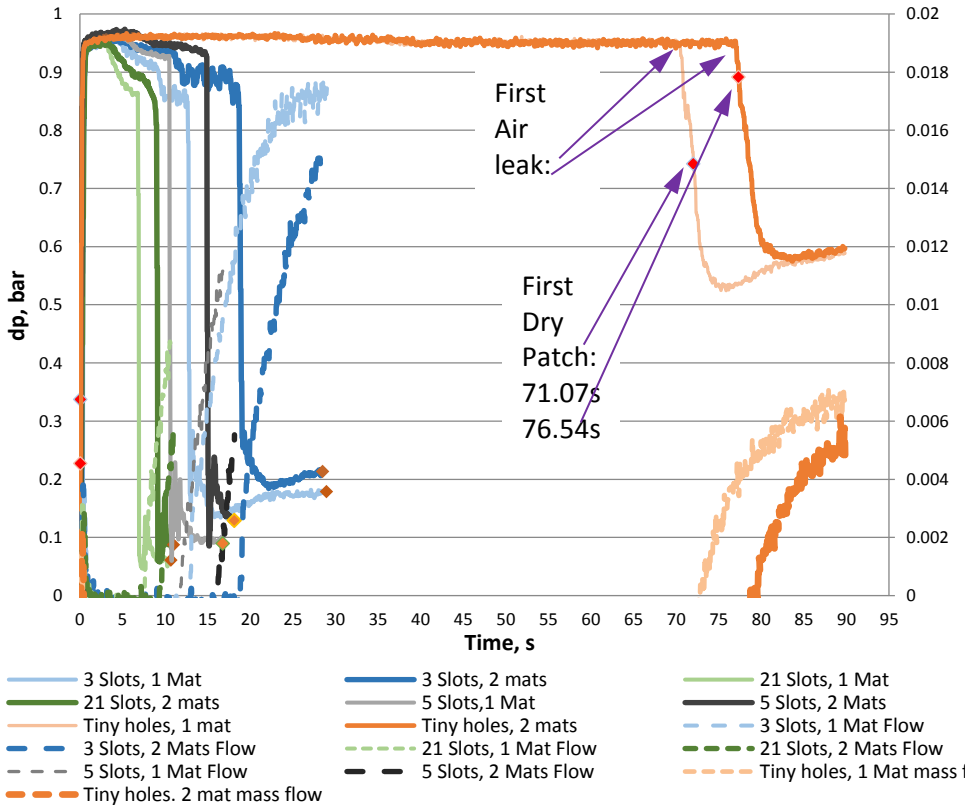


Figure 6.8 Perforated plate dewatering tests results: pressure drop and air mass flow rate vs. time

6.3.3 Nylon mesh permeability and mats

As a baseline, one layer of coarse nylon mesh and one layer of medium mesh was attached around the deposition drum before deposition began. Figure 6.9 shows the fibre orientation of a 30gsm 12mm fibre mat which was manufactured with this original configuration of meshes. There are some black dots on the mat which indicate the position of holes, and the fibre orientation is clearly affected by the lateral liquid flow caused by uneven pressure distribution. Therefore to optimise the configuration of pressure distribution media and improve the fibre alignment quality a DOE was undertaken.

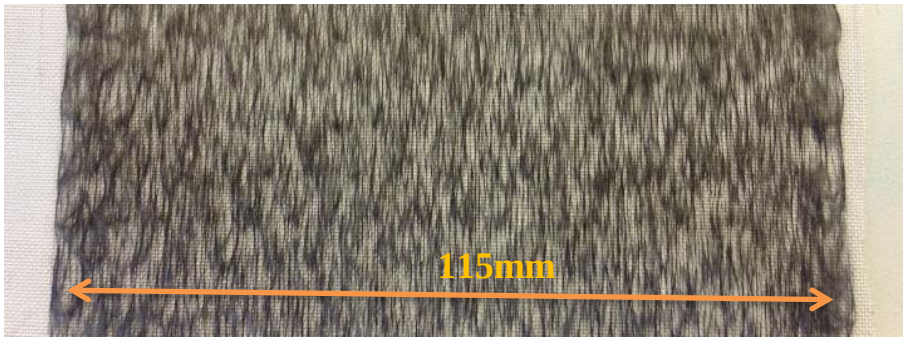


Figure 6.9 – 30gsm fibre mat made by the new alignment rig (12mm fibre length).

The permeability results for a single layer of fine, medium coarse and coarse mesh are given in Figure 6.10. Where multiple layers are used the meshes will exhibit self-compaction behaviour. In order to describe this behaviour a flow resistance number was introduced and defined as:

$$\text{Flow resistance number} = \frac{permeability}{sample\ thickness} \qquad \text{Equation 6.1}$$

Basing on the Darcy's law, the flow resistance number is used to indicate the relationship between the pressure drop across the material and the volume flow rate of the liquid. The flow resistance number of various nylon meshes are given in Figure 6.11, and the corresponding images of aligned fibre mats obtained are in Figure 6.12. Comparing with the original lay-up order (1-1-0, one coarse and one media mesh), additional layers of coarse mesh cannot make a significant improvement in fibre orientation (photo a &b in Figure 6.12). Replacing a layer of course mesh with a layer or medium mesh (2-2-0 instead of 3-1-0) results in a 0.8% increase in the flow resistance number. The alignment quality has been improved as shown in Figure 6.12_c, although fibres become small bundles and the gaps among them are clearly visible.

In the final stage of testing the influence of a fine mesh was investigated. The 2-2-1 configuration makes the flow resistance number increase by 6%, compared with 2-2-0. Furthermore, fibres are uniformly aligned as shown in Figure 6.12_d. The inclusion of a fine mesh greatly improves the performance of the set-up.

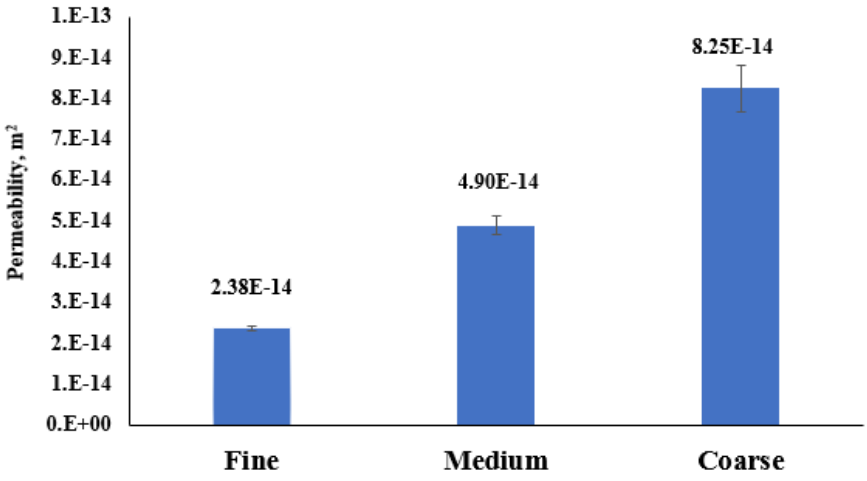


Figure 6.10 Permeability results of fine, medium coarse and coarse mesh

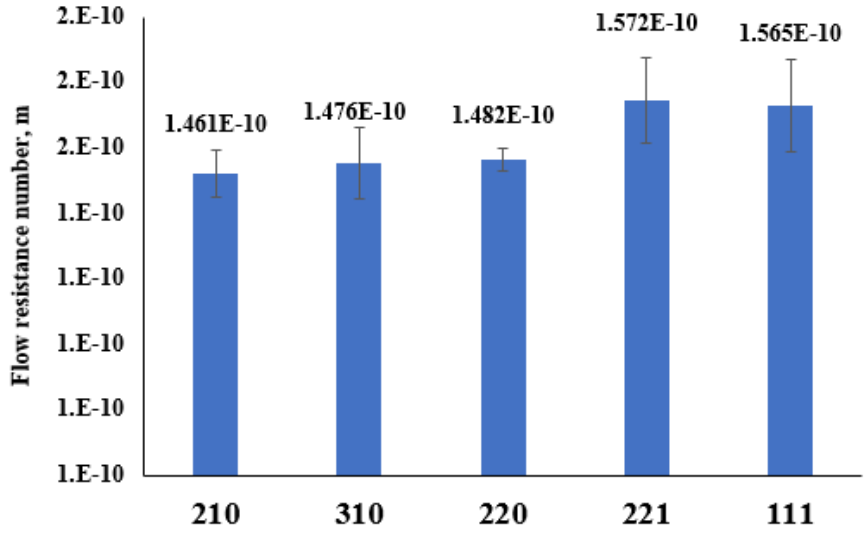


Figure 6.11 Flow resistance number of different nylon mesh lay-up orders: 2-1-0 – 2 coarse, 1medium; 3-1-0 – 3 coarse, 1medium; 2-2-0 –

2 coarse, 2 medium; 2-2-1 – 2 coarse, 2 medium, 1fine; 1-1-1 – 1 coarse, 1 medium, 1fine.

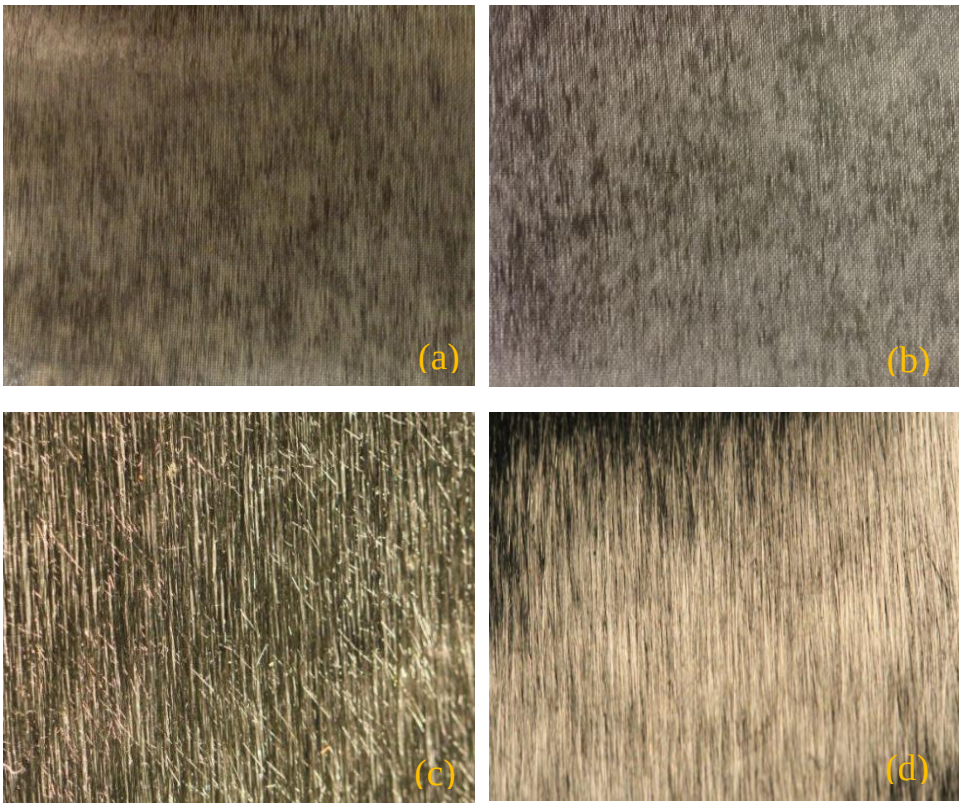


Figure 6.12 Fibre orientation: (a) 30gsm - 2 coarse, 1medium; (b) 30gsm - 3 coarse, 1medium; (c) 30gsm - 2 coarse, 2medium; (d) 50gsm - 2 coarse, 2medium, 1fine.

6.4 Conclusion

Vacuum plates were designed with four different open area geometry (3-slots, 5-slots, 21-slots and perforated plate). Dewatering tests were undertaken to evaluate the performance of each plate. Among the slot design plates, 21-slot vacuum plate, with highest open area density and smallest solid space between slots provides the most even pressure difference distribution which makes the localised dry patches almost invisible. The perforated plate displays similar behaviour. However, the perforated plate can provide a more uniform pressure distribution with a lower air flow rate and it will thus require

a lower power consumption for the pump. The 2-2-1 mesh lay-up method (two layers coarse mesh, two layers medium coarse mesh and one layer fine mesh) achieved the highest flow resistance number and the most uniformly aligned fibre mat. The 1-1-1 configuration can provide a similar flow resistance number but can reduce the labour associated with preparation as there are fewer layers involved.

7. Conclusions

7.1 Behaviour of fibre suspension jet and improvements in nozzle design

It has been assumed by other researchers that in depositing process the fibre orientation of aligned mat is consist with the orientation which is generated in converging nozzle. However, the stability of suspension jets has a significant influence on fibre alignment quality. The jet stability testing has been undertaken with the variables: fibre suspension viscosity, the Re number of suspension flow, fibre length and fibre volume concentration in the suspension. The results can be concluded as that by increasing either fibre length, or fibre volume concentration in suspension, the fibre-fibre interaction become more significant and resulting a reduced stability of fibre suspension jet. Furthermore, the aligned fibre orientation is beneficial to the jet stability.

Both numerical modelling and experimental work were undertaken to explore the optimised nozzle which can generate good stability jet and improve the fibre alignment quality in nozzle. Concave nozzle can provide high stability as there is less influence of wall shear on the flow, reffering to the data expoted from CFD simulation. The fibre orientation in concave nozzle was investigated in this work. The appropriate increment of contraction angle of concave nozzle makes the shear rate increase continuously which consequently gives a good fibre alignment quality. Thus, the concave nozzle is suggested to be applied in the hydrodynamic alignment process, due to it can provide a good fibre alignment in nozzle and maintain this thtough good jet stability in deposition.

7.2 Characterisation of aligned mats and composites

The processing factors which can influent alignment quality in hydrodynamic alignment process have been explored. With the improved fibre dispersion process, fibre volume concentration in the suspension is not a main effect for aligning 3mm fibre and 12 mm fibre. Higher dewatering suction pressure is beneficial to the fibre alignment for 12 mm fibres. However, if high vacuum level was applied around the depositing drum, 3mm fibres will move along the glycerine flow direction during dewatering process and the pre-aligned orientation will be affected. Thus, lower vacuum level is required for 3mm fibre to maintain aligned fibre orientation. Higher drum/jet velocity ratio can improve the alignment quality with both 3mm and 12mm fibre.

The composite laminates were made with 3mm carbon fibre under 7 bar curing pressure and had a tensile modulus of 98GPa and tensile strength of 826 MPa with a fibre volume fraction of 46%. True recycled fibre was also introduced in this work, and a tensile modulus of 60GPa and tensile strength of 322 MPa was achieved by 1.15mm mean fibre length recycled fibre laminate composites with a fibre volume fraction of 38%. Demonstrating the potential of fibre alignment to produce high value composites that give specific mechanical properties better than other widely used low costs metallic and composite materials and approaching those of virgin carbon fibre composites.

7.3 Through thickness permeability of aligned fibre mat

A permeability testing rig was designed based on the Darcy's law. The highly close packed structure makes the fibre mat has a small permeability. In addition, the permeability of aligned fibre mat is decreasing with the

increasing load and this is due to its self-compaction behaviour. Based on the experimental permeability results, the Kozeny-Carman constant, C, is defined as 10.92 for the aligned fibre mat. Thus, Kozeny-Carman equation was applied to predict the permeability value in the subsequent analytical model related to vacuum pump selection and energy cost consumption. For the current deposition process, the target fibre mat areal density is set as 100gsm. If the leaking area ratio is above 2.5%, a high pressure radial blower is the optimal choice, it can maintain 0.084bar suction pressure under 6kw energy cost and high production rate become achievable. 2-stage channel blower is preferred when the target areal density if 300gsm, but the leaking area ratio should be limited to below 2%. A liquid ring pump is an appropriate choice when an extremely thick mat is expected (more than 500gsm). However, the leaking area ratio is strictly restricted to below 0.75%. The analytical model described in this chapter can be used to optimise the current process and be considered as a design guideline for process scale up.

7.4 Characterisation of dewatering behaviour

Vacuum plates were designed with four different open area geometry (3-slots, 5-slots, 21-slots and perforated plate). Dewatering tests were undertaken to evaluate the performance of each plate. The perforated plate can provide a more uniform pressure distribution with a lower air flow rate and it will thus require a lower power consumption for the pump. Nylon meshes are used as the pressure distribution media and attaced around the deposition drum. The 1-1-1 mesh lay-up configtation (one layer coarse mesh, one layer medium mesh and one layer fine mesh) achieved the high flow resistance number and

the uniformly aligned fibre mat. Furthermore, this lay-up method can reduce the labour associated with preparation as there are fewer layers involved.

Future work can focus on further development of the alignment process with considering process capital and operating costs.

7.5 Future research recommendations

The alignment process at this stage has a single nozzle travelling transversely during depositing. This may lead to a flodding at the near nozzle side of drum when there is a air leakage at the other side. This will result an effect on fibre orientation and an extra energy cost. In addition, raletively low production rate is another drawback from this single nozzle setting. Thus, either a full weith nozzle (covering the full mat weith) or series of nozzles could be applied in the further development. CFD simulation can be used to calculate the fluid properties in depositing, and combining with the fibre orientation tensors, the fibre orientation distribution of the aligned fibre mat can be predicted.

Continuous process should be the next generation after this batch type alignment rig. Based on the through thickness permeability which were evaluated in this thesis, an analytical model, combing the fibre mat areal mass building up procedure, dewatering process and energy costs from vacuum pump, could be developed for the continuous process. So that commercially viable processes are available to support future expansion of the emerging carbon fibre recycling industry.

The dispersion media involved in this work is glycerine/water solution as it is a Newtonian fluid and the viscosity can be easily adjusted by changing the weight percentage of water in the solution. As the drawback, it requires a

washing process before applying binder and the glycerine residual can make a significant reduction on the mechanical properties of the composites. Some substitute dispersion media, such as water and cellosize have been suggested by other researchers. However, the low viscosity makes water can’t disperse longer recycled fibres (over 12mm), and cellosize requires a long preparation time.

Appendix – publications

The following papers have been produced as a result of this work, some of which are in press or to be submitted at the time of writing.

1. ‘Effect of fibre length and suspension concentration on alignment quality of discontinuous recycled carbon fibre’,
   Z. Liu, K. H. Wong, T. A. Turner, S.J. Pickering,
   20th International Conference on Composite Materials (ICCM20), Copenhagen, Danmark, July 2015.
2. ‘Applications for carbon fibre recovered from composites’,
   S.J. Pickering, Z. Liu, T. A. Turner, K. H. Wong,
   37th Risø International Symposium on Materials Science,
   Frederiksborgvej, Danmark, September 2016
3. ‘Processing factors influencing alignment quality of discontinuous carbon fibre in hydrodynamic alignment process’,
   Z. Liu, K. H. Wong, T. A. Turner, S.J. Pickering,
   Awaiting subbmition.
4. ‘Effect of fibre suspension jet stability on alignment quality of discontinuous carbon fibre mat’,
   Z. Liu, K. H. Wong, T. A. Turner, S.J. Pickering,
   Awaiting subbmition.